EXHIBIT 6

BIOCHEMICAL ENGINEERING FUNDAMENTALS

Second Edition

James E. Bailey
California Institute of Technology

David F. Ollis
North Carolina State University

McGraw-Hill Publishing Company

New York St. Louis San Francisco Auckland Bogotá Caracas
Hamburg Lisbon London Madrid Mexico Milan
Montreal New Delhi Oklahoma City Paris San Juan
São Paulo Singapore Sydney Tokyo Toronto

This book was set in Times Roman.
The editors were Kiran Verma and Cydney C. Martin.
The production supervisor was Diane Renda;
the cover was designed by John Hite;
project supervision was done by Albert Harrison, Harley Editorial Services.
Halliday Lithograph Corporation was printer and binder.

BIOCHEMICAL ENGINEERING FUNDAMENTALS

67891011 HDHD 99876543210

ISBN 0-07-003212-2

Library of Congress Cataloging-in-Publication Data

Bailey, James E. (James Edwin), 1944-
Biochemical engineering fundamentals.

(McGraw-Hill chemical engineering series)
Includes bibliographies and index.
1. Biochemical engineering. I. Ollis, David F.
II. Title. III. Series
TP248.3.B34 1986 660'.63 85-19744
ISBN 0-07-003212-2

To Sean
and
Andrew, Mark, Stephen, and Matthew

Structured growth models. See Refs. 5–8 above and

15. A. G. Fredrickson, "Formulation of Structured Growth Models," *Biotechnol. Bioeng.*, **18**: 1481, 1976.
16. F. M. Williams, "A Model of Cell Growth Dynamics," *J. Theoret. Biol.*, **15**: 190, 1967.
17. A. Harder and J. A. Roels, "Application of Simple Structured Models in Bioengineering," p. 55. In *Advances in Biochemical Engineering*, vol. 21, A. Fiechter (ed.), Springer-Verlag, Berlin, 1982.
18. A. H. E. Bijkerk and R. J. Hall, "A Mechanistic Model of the Aerobic Growth of *Saccharomyces cerevisiae*," *Biotechnol. Bioeng.*, **19**: 267, 1977.
19. N. B. Pamment, R. J. Hall, and J. P. Barford, "Mathematical Modeling of Lag Phases in Microbial Growth," *Biotechnol. Bioeng.*, **30**: 349, 1978.
20. M. L. Shuler and M. M. Domach, "Mathematical Models of the Growth of Individual Cells," p. 101 in *Foundations of Biochemical Engineering*, H. W. Blanch, E. T. Papoutsakis, and G. Stephanopoulos (eds.), American Chemical Society, Washington, D. C., 1983.
21. D. Ramkrishna, "A Cybernetic Perspective of Microbial Growth," p. 161 in *Foundations of Biochemical Engineering*, H. W. Blanch, E. T. Papoutsakis, and G. Stephanopoulos (eds.), American Chemical Society, Washington, D.C., 1983.
22. D. S. Kompala, D. Ramkrishna, and G. T. Tsao, "Cybernetic Modeling of Microbial Growth on Multiple Substrates," *Biotechnol. Bioeng.*, **26**: 1272, 1984.

Product formation kinetics:

23. E. L. Gaden, *Chem. Ind. Rev.* **1955**: 154; *J. Biochem. Microbiol. Technol. Eng.*, **1**: 413, 1959.
24. F. H. Deindoerfer, "Fermentation Kinetics and Model Processes," *Adv. Appl. Microbiol.*, **2**: 321, 1960.
25. D. F. Ollis, "A Simple Batch Fermentation Model: Theme and Variations," *Ann. N.Y. Acad. Sci.*, **413**: 144, 1983.
26. S. Pažoutova, J. Votruba, and Z. Řeháček, "A Mathematical Model of Growth and Alkaloid Production in the Submerged Culture of *Claviceps purpurea*," *Biotechnol. Bioeng.*, **23**: 2837, 1981.
27. S. B. Lee and J. E. Bailey, "Analysis of Growth Rate Effects on Productivity of Recombinant *Escherichia coli* Populations," *Biotechnol. Bioeng.*, **26**: 66, 1984.
28. S. B. Lee and J. E. Bailey, "Genetically Structured Models for *lac* Promoter-Operator Function in the *Escherichia coli* Chromosome and in Multicopy Plasmids: *lac* Operator Function," *Biotechnol, Bioeng.*, **26**: 1372, 1984.

Segregated kinetic models:

29. D. Ramkrishna, "Statistical Models of Cell Populations," *Adv. in Biochem. Eng.*, **11**: 1, 1979.
30. Y. Nishimura and J. E. Bailey, "On the Dynamics of Cooper-Helmstetter-Donachie Procaryote Populations," *Math. Biosci.*, **51**: 505, 1980.
31. M. A. Hjortso and J. E. Bailey, "Steady-State Growth of Budding Yeast Populations in Well-Mixed Continuous Flow Microbial Reactors," *Math. Biosci.*, **60**: 235, 1982.
32. P. Shu, "Mathematical Models for the Product Accumulation in Microbial Processes," *J. Biochem. Microbiol, Technol. Eng.*, **3**: 95. 1961.

An excellent introduction to the literature on sterilization:

33. N. Blakebrough, "Preservation of Biological Materials Especially by Heat Treatment," in N. Blakebrough (ed.), *Biochemical and Biological Engineering Science*, vol. 2, Academic Press, Inc., New York, 1968.

The factors affecting organisms' susceptibility to sterilization are reviewed in Chaps. 20 and 21 of Frobisher (Ref. 2 of Chap. 1); consideration of phage destruction:

34. Hango et al, "Phage Contamination and Control," in *Microbial Production of Amino Acids*, Kodansha Ltd., Tokyo, and John Wiley & Sons, Inc., New York, 1973.

CHAPTER

EIGHT

TRANSPORT PHENOMENA IN BIOPROCESS SYSTEMS

The previous chapters have considered progressively larger scales of distance: from molecular through cellular to fluid volumes containing millions or billions of cells per milliliter. As the sources and sinks of entities such as nutrients, cells, and metabolic products become further separated in space, the probability increases that some physical-transport phenomena, rather than a chemical rate, will influence or even dominate the overall rate of solute processing in the reaction volume under consideration. Indeed, according to the argument of Weisz [1], cells and their component catalytic assemblies operate at Thiele moduli near unity; they are operating at the maximum possible rate without any serious diffusional limitation. If, in bioprocess circumstances, a richer supply of carbon nutrients is created, evidently the aerobic cell will be able to utilize them fully only if oxygen can also be maintained at a higher concentration in the direct vicinity of the cell. This situation may call for increased *gas–liquid mass transfer* of oxygen, which has sparingly small solubility in aqueous solutions, to the culture.

Evidently, the boundary demarcating aerobic from anaerobic activity depends upon the local bulk-oxygen concentration, the O_2 diffusion coefficient, and the local respiration rates in the aerobic region. This line divides the viable from dying cells in strict aerobes such as mold in mycelial pellets or tissue cells in cancer tumors; it determines the depth of aerobic activity near lake surfaces; and it divides the cohabitating aerobes from anaerobic microbial communities in soil

particles. Thus, while the modern roots of biological-process oxygen mass transfer began with World War II penicillin production in the 1940s, its implications are now established to include many natural processes such as food spoilage via undesired oxidation and lake eutrophication due either to inadequate system aeration by natural oxygen supplies or to an excessive concentration of material such as phosphate or nitrate.

Other sparingly soluble gases are also of fermentation interest. Methane and other light hydrocarbons have been explored as gaseous substrates for single cell protein production; in this demanding conversion, *both* oxygen and methane must be dissolving continuously at rates sufficient to meet the biological demand. Methane transfer out of solution is important in anaerobic waste treatment, at the metabolic end of which light carboxylic acids (primarily acetic acid) are decarboxylated to give the corresponding alkanes.

Carbon dioxide is generated in nearly all microbial activity. In spite of its large solubility, the interconversion between gaseous and the various forms of dissolved carbon dioxide (CO_2, H_2CO_3, HCO_3^-, CO_3^{2-}) couples its mass transfer rate to the pH variation; this topic figures importantly in controlling the pH of acid-sensitive anaerobic digestors (Chapter 14) where CO_2 and CH_4 removal occur simultaneously.

Liquid–liquid mass transfer is important in SCP production from liquid hydrocarbon feedstocks, as well as in fermentation recovery operations; e.g., filtered or whole broth extraction of pharmaceuticals (Chapter 11) employing organic solvents.

Renewable resource bioconversions, such as the use of cellulosic, hemicellulosic, and lignin fractions of agricultural and forest wastes as fermentation feedstocks, typically involve rate processes (biomass solubilization, liquefaction, hydrolysis) limited by available particulate substrate surface areas and solute diffusion rates. Other topics also involving *liquid–solid mass transfer* include various sorption and chromatographic methods for product recovery and purification, and liquid phase oxygen transfer to mold pellets or beads and biofilms containing immobilized cells.

Operation at high cell densities may often result in mass-transfer limited conditions, as observed in reactors as diverse as laboratory shake flasks or large scale fermentors for penicillin or extracellular biopolymers (xanthan gum) or activated sludge waste plants. The process engineer must, accordingly, know when transport phenomena or biological kinetics are rate-limiting in order properly to design bioreactors.

Strong coupling often occurs between solute diffusion and momentum transport or chemical reactions or (even more complex) both. The case of diffusion and reaction interaction has been considered in Chap. 4. In such circumstances, the Thiele modulus and a saturation parameter K_s/s_0 provide the unifying parameters needed to completely describe cell and enzyme performance; i.e., effectiveness factor, for such systems. Unfortunately, the variety of circumstances under which mass transfer couples with momentum transfer, i.e., fluid mechanics, is enormous; indeed, it is the substance of a major fraction of the chemical

engineering literature. For this text, we content ourselves with fundamental concepts and tabulated formulas for calculation or estimation of the appropriate mass-transfer coefficients for solutes.

A final brief section of this chapter concerns instances where heat transfer may provide an important transport effect which strongly influences the bioprocess system's behavior through spatial temperature inhomogeneity. Examples here include relatively exothermic fermentation processes, such as trickling-filter operation for wine-vinegar production or wastewater treatment, and that gardener's delight, the compost heap (municipal dump, etc.) and other solid-state fermentations.

8.1 GAS–LIQUID MASS TRANSFER IN CELLULAR SYSTEMS

The general nature of the mass-transfer problem of primary concern in this chapter is shown schematically in Fig. 8.1. A sparingly soluble gas, usually oxygen, is transferred from a source, say a rising air bubble, into a liquid phase containing cells. (Any other sparingly soluble substrate, e.g., the liquid hydrocarbons used in hydrocarbon fermentations, will give the same general picture.) The oxygen must pass through a series of transport resistances, the relative magnitudes of which depend on bubble (droplet) hydrodynamics, temperature, cellular activity and density, solution composition, interfacial phenomena, and other factors.

These arise from different combinations of the following resistances (Fig. 8.1):

1. Diffusion from bulk gas to the gas–liquid interface
2. Movement through the gas–liquid interface
3. Diffusion of the solute through the relatively unmixed liquid region adjacent to the bubble into the well-mixed bulk liquid
4. Transport of the solute through the bulk liquid to a second relatively unmixed liquid region surrounding the cells
5. Transport through the second unmixed liquid region associated with the cells
6. Diffusive transport into the cellular floc, mycelia, or soil particle
7. Transport across cell envelope and to intracellular reaction site

All of these resistances appear in Fig. 8.1. When the organisms take the form of individual cells, the sixth resistance disappears. Microbial cells themselves have some tendency to adsorb at interfaces. Thus, cells may preferentially gather at the vicinity of the gas-bubble–liquid interface. Then, the diffusing solute oxygen passes through only one unmixed liquid region and no bulk liquid before reaching the cell. In this situation, the bulk dissolved O_2 concentration does not represent the oxygen supply for the respiring microbes.

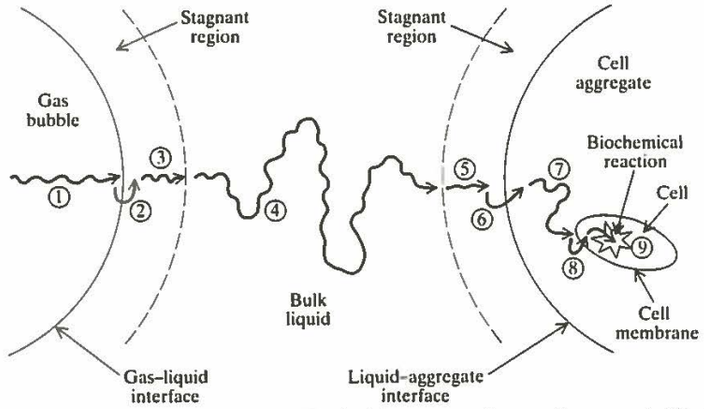

Figure 8.1 Schematic diagram of steps involved in transport of oxygen from a gas bubble to inside a cell.

Similarly, in the microbial utilization of other sparingly soluble substrates such as hydrocarbon droplets, cell adsorption on or near the hydrocarbon-emulsion interface has been frequently observed. A reactor model for this situation is considered in Chap. 9.

The variety of macroscopic physical configurations by which gas–liquid contacting can be effected is indicated in Fig. 8.2. In general, we can distinguish fluid motions induced by freely rising or falling bubbles or particles from fluid motions which occur as the result of applied forces other than the external gravity field (forced convection). The distinction is not clear-cut; gas–liquid mixing in a slowly stirred semibatch system may have equal contributions from naturally convected bubbles and from mechanical stirring. The central importance of hydrodynamics requires us to examine the interplay between fluid motions and mass transfer. Before beginning this survey, some comments and definitions regarding mass transfer are in order.

8.1.1 Basic Mass-Transfer Concepts

The solubility of oxygen in aqueous solutions under 1 atm of air and near ambient temperature is of the order of 10 parts per million (ppm) (Table 8.1). An actively respiring yeast population may have an oxygen consumption rate of the order 0.3 g of oxygen per hour per gram of dry cell mass. The peak oxygen consumption for a population density of 10^9 cells per milliliter is estimated by assuming the cells to have volumes of 10^{-10} mL, of which 80 percent is water. The absolute oxygen demand becomes

$$\frac{0.3\ \text{g O}_2}{\text{g dry mass} \cdot \text{h}}\left(10^9\ \frac{\text{cells}}{\text{mL}}\right)(10^{-10}\ \text{mL})\left(1\ \frac{\text{g cell mass}}{\text{cm}^3}\right)\left(0.2\ \frac{\text{g dry cell mass}}{\text{g cell mass}}\right)$$
$$= 6 \times 10^{-3}\ \text{g/(mL} \cdot \text{h)} = 6\ \text{g O}_2\text{/(L} \cdot \text{h)}$$

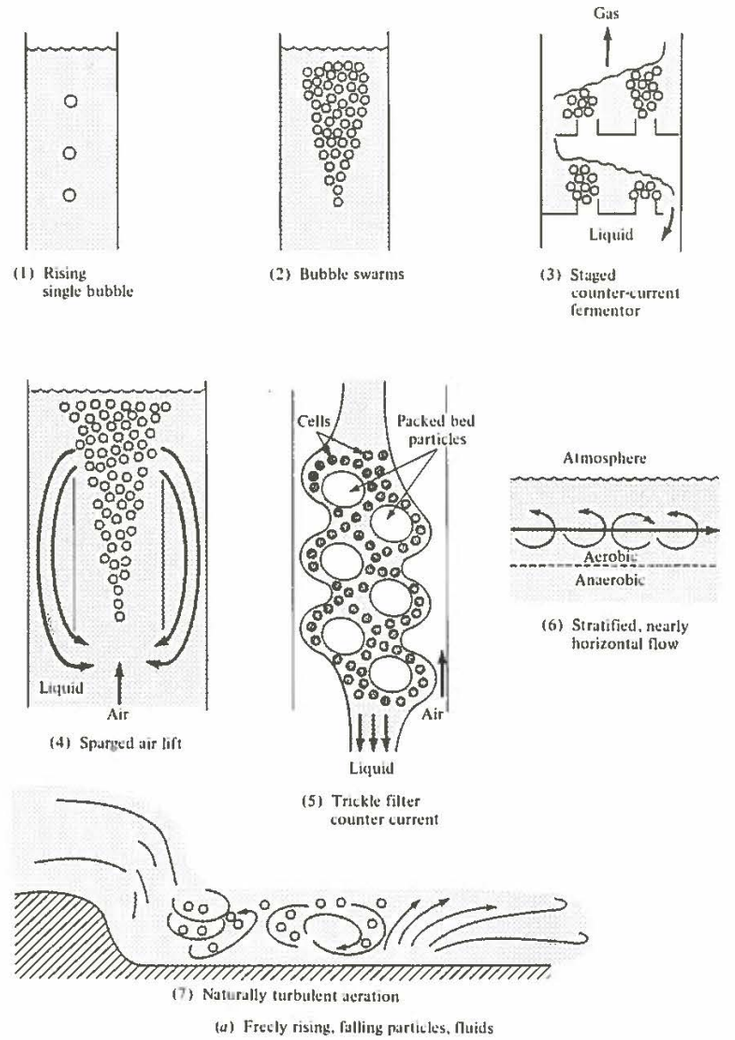

Figure 8.2 Gas–liquid contacting modes: (*a*) freely rising, falling particles, fluids.

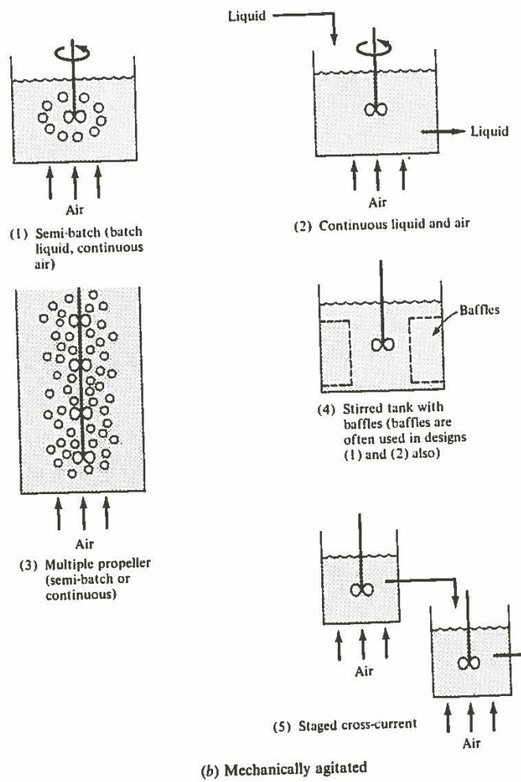

(1) Semi-batch (batch liquid, continuous air)

(2) Continuous liquid and air

(4) Stirred tank with baffles (baffles are often used in designs (1) and (2) also)

(3) Multiple propeller (semi-batch or continuous)

(5) Staged cross-current

(*b*) Mechanically agitated

Figure 8.2 (*continued*) (*b*) mechanically agitated.

Thus, the actively respiring population consumes oxygen at a rate which is of the order of 750 times the O_2 saturation value per hour. Since the inventory of dissolved gas is relatively small, it must be continuously added to the liquid in order to maintain a viable cell population. This is not a trivial task since the low oxygen solubility guarantees that the concentration difference which drives the transfer of oxygen from one zone to another is always very small.

For sparingly soluble species such as oxygen or hydrocarbons in water, the two equilibrated interfacial concentrations c_{gi} and c_{li} on the gas and liquid sides,

Table 8.1 Solubility of O_2 at 1 atm O_2 in water at various temperatures and solutions of salt or acid at 25°C†

Temp, °C	Water, O_2 mmol/L	Temp. °C	Water, O_2 mmol/L
0	2.18	25	1.26
10	1.70	30	1.16
15	1.54	35	1.09
20	1.38	40	1.03

Aqueous solutions at 25°C

Electrolyte conc, *M*	O_2, mmol/L		
	HCl	H_2SO_4	NaCl
0.0	1.26	1.26	1.26
0.5	1.21	1.21	1.07
1.0	1.16	1.12	0.89
2.0	1.12	1.02	0.71

† Data from *International Critical Tables*, vol. III, p. 271, McGraw-Hill Book Company, New York, 1928, and F. Todt, *Electrochemische Sauerstoffmessungen*, W. de Guy and Co., Berlin, 1958.

respectively, may typically be related through a linear partition-law relationship such as Henry's law

$$Mc_{li} = c_{gi} \tag{8.1}$$

provided that the solute exchange rate across the interface is much larger than the net transfer rate, as is typically the case: at 1 atm of air and 25°C, the O_2 collision rate at the surface is of the order of 10^{24} molecules per square centimeter per second, a value greatly in excess of the net flux for typical microbial consumption requirements cited above.

At steady state, the oxygen transfer rate to the gas–liquid interface equals its transfer rate through the liquid-side film (Fig. 8.1). Taking c_g and c_l to be the oxygen concentrations in the bulk gas and bulk liquid respectively, we can write the two equal transfer rates

$$\begin{aligned} \text{Oxygen flux} &= \text{mol } O_2/(\text{cm}^2 \cdot \text{s}) \\ &= k_g(c_g - c_{gi}) \quad \text{gas side} \\ &= k_l(c_{li} - c_l) \quad \text{liquid side} \end{aligned} \tag{8.2}$$

Since the interfacial concentrations are usually not accessible in mass-transfer measurements, resort is made to mass-transfer expressions in terms of the overall mass-transfer coefficient K_l and the overall concentration driving

force $c_l^* - c_l$, where c_l^* is the liquid-phase concentration which is in equilibrium with the bulk gas phase

$$Mc_l^* \equiv c_g \tag{8.3}$$

In terms of these overall quantities, the solute flux is given by

$$\text{Flux} = K_l(c_l^* - c_l) \tag{8.4}$$

Utilization of Eqs. (8.1), (8.2), (8.3), and (8.4) results in the following well-known relationship between the overall mass-transfer coefficient K_l and the physical parameters of the two-film transport problem, k_g, k_l, and M:

$$\frac{1}{K_l} = \frac{1}{k_l} + \frac{1}{Mk_g} \tag{8.5}$$

For sparingly soluble species, M is much larger than unity. Further, k_g is typically considerably larger than k_l. Under these circumstances we see from Eq. (8.5) that K_l is approximately equal to k_l. Thus, essentially all the resistance to mass transfer lies on the liquid-film side.

The oxygen-transfer rate per unit of reactor volume Q_{O_2} is given by

$$\begin{aligned} Q_{O_2} = \text{oxygen absorption rate} &= \frac{(\text{flux})(\text{interfacial area})}{\text{reactor liquid volume}} \\ &= k_l(c_l^* - c_l)\frac{A}{V} \\ &= k_l a'(c_l^* - c_l) \end{aligned} \tag{8.6}$$

where $a' = A/V$ is the gas–liquid interfacial area per unit liquid volume and the approximation $K_l \approx k_l$ just discussed has been invoked. Since our major emphasis in this chapter is aeration, we shall concentrate on oxygen transfer and henceforth use k_l in place of K_l as the appropriate mass-transfer coefficient. The symbol a, which appears in several correlations, is the gas–liquid interfacial area per unit volume of bioreactor (gas + liquid) contents. Head space gas is not included.

It is important to recognize that Q_{O_2} is defined "at a point." It is a local volumetric rate of O_2 consumption; the average volumetric rate of oxygen utilization (moles per time per volume) $\bar{Q}_{O_2}$ in an entire liquid volume V is given by

$$\bar{Q}_{O_2} = \frac{1}{V}\int_0^V Q_{O_2}\, dV \tag{8.7}$$

In general, $\bar{Q}_{O_2}$ is equal to Q_{O_2} only if hydrodynamic conditions, interfacial area/volume, and oxygen concentrations are uniform throughout the vessel.

For example, a complete description of the phenomena underlying the observed average transfer rate in a bioreactor depends on power input per unit volume, fluid and dispersion rheology, sparger characterization, and gross flow patterns in the vessel. Figure 8.3 indicates the relationship between observed average transfer rate and the causative phenomena. Since we generally lack

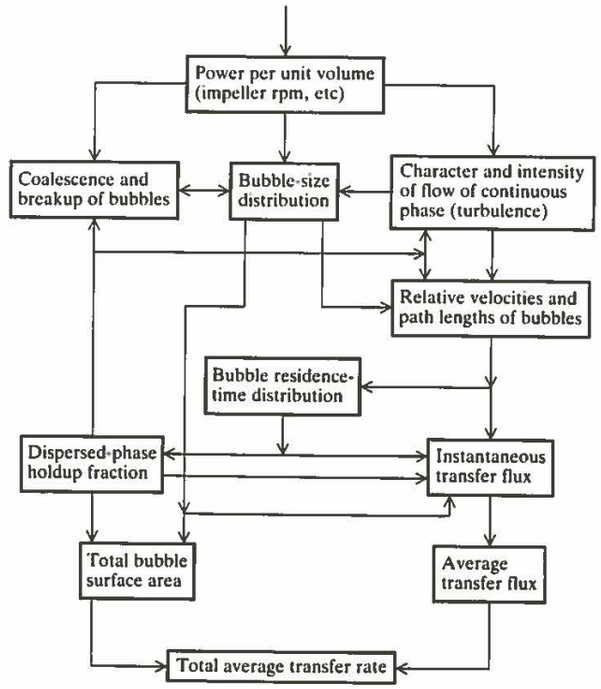

Figure 8.3 Relationships between input agitation intensity and resultant gas transfer rate. *(After W. Resnick and B. Gal-Or, Adv. Chem. Eng., vol. 7, p. 295 (1968). Reprinted by permission of Academic Press.)*

crucial fundamental information on coalescence and redispersion rates, bubble size and residence time distribution, we are typically forced to develop correlations based on appropriate averages of bubble size, holdup (gas volume fraction), gas bubble and liquid residence times, etc.

In Table 8.1 we saw that c_l^* is determined by the temperature and composition of the medium. Composition influences become more complicated when the dissolved gas can undergo liquid-phase reaction. This is the case for carbon dioxide, which may exist in the liquid phase in any of four forms: CO_2, H_2CO_3, HCO_3^-, and CO_3^{2-}. The equilibrium relations

$$K_1 = \frac{[H^+][HCO_3^-]}{[CO_2] + [H_2CO_3]} = 10^{-6.3}\,\text{M} \tag{8.8}$$

$$K_2 = \frac{[H^+][CO_3^{2-}]}{[HCO_3^-]} = 10^{-10.25}\,\text{M} \tag{8.9}$$

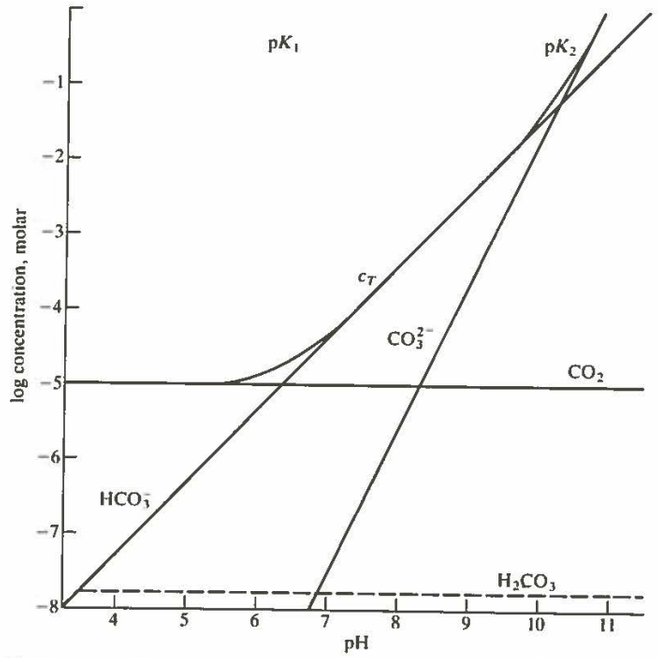

Figure 8.4 Equilibrium concentrations of dissolved CO_2, HCO_3^-, $CO_3^=$ and H_2CO_3. c_T is total concentration of all four forms of CO_2. [$p_{CO_2} = 10^{-3.5}$ atm (ambient concentration); pH adjusted with strong acid or strong base.] *(After W. Stumm and J. J. Morgan, "Aquatic Chemistry," John Wiley and Sons, N.Y. p. 127, 1970.)*

(values at 25°C) indicate that the total dissolved carbon concentration, c_T, as carbon dioxide is quite pH sensitive:

$$c_T = [CO_2] + [H_2CO_3] + [HCO_3^-] + [CO_3^{2-}]$$
$$= c_0\left[1 + \frac{K_1}{[H^+]} + \frac{K_1K_2}{[H^+]^2}\right] \tag{8.10}$$

This relation appears in Fig. 8.4, showing that below pH 5, nearly all carbon is dissolved molecular CO_2, while bicarbonate dominates when $7 < pH < 9$ and carbonate for $pH > 11$. Only the dissolved CO_2 molecule is transported across the gas–liquid interface, and we may again write Eq. (8.2) for the interfacial transfer rate.

The coupling of reaction and mass transfer may occur under neutral to basic conditions. While the reversible reaction (8.11) is rapid,

$$H_2CO_3 \rightleftharpoons HCO_3^- + H^+ \tag{8.11}$$

$$K_{eq}(T = 28°C) = \frac{[H^+][HCO_3^-]}{[H_2CO_3]} = 2.5 \times 10^{-4}\ \text{mol/L} \tag{8.12}$$

the important reaction

$$H_2CO_3 \underset{k_{-1}}{\overset{k_1}{\rightleftharpoons}} CO_2 + H_2O \tag{8.13}$$

is far slower, with $k_1 = 20\,s^{-1}$ and $k_{-1} = 0.03\,s^{-1}$ (25°C). Thus, depending on circumstances, the slow step in CO_2 removal to the gas phase could be chemical [Eq. (8.13)] or physical [CO_2 (dissolved) → CO_2 (gas)].

8.1.2 Rates of Metabolic Oxygen Utilization

In design of aerobic biological reactors we frequently use correlations of data more or less approximating the situation of interest to establish whether the slowest process step is the oxygen transfer rate or the rate of cellular utilization of oxygen (or other limiting substrate). The maximum possible mass-transfer rate is simply that found by setting $c_l = 0$: all oxygen entering the bulk solution is assumed to be rapidly consumed. The maximum possible oxygen utilization rate is seen from Chap. 7 to be $x\mu_{max}/Y_{O_2}$, where x is cell density and Y_{O_2} is the ratio of moles of cell carbon formed per mole of oxygen consumed.

Evidently, if $k_l a' c_l^*$ is much larger than $x\mu_{max}/Y_{O_2}$, the main resistance to increased oxygen consumption is microbial metabolism and the reaction appears to be biochemically limited. Conversely, the reverse inequality apparently leads to c_l near zero, and the reactor seems to be in the mass-transfer-limited mode.

The situation is actually slightly more complicated. At steady state, the oxygen absorption and consumption rates must balance:

$$Q_{O_2} = \text{absorption} = \text{consumption} = xq_{O_2}$$

$$k_l a'(c_l^* - c_l) = \frac{x\mu}{Y_{O_2}} \tag{8.14}$$

Assuming that the dependence of μ on c_l is known, we can use Eq. (8.14) to evaluate c_l and hence the rate of oxygen utilization.

In general, above some critical bulk oxygen concentration, the cell metabolic machinery is saturated with oxygen. In this case, sufficient oxygen is available to accept immediately all electron pairs which pass through the respiratory chain, so that some other biochemical process within the cell is rate-limiting (Chap. 5). For example, if the oxygen dependence of the specific growth rate μ follows the Monod form, then

$$Y_{O_2}k_l a'(c_l^* - c_l) = x\mu_{max}\frac{c_l}{K_{O_2} + c_l} \tag{8.15}$$

A general solution to an equation of this form was given in Sec. 4.4.1., but here for the sake of illustration we assume that the value of c_l is considerably less than c_l^*. This is not an uncommon situation in biological reactors. Subject to the assumption that $c_l \ll c_l^*$, c_l is easily seen to be

$$c_l = c_l^*\left[\frac{Y_{O_2}K_{O_2}k_l a'/x\mu_{max}}{1 - Y_{O_2}c_l^*k_l a'/x\mu_{max}}\right] \tag{8.16}$$

Table 8.2 Typical values of $c_{O_2,cr}$ in the presence of substrate†

Organism	Temp, °C	$c_{O_2,cr}$, mmol/L
Azotobacter vinelandii	30	0.018–0.049
E. coli	37.8	0.0082
	15	0.0031
Serratia marcescens	31	~0.015
Pseudomonas denitrificans	30	~0.009
Yeast	34.8	0.0046
	20	0.0037
Penicillium chrysogenum	24	~0.022
	30	~0.009
Aspergillus oryzae	30	~0.020

† Summarized by R. K. Finn, p. 81 in N. Blakebrough (ed.), *Biochemical and Biological Engineering Science*, vol. 1, Academic Press, Inc., New York, 1967.

If the resulting value of c_l is greater than the critical oxygen value c_{cr} (about $3K_{O_2}$), the rate of microbial oxygen utilization is limited by some other factor, e.g., low concentration of another substrate, even though the bulk solution has a dissolved oxygen level considerably below the saturation value. The critical oxygen values for organisms lie in the range of 0.003 to 0.05 mmol/L (Table 8.2) or of the order of 0.1 to 10 percent of the solubility values in Table 8.1, that is, 0.5 to 50 percent of the air saturation values. For the higher critical oxygen values such as obtained for *Penicillium* molds, oxygen mass transfer is evidently extremely important.

Many factors can influence the total microbial oxygen demand $x\mu/Y_{O_2}$, which in turn sets the minimum values of $k_l a'$ needed for process design through Eq. (8.14). The more important of these are cell species, culture growth phase, carbon nutrients, pH, and the nature of the desired microbial process, i.e., substrate utilization, biomass production, or product yield (Chap. 7).

In the batch-system results of Fig. 8.5, a maximum in *specific* O_2 demand occurs in the early exponential phase although x is larger at a later time. A peak in the product $x\mu$, and thus the total oxygen demand, occurs near the end of the exponential phase and the approach to the stationary phase; this is later than the time of achievement of the largest specific growth rate.

The carbon nutrient affects oxygen demand in a major way. For example, glucose is generally metabolized more rapidly than other carbohydrate substances. Peak oxygen demands of 4.9, 6.7, and 13.4 mol/(L · h) have been observed for *Penicillium* mold utilizing lactose, sucrose, and glucose, respectively [2].

The component parts of oxygen utilization by the cell include cell maintenance, respiratory oxidation for further growth (more biosynthesis), and oxidation of substrates into related metabolic end products. In examining metabolic stoichiometry in Chap. 5, we have seen that oxygen utilization for growth is typically coupled directly to the amount of carbon-source substrate consumed. Furthermore, more reduced substrates such as paraffins and methane require greater oxygen uptake by the cell than substrates such as glucose which have approximately the same carbon oxidation state as the cell. For example, the yield factors $Y_{O_2/C}$ giving moles oxygen used per mole of carbon source metabolized are 1.34, 1.0, and 0.4 for typical microorganisms growing on methane, paraffins, and carbohydrates, respectively.

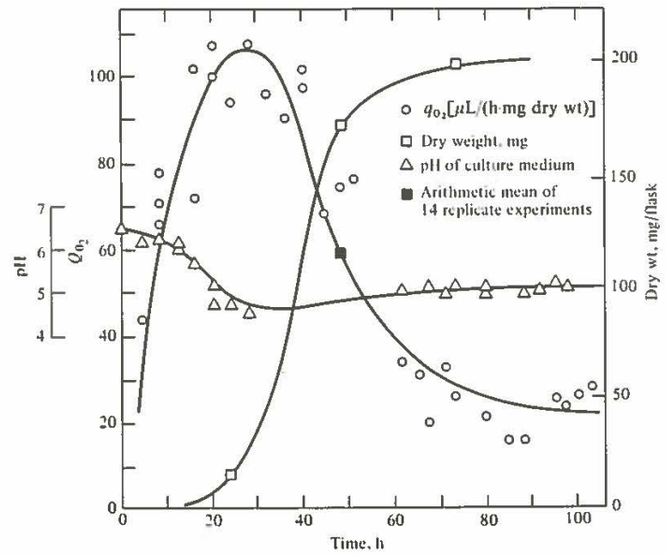

Figure 8.5 Oxygen utilization rate in batch culture of *Myrothecium verrucaria* [*Reprinted from R. T. Darby and D. R. Goddard, Am. J. Bot., vol. 37, p. 379 (1950).*]

Oxygen may also be consumed as a reactant in a *biotransformation*. For example, 5-ketogluconic acid production from glucose by batch cultivation of *Acetobacter* begins with a growth phase in which some medium glucose is converted to gluconic acid. Here O_2 use for both growth and product formation occurs. After glucose exhaustion, growth ceases, and gluconic acid is converted to 5-ketogluconic acid with stoichiometry

$$C_6H_{12}O_7 + \tfrac{1}{2}O_2 \rightarrow C_6H_{10}O_7 + H_2O \qquad (8.17)$$

In the final phase of the process which involves only this biotransformation, oxygen demand is directly coupled to product formation through the stoichiometry of Eq. (8.17).

8.2 DETERMINATION OF OXYGEN TRANSFER RATES

Ideally, oxygen transfer rates should be measured in biological reactors which include the nutrient broth and cell population(s) of interest. As this requires all the accoutrements for inoculum and medium preparation, prevention of contamination, and environmental control for the cell culture, it is an inconvenient and troublesome way to conduct mass-transfer experiments. Consequently, a common strategy for study of oxygen transfer rates is to use synthetic systems which approximate bioreaction conditions without the complications of a living culture. In such approaches, the major objective is to elucidate the dependence of $k_l a'$ on hydrodynamics.

In order for such synthetic media to represent the cellular broth of interest reliably, the following properties of the synthetic media and actual broth should be identical:

1. Solution viscosity and other rheological characteristics (see Sec. 8.8).
2. Gas-liquid interfacial resistance.
3. Bubble coalescense tendencies
4. Oxygen solubility and diffusivity.

In general, the usefulness of a synthetic (cell-free) situation for approximating a bioreaction situation depends on the degree to which these conditions are met. Experiments with oxygen absorption into pure water, for example, satisfy few of these criteria. We shall examine the quantitative influence of fluid viscosity, surface-active agents, and nature of mixing shortly.

8.2.1 Measurement of $k_l a'$ Using Gas-Liquid Reactions

Considering now the transport paths in Fig. 8.1, we see that if oxygen is consumed by chemical reaction in the bulk liquid at a sufficiently large rate we will find $c_l \approx 0$. Then the bulk-phase chemical-reaction rate is equal to $k_l a' c_l^*$, from which the $k_l a'$ value readily follows. A common bulk-phase oxygen sink in many previous mass-transfer studies is the oxidation of sodium sulfite to sulfate in the presence of catalytic metal ions such as Co^{2+}:

$$SO_3^{2-} + \tfrac{1}{2}O_2 \xrightarrow{\text{catalyst}} SO_4^{2-} \tag{8.18}$$

The kinetics of the rate of oxidation of sulfite solutions to sulfate is complex. The reaction orders for oxygen and sulfite depend on the catalyst used and its concentration, apparently implying a nontrivial series of elementary steps leading to the overall result above. Regardless of the reaction order, the condition sufficient to ensure that the chemical reaction occurs to a negligible extent in the liquid film adhering to each bubble (and thus represents the situations in Fig. 8.1) is a negligible total reaction rate in the film compared with the mass-transfer rate

$k_l(c^* - c)$. If ζ denotes the mass-transfer film thickness, this criterion can be restated mathematically as

$$\zeta \times \text{rate}\Big|_{\text{film}} < k_l(c^* - c) \tag{8.19}$$

The rate in the film will be less than that corresponding to bulk sulfite and saturation oxygen levels, i.e., rate (c^*, $\text{sulfite}_{\text{bulk}}$), and so in terms of these measurable or calculable quantities (c^*, $\text{sulfite}_{\text{bulk}}$) a conservative criterion for negligible film reaction is

$$\zeta \times \text{rate}(c^*, \text{sulfite}_{\text{bulk}}) < k_l(c^* - c) \tag{8.20}$$

The "thickness" of the mass-transfer film is given by

$$\zeta = \frac{\mathscr{D}_{O_2}}{k_l} \tag{8.21}$$

Assuming the reaction to be of order α_1 in oxygen and α_2 in sulfite leads to the inequality

$$\frac{\mathscr{D}_{O_2}[k_r(c^*)^{\alpha_1}\text{sulfite}^{\alpha_2}]}{k_l} < k_l(c^* - c) \tag{8.22}$$

Thus

$$k_l > \left[\frac{\mathscr{D}_{O_2}[k_r(c^*)^{\alpha_1}\text{sulfite}^{\alpha_2}]}{c^* - c}\right]^{1/2} \tag{8.23}$$

An illustrative example of Danckwerts' considers an experiment using $10^{-5}\,M$ cobalt catalyst (known to give $\alpha_1 = 2$) and sufficient sulfite (say 0.5 M) for α_2 to be 0. For $c \ll c^*$, the above inequality becomes

$$k_l > [\mathscr{D}_{O_2} k_r c^*]^{1/2} \tag{8.24}$$

Taking $\mathscr{D}_{O_2} = 1.6 \times 10^{-5}\,\text{cm}^2/\text{s}$, k_r for cobalt catalyst $= 0.85 \times 10^8\,\text{cm}^3/(\text{g mol} \cdot \text{s})$, $c^* = 1.35 \times 10^{-7}\,\text{g mol/cm}^3$ gives

$$k_l \gg 0.01\,\text{cm/s}$$

A less effective catalyst (smaller k_r) would reduce the right-hand side.

Reference to the correlations to be presented later in this section indicates that for large bubbles in water, $k_l \sim 0.04\,\text{cm/s}$, and for small bubbles $k_l \sim 0.01\,\text{cm/s}$. Thus this inequality places a minimum size on the bubbles which may be used for such an interpretation. Smaller bubbles rising more slowly will have an appreciable reaction rate in the adhering fluid film under these specific conditions. Similarly, larger bubbles in media more viscous than water will exhibit reduced mass-transfer coefficients. However, an enhancement factor E to account for film reaction can be calculated provided the reaction-rate constant and reaction order are known [3–5].

A closing series of caveats for sulfite oxidation is illuminating: the rate constant k_r depends on (1) the catalyst and its concentration, (2) the ionic strength of the solution, (3) the presence of catalytic impurities, and (4) the solution pH; for example, in 10^{-5} M cobalt, k_r increases by a factor of 10 between pH 7.50 and 8.50 at 20°C. (The overall reaction generates H^+, so that base must be added to maintain pH constant).

In spite of these difficulties, the literature contains examples of reactors where $k_l a'$ determined from sulfite measurements for a given sparger, stirring rate, etc., correlate closely with the $k_l a'$ values observed in an actual fermentation (counterexamples are also evident). Assuming that the configuration in Fig. 8.1 represents the bioreaction of interest, there is essentially no O_2 consumption in the bubble liquid-side film. Thus, any chemical measure of O_2 absorption attempting to simulate such cell broths must, inter alia, satisfy the fundamental inequality (8.19) above. On the other hand, if growing cells are concentrated in the bubble liquid-side film, a different model chemical reaction situation may be required.

We can measure oxygen transfer rates in several other ways. If the experimental system is strictly a batch operation, with no addition or removal of liquid or gas, $\bar{Q}_{O_2}$ is revealed by monitoring the gas volume or pressure changes with time. Also, as discussed in the next section, measurement of c_l aids in $k_l a'$ estimation.

When gas is continuously added to and removed from the liquid, we use the following O_2 mass balance on the gas phase to determine $\bar{Q}_{O_2}$:

$$\bar{Q}_{O_2} = [F_{g_{inlet}}(p_{O_2})_{inlet} - F_{g_{exit}}(p_{O_2})_{exit}]/VRT \tag{8.25}$$

Here F_g is the volumetric gas flow rate and p_{O_2} is the partial pressure of O_2. [What assumptions are necessary to justify Eq. (8.25)? Are they generally valid for bioreaction processes?]

We would like to use these $\bar{Q}_{O_2}$ values to determine $k_l a'$, but, as Eqs. (8.6) and (8.7) and the associated discussion reveal, this requires uniformity of conditions within the vessel, so that the local and average oxygen utilization rates are identical. Consequently, stirred vessels [Fig. 8.2*b*(2)] are frequently employed in laboratory mass-transfer studies for biological-reactor design.

When the problem of spatial uniformity has been resolved, $k_l a'$ can be extracted from Eq. (8.6) if c_l^* and c_l are known. The first of these is available from solubility data such as Table 8.1, and direct measurement of c_l is now feasible (even in pure microbial cultures) with the polarographic sterilizable oxygen electrode. The operating principles of this electrode, which produces a current proportional to local dissolved oxygen partial pressure, are described in Chap. 10. An additional method for $k_l a'$ estimation based on dynamic measurements with an oxygen electrode is also described in Chap. 10.

In many reactor configurations or processes of natural origin, the local oxygen transfer rate varies with position. If such variations occur in the vessel in which mass-transfer rates are measured, the observed vessel-averaged value of $k_l a'$ cannot properly be used effectively in scale-up, the process of transferring

laboratory scale results into large capacity units. Design methods for such scale-up are considered later in this chapter. Variations of dissolved O_2 within a "homogeneous" phase (bulk fluid, mold pellet, microbial films, etc.) have been examined with miniaturized oxygen probes, the sensing head being of the order of 10 micrometers in diameter. Applications of this instrument include study of local oxygen profiles in mold pellets and the determination of diffusion coefficients in microbial aggregates.

8.3 MASS TRANSFER FOR FREELY RISING OR FALLING BODIES

The rate of material exchange between different regions is governed by the equations of change which describe conservation of mass, conservation of species (such as oxygen), and the momentum balance. When the equations of change are rendered dimensionless in distance, velocity, and concentrations for situations where the density difference between the two contacting phases provides the major driving force for fluid motion, three dimensionless parameters appear in the final expressions. These are the Grashof, Sherwood, and Schmidt numbers, which, for mass transfer, are defined by

$$\text{Grashof number} = \text{Gr} = \frac{D^3 \rho_l (\rho_l - \rho_g) g}{\mu_l^2} \tag{8.26a}$$

$$\text{Sherwood number} = \text{Sh} = \frac{k_l D}{\mathscr{D}_{O_2}} \tag{8.26b}$$

$$\text{Schmidt number} = \text{Sc} = \frac{\mu_l}{\rho_l \mathscr{D}_{O_2}} \tag{8.26c}$$

where D is a characteristic dimension and μ_l is the viscosity of the continuous phase. Consequently, we expect mass-transfer-coefficient correlations for such convective motion to involve only these three groups.

8.3.1 Mass-Transfer Coefficients for Bubbles and Bubble Swarms

The mass-transfer coefficient for a bubble, for example, is the proportionality constant between the total bubble flux and the overall driving force, $c_l^* - c_l$. The local flux at the gas–liquid surface is $-\mathscr{D}_{O_2}(\partial c/\partial z)_{z=0}$ (valid for low mass-transfer rates), where z is the coordinate measured into the liquid phase. Thus,

$$k_l = \frac{-1}{c_l^* - c_l} \mathscr{D}_{O_2} \left.\frac{\partial c}{\partial z}\right|_{z=0} \tag{8.27}$$

or, nondimensionally,

$$\text{Sh} = \frac{k_l D}{\mathscr{D}_{O_2}} = \frac{-1}{1 - \bar{c}_l} \left(\frac{\partial \bar{c}}{\partial \bar{z}}\right)_{\bar{z}=0} \tag{8.28}$$

Near the gas–liquid interface, the dimensionless concentration $\bar{c}$ has a solution from the transport equations of the form

$$\bar{c} = f(\bar{z}, \text{Sh}, \text{Sc}, \text{Gr}) \tag{8.29}$$

Using this expression to evaluate the derivative $(\partial\bar{c}/\partial\bar{z})_{\bar{z}=0}$ in Eq. (8.28), which is possible in principle, leaves the desired mass-transfer coefficient k_l in the form of the Sherwood number

$$\text{Sh} = \frac{k_l D}{\mathscr{D}_{O_2}} = g(\text{Sc}, \text{Gr}) \tag{8.30}$$

Thus, the dimensionless mass-transfer coefficient Sh is a function of only the two parameters Sc and Gr. Here D denotes characteristic bubble diameter.

Correlations for mass-transfer coefficients for falling or rising bubbles, droplets, or solids have appeared in the literature using other dimensionless groups such as the Reynolds number ($\text{Re} = \rho_l D u/\mu_l$) or the Peclet number ($\text{Pe} = uD/\mathscr{D}_{O_2}$). The velocity u applied here is the velocity of the gas bubble relative to the liquid velocity. In both instances, when an expression for the characteristic velocity u in terms of the density difference $\Delta\rho = (\rho_l - \rho_g)$ is substituted, the final result depends only on Gr and Sc according to Eq. (8.30).

Mass transfer from an isolated sphere with a rigid interface, a reasonable approximation to small bubbles in a fermentation broth containing surface-active agents, may be determined theoretically for the case $\text{Re} = \rho_l D u/\mu_l \ll 1$ and $\text{Pe} \equiv uD/\mathscr{D}_{O_2} \gg 1$. (Thus $uD/\mathscr{D}_{O_2} \gg 1 \gg \rho_l D u/\mu_l$, which implies that $\mu_l/\rho_l\mathscr{D}_{O_2} = \text{Sc} \gg 1$. Is the converse true?) In aqueous liquids, since the kinematic viscosity $\nu = \mu_l/\rho_l$ is about 10^{-2} cm^2/s and $\mathscr{D}_{O_2}$ is of the order of 10^{-5} cm^2/s, the Schmidt number is typically of the order of 10^3. Consequently, for Re of the order of 10^{-1}–10^{-2}, the theoretical result of Eq. (8.31) applies.

$$\text{Sh} = 1.01\ \text{Pe}^{1/3} = 1.01(uD/\mathscr{D}_{O_2})^{1/3} \tag{8.31}$$

For small Reynolds numbers for which this prediction applies, the terminal velocity u_t of a sphere is given by

$$u_t = \frac{D^2 \Delta\rho\, g}{18\mu_l} \tag{8.32}$$

Replacing u in Eq. (8.31) with u_t from Eq. (8.32) gives

$$\text{Sh} = 1.01\left(\frac{D^3\,\Delta\rho\, g}{18\mu_l\mathscr{D}_{O_2}}\right)^{1/3} = 1.01\left(\frac{D^3\rho_l\Delta\rho\, g}{18\mu_l^2}\right)^{1/3}\left(\frac{\mu_l}{\rho_l\mathscr{D}_{O_2}}\right)^{1/3} = 0.39\ \text{Gr}^{1/3}\text{Sc}^{1/3} \tag{8.33}$$

[The grouping $(D^3\ \Delta\rho\ g)/\mu_l\mathscr{D}_{O_2}$ is also known as the Rayleigh number Ra.] Notice here that $\text{Sh} = f(\text{Gr}, \text{Sc})$, as expected.

For a larger Reynolds number, the single-bubble result for a noncirculating sphere in laminar flow is

$$\text{Sh} = 2.0 + 0.60\ \text{Re}^{1/2}\text{Sc}^{1/3} \qquad \text{Re} \gg 1 \tag{8.34}$$

Note that Sh varies as the square root rather than the cube root of the velocity, indicating that a different hydrodynamic regime is present. Again, replacement of u by an appropriate terminal velocity expression will yield $\text{Sh} = f(\text{Gr}, \text{Sc})$.

In many industrial air-sparged reactors (Fig. 8.2 configurations), air bubbles are produced in swarms or clusters of sufficient intimacy that single isolated-bubble hydrodynamics and mass-transfer results fail to describe fluid motion and mass transport accurately in the vicinity of the gas–liquid interface. Calderbank and Moo-Young [10] report that two correlations are sufficient to describe their data for absorption of sparingly soluble gases into liquids which consume the gas chemically. Two distinct regimes of bubble-swarm mass-transfer are evident, the division between them being indicated by a critical bubble diameter D_c. In the absence of surfactants $D_c \approx 2.5$ mm. Bubbles larger than this are typically encountered with pure water in agitated tanks and in sieve-plate columns. Smaller bubbles are frequently found in sintered-plate columns and in agitated vessels containing hydrophilic solutes in aqueous solution.

For $D < D_c = 2.5$ mm

$$\text{Sh} = \frac{k_l D}{\mathscr{D}_{O_2}} = 0.31\ \text{Gr}^{1/3}\text{Sc}^{1/3} = 0.31\ \text{Ra}^{1/3} \tag{8.35}$$

For $D > D_c = 2.5$ mm

$$\text{Sh} = \frac{k_l D}{\mathscr{D}_{O_2}} = 0.42\ \text{Gr}^{1/3}\text{Sc}^{1/2} \tag{8.36}$$

Thus Eqs. (8.33) and (8.35) indicate that in bubble swarms, the mass-transfer coefficient for the same Schmidt and Grashof numbers is reduced about 20 percent compared with the isolated single-bubble case with an immobile surface. Equation (8.36) has also been verified for air-lift operation, Fig. 8.2*a*, using a coefficient of 0.50 rather than 0.42.

The change of Schmidt number exponent in Eq. (8.36) indicates a changed hydrodynamic regime from Eq. (8.35). For Newtonian fluids, i.e., viscosity = constant, independent of shear rate due to stirring speed, bubble velocity, etc., the transition from the $D < D_c$ region to the $D > D_c$ regime is accompanied by a change of bubble shape from nearly spherical (small bubbles) to hemispheric and caplike shapes. For further discussion of bubble hydrodynamics in these swarms, see Ref. [10]. The transition value of D varies with surfactant; values as high as 7.0 mm have been reported. In some non-Newtonian fluids, which will be discussed further later, transition with D is much more gradual than the abrupt change observed for Newtonian fluids.

Mass-transfer results for small particles show that as the density difference $\Delta\rho$ diminishes, the Sherwood number approaches 2.0 as a lower limit. For individual cells, clumps, flocs, etc., as well as for gas oil or other hydrocarbon dispersions, a more accurate form of the Sherwood number is

$$\text{Sh} = \frac{k_l D}{\mathscr{D}_{O_2}} = 2.0 + 0.31\ \text{Ra}^{1/3} \tag{8.37}$$

or

$$\frac{k_l}{\mathscr{D}_{O_2}} = \frac{2.0}{D} + 0.31\left[\frac{\Delta\rho\, g}{\mu_l \mathscr{D}_{O_2}}\right]^{1/3} \tag{8.38}$$

Thus the relative importance of the pure-diffusion result ($\Delta\rho \equiv 0$, $k_l = 2.0\mathscr{D}_{O_2}/D$) vs. the buoyancy term diminishes as particle size increases. For an isolated cell, $2\mathscr{D}_{O_2}/D$ is of the order of 10^{-1} cm/s compared with 10^{-2} cm/s for the Raleigh number term; the mass transfer near its surface therefore resembles that for a sphere in a more or less stagnant medium. Larger diameters due to flocs, films, etc., lead to greater relative contributions from the second term.

8.3.2 Estimation of Dispersed Phase Interfacial Area and Holdup

Having evaluated k_l from the appropriate previous formulas, we still must determine the interfacial area a' per unit volume. The value of a' can be estimated from sparger orifice diameter, overall reactor information, or photographic data, among other means. If bubble residence time in the reactor is t_b, volumetric flow rate per orifice is F_0, and total number of (equal) orifices is n, then the interfacial area per unit volume a' (neglecting coalescence and change of D with hydrostatic head or absorption) is given by

$$a' = \frac{1}{\text{volume}}\, nF_0 t_b \frac{\pi D^2}{\pi D^3/6} = \frac{nF_0 t_b}{V}\frac{6}{D} \tag{8.39}$$

In the following discussion, then, we consider the factors which appear on the right-hand side of Eq. (8.39). In particular, we will examine in detail the physical processes which determine bubble size. Based on these, we will explore the feasibility of predicting bubble size as a function of operating conditions, contactor design, and fluid properties. While introduced here in the context of rising bubbles and bubble swarms, many of the concepts described are also central in determining transport properties in vessels with mechanical agitation.

There are three main factors which interact to determine the size of bubbles in bioreactors (similar comments apply also to dispersion of a sparingly soluble second liquid phase). These are bubble formation, bubble breakup, and bubble coalescence. Bubble formation is dictated by instabilities in the gas stream entering the liquid phase which result in this stream breaking into discrete bubbles rather than flowing through the vessel as a continuous stream. Bubble breakup depends on the competition between surface tension, which stabilizes the bubble, and local fluid forces, which tend to tear the bubble apart.

The probability of bubble coalescence depends on the properties of the gas-liquid interface. In the predominantly aqueous mixtures commonly encountered in bioprocessing, coalescence properties are determined primarily by liquid phase solutes such as fatty acids, polyalcohols, electrolytes, and ketones. Addition of these components suppresses coalescence. In subsequent discussions, it will be useful to consider two limiting cases: coalescing dispersions (e.g., air–pure water) and noncoalescing dispersions (e.g., air–water with electrolyte).

Let us first consider the process of bubble formation as gas flows at volumetric flow rate F_0 through a single orifice of diameter d. The diameter of the initially formed bubble will be denoted D_0. Two regimes can be identified. At low gas flow rates, bubbles form one at a time at the orifice. The simplest analysis of this situation is based on a force balance for a bubble leaving an orifice. Bubble departure occurs when the buoyant force $(\pi D_0^3\, \Delta\rho\, g)/6$ equals the restraining force $\pi\sigma d$:

$$\frac{g\,\Delta\rho\, D_0^3}{\sigma d} = 6 \tag{8.40}$$

More elaborated theories are summarized in Ref. [21].

At some critical gas flow rate F_0^*, there is a transition from departure of single gas bubbles from the orifice to appearance of a gas jet at the orifice. Precise predictions are not presently possible, but this critical gas flow rate falls in the range indicated by

$$\sqrt{\frac{2\pi^2\sigma d^3}{16\rho_g}} \le F_0^* \le 20.4\,\frac{\sigma}{\rho_l}\sqrt{\frac{d}{g}}\ (\text{cm}^3/s) \tag{8.41}$$

At gas flow rates greater than F_0^*, initial bubble formation occurs by breakup of the gas jet due to instability of the interface. Based on stability theory developed first by Rayleigh, the expected bubble diameter for gas jet breakup in laminar liquid flow is approximately

$$D_0 = d(12\pi/0.485)^{1/3} = 4.27d \tag{8.42}$$

provided [21]

$$\frac{\sigma\rho_l d}{\mu_l} > 36 \tag{8.43}$$

This inequality is usually satisfied under bioprocess conditions.

For sparging into viscous broths, liquid viscosity rather than bubble surface tension provides the predominant resistance to new bubble formation. Where the bubbles are formed, the ratio of bubble to sparger orifice diameter, (D/d), is given by

$$\left(\frac{D}{d}\right) = 3.23\ \text{Re}_0^{-0.1}\ \text{Fr}_0^{0.21} \tag{8.44}$$

where the orifice Reynolds and Froude numbers are given by Eqs. (8.45) and (8.46):

$$\text{Re}_0 = \frac{4\rho_c F_0^*}{\pi\mu_l d} \tag{8.45}$$

$$\text{Fr}_0 = \frac{(F_0^*)^2}{d^5 \cdot g} \tag{8.46}$$

In some circumstances, the bubbles found in the gas–liquid dispersion are smaller than those formed at the gas distributor. This occurs because of instability of bubbles under the forces applied on the bubbles by the moving continuous phase. For a dispersed liquid or gas phase in a continuous liquid phase, the maximum size of dispersed-phase diameters for either freely rising (falling) or agitated configurations is due to a balance of opposing forces:

1. The dynamic pressure τ (the sum of shearing and normal stress differences) tends to draw out the droplets into shapes which eventually disintegrate into smaller pieces; this subdivision process is resisted by the following two forces.
2. The surface-tension forces σ/D of the particle tend to restore the droplet to spherical shape (minimum surface-energy configuration).
3. The viscous resistance of the dispersed phase to deformation is proportional to the term $\mu_d D^{-1}\sqrt{\tau/\rho_d}$, where subscript d indicates a dispersed-phase property.

In gas–liquid systems, term 3 will be negligible compared with term 2. In liquid–liquid contactors the last term should be relatively larger, but a later result of Example 9.2 indicates again that the forces in term 2 appear to predominate even for these all-liquid systems.

The last two restoring forces diminish as $D^{-\beta}$, where β is a positive number. Thus, at some critical diameter D_c, the dynamic pressure will override the two countering resistances and rearrange the bubble or droplet into smaller portions. At the critical diameter, evidently the following equality holds:

$$m_1 \frac{\sigma}{D} + m_2 \cdot \mu_d D^{-1}\left[\frac{\tau}{\rho_d}\right]^{1/2} = \tau \tag{8.47}$$

where m_1 and m_2 are constants.

If the surface-tension forces are much more significant than the viscous forces, as argued, then at the critical bubble size

$$m_1 \frac{\sigma}{D_c} = \tau \quad \text{or} \quad m_1 = \tau \frac{D_c}{\sigma} \quad \text{or} \quad D_c = \frac{m_1 \sigma}{\tau} \tag{8.48}$$

Equation (8.48) states that the maximum stable bubble size is a dimensionless constant (m_1) times surface tension divided by dynamic pressure. Thus, with greater dynamic pressure, increasingly smaller bubbles will be broken up.

Theoretical relations or correlations describing the relationship between the maximum stable bubble (or drop) size and fluid and flow properties typically employ a dimensionless group based on the form of Eq. (8.48). The Weber number We is defined by

$$\mathrm{We} = \tau \frac{D}{\sigma} \tag{8.49}$$

The *critical* Weber number We_c is the value of We for $D = D_c$ which, according to Eq. (8.48), is a characteristic constant. Experiments for clean air–water systems and theoretical calculations indicate that We_c is approximately unity (actually 1.05).

In order to calculate the maximum stable bubble size using these concepts, we need to determine a suitable value of the dynamic pressure τ for different flow situations. For freely rising bubbles, τ is given by

$$\tau = \frac{\rho_l u_t^2}{2} \tag{8.50}$$

where u_t is the bubble terminal velocity, given by Eq. (8.32) for spherical bubbles. In a complicated turbulent flow, estimation of the dynamic pressure is difficult. Turbulence is expected in bubble columns, for example, near aeration nozzles. Faced with this problem, we now consider some general concepts in turbulence which will be useful in several contexts which follow.

In the statistical theory of turbulence formulated by Kolmogorov and others, the turbulent flow field is regarded as a collection of superposed eddies or velocity fluctuations characterized by their fluctuation frequency (or length scale) and magnitude. The largest vortex elements or primary eddies have the scale of the main flow. These largest eddies are unstable and disintegrate into smaller eddies which are unstable and disintegrate into still smaller eddies and so on. Kinetic energy flows through this cascade from largest eddies to the smallest eddies until ultimately this energy is dissipated as heat. As the energy is transferred through this cascade, the directional character of the primary eddies, which depends on the geometry of the vessel, entering jets, mixers, and the like, decays. Kolmogorov's theory asserts that the smaller eddies are statistically independent of the primary eddies and are locally isotropic (spatially uniform). The smallest vortices which dissipate the turbulence energy have length scale λ_0 given by

$$\lambda_0 = \frac{\mu_l^{3/4}}{\rho_l^{1/2}}\left(\frac{P}{V_l}\right) \tag{8.51}$$

where P/V_l is the power input per unit volume.

In examining the effects of turbulence, we commonly use time-averaged quantities. The rms velocity $u_{\mathrm{rms}} \equiv \langle u^2(t)\rangle^{1/2}$ ($\langle\ \rangle$ denotes time averaging over the instantaneous velocity fluctuations) reflects the typical average magnitude of the local velocity variations. For length scales l much smaller than the scale of the primary eddies and much greater than λ_0, the rms velocity of vortices with characteristic size l is given by

$$u_{\mathrm{rms}}\Big|_{\text{eddies of scale } l} = \alpha\left(\frac{P}{V_l}\right)^{1/3}\left(\frac{l}{\rho_l}\right)^{1/3} \tag{8.52}$$

where α is a constant.

Returning now to a suitable choice of dynamic pressure for use in the Weber number in turbulent flows, we can use

$$\tau = \rho_l \left(u_{\text{rms}} \Big|_{\substack{\text{eddies of} \\ \text{scale } D_c}} \right)^2 \tag{8.53}$$

since this gives a measure of the turbulent shear stress which acts on a bubble of size D_c. Combining Eqs. (8.49), (8.52), and (8.53), we obtain

$$D_c = \alpha' \frac{\sigma^{0.6}}{(P/V_l)^{0.4} \rho_l^{0.2}} \tag{8.54}$$

where α' is a constant. Thus, the maximum stable bubble size is reduced if the power dissipation per unit volume is increased.

It is significant that, according to the theory of isotropic turbulence, the power input per unit volume is a key parameter in determining the scales of eddies obtained and the intensity of turbulent velocity fluctuations of length scales comparable to bubble and drop sizes. Local isotropic turbulence is an idealized situation not always obtained in practice; however, it is important to remember this physical view of the mechanism by which energy input to a process in the form of gas compression or mechanical agitation is ultimately transmitted to bubbles, drops, flocs, and mycelial pellets. Furthermore, Eqs. (8.52) and (8.54) above prepare us well to expect important effects of P/V_l on mass transfer coefficients in sparged towers and agitated tanks. Another important aspect of this theory deserves special emphasis: what matters is the local energy dissipated per unit volume, regardless of the means by which that energy is delivered to the mixture (for example injection of compressed gas versus mechanical mixing, one impeller or two, etc.). Again, this is an idealization, but it is one that is consistent with experimental observations in some cases.

Having considered coalescence, bubble formation, and bubble breakup separately, let us now examine the different possible outcomes of interaction of these processes in a sparged column. First we shall suppose that bubble (or droplet) coalescence is slow in the two-phase dispersion considered. If the initial bubble diameter D_0 is less than the maximum stable bubble diameter D_c evaluated under conditions of greatest dynamic pressure (typically in the region of bubble formation in a sparged column), the characteristic bubble diameter is D_0 (Table 8.3). If D_0 exceeds this maximum stable diameter, bubble breakup tending toward a characteristic diameter equal to D_c is expected.

On the other hand, if coalescence occurs rapidly, bubbles initially formed will coalesce and grow in size until they exceed the maximum stable bubble size after which breakup occurs. In this case, except in the region of the sparger, the initial bubble size D_0 has little influence on bubble size in the vessel. Remembering that turbulent velocity fluctuations generally vary from point to point in the vessel so that D_c does also, the coalescing system is characterized by a tendency at each point toward local coalescence-breakup equilibrium with characteristic bubble size given by D_c.

Table 8.3 Characteristic bubble diameter D depends on bubble coalescence properties and on the relationship between bubble diameter at formation (D_0) and the maximum stable bubble diameter (D_c)

Condition	Noncoalescing	Coalescing
$D_0 < D_c$	$D \sim D_0$	Transition toward dispersion equilibrium
$D_0 > D_c$	$D \sim D_c \Big\vert_{\substack{\text{sparger} \\ \text{(stirrer)}}}$	$D \sim D_c \Big\vert_{\text{local}}$

These observations have important implications for equipment design. In a noncoalescing system, energy dissipated for gas dispersion is most efficiently expended at the point of initial bubble formation and dispersion. Uniform dissipation of energy for dispersion is best when coalescence is important. These facts have motivated invention, characterization, and application of many alternative contacting and mixing configurations for bioreactors as we shall see in Chap. 9. These points and other related qualitative ones may be at present the most practically useful results from the preceding discussion of mechanisms. In fact, spatial inhomogeneities in flow patterns, turbulence properties, and gas/liquid volume fractions are so complicated in most situations that quantitative prediction is difficult, requiring recourse to correlations to obtain useful numbers. Armed with the physical insight just gained, however, we now should be alert to check the basis for various correlations before applying them. A correlation based on data from a clean air–water, and hence coalescing system, will likely have little relevance for a process containing a relatively noncoalescent two-phase mixture.

Returning now to the factors in Eq. (8.39) which determine interfacial area per unit volume a', we consider the bubble residence time t_b. This time may be estimated from the bubble rise velocity integrated over the reactor height h_r

$$t_b = \int_0^{h_r} \frac{dz}{u_b(z)} \approx \frac{h_r}{u_t} \tag{8.55}$$

where in the approximate expression on the right-hand side the bubble rise velocity has been taken to be the bubble terminal velocity. For isolated small bubbles at small Reynolds numbers the terminal velocity given in Eq. (8.32) can be used. In the case of large, spherical-cap shaped bubbles (diameter D) in Newtonian fluids, the terminal rise velocity to be used in these calculations is

$$u_t = 0.711(gD)^{1/2} = 22.26\sqrt{D} \quad \text{cm/s} \tag{8.56}$$

For bubble clouds or swarms, calculation of the characteristic bubble rise velocity is more difficult, since neighboring bubbles influence each other's motion

and since bubble coalescence and breakup may occur. As a crude approximation, comparison of Eqs. (8.33) and (8.35) suggests that for identical Sc and Sh,

$$\left[\frac{u_t\ (\text{bubble cloud})}{u_t\ (\text{single bubble})}\right]^{1.3} = \frac{0.31}{0.39} \tag{8.57}$$

so that

$$u_t\ (\text{bubble cloud}) \approx 0.50 u_t\ (\text{single bubble}) \tag{8.58}$$

Any real dispersion will generally contain a distribution of bubble sizes. This raises the question of suitable definition of a characteristic or mean size. The value of D for Eqs. (8.35) to (8.38) is the surface-averaged, or Sauter mean bubble diameter D_{sm}:

$$D_{sm} = \frac{\sum m_j D_j^3}{\sum m_j D_j^2} \tag{8.59}$$

where m_j is the number of bubbles of diameter D_j.

The quantity $nV_b t_b$ in Eq. (8.39) is the total bubble volume in the reactor. The bubble volume per reactor volume is known as the holdup H (volume gas per volume reactor). If the holdup value is available from other laboratory, plant, or literature correlations (Example 8.1), it is used directly in

$$a = H\frac{6}{D} \tag{8.60}$$

When writing mass balances on the liquid phase volume only, it was convenient to define an interfacial area per *liquid volume*, a', as in Eqs. (8.14) and (8.15). A second common quantity is a, the interfacial area per (liquid + gas) volume. These two interfacial measures are related through the holdup H:

$$a'(1 - H) = a \tag{8.61}$$

Thus, in using correlations for mass transfer, care must be taken to note whether the original reference calculated $k_L a$ or $k_L a'$.

Example 8.1 Holdup correlations

Bubble column[1]

$$H/(1 - H)^4 = 0.20(\text{Bo})^{1.8}(\text{Ga})^{1.12}\text{Fr} \tag{8E1.1}$$

where Bo Bond no. $gd_t^2\rho_L/\sigma$
Ga Galileo no. $gd_t^3\rho_L^2/\mu_L^2$
Fr Froude no. $u_G/\sqrt{gd_t}$
u_G gas superficial velocity
d_t tower (tank) diameter

[1] M. Chakravarty, S. Begum, H. D. Singh, J. N. Baruah, and M. S. Iyengar, *Biotech. Bioeng. Symp.*, 4: 363, 1973.

Laboratory-scale gas-lift column[1] Holdup interior to draft tube (sparged):

$$H_1 = \left[(\mu_L/\mu_{H_2O})^{2.5} + 1.61\frac{73.3}{74.1}\frac{\sigma}{\sigma}\right]10^{-4}u^{0.88} \tag{8E1.2}$$

Holdup in annulus:

$$H_2 = 1.23 \times 10^{-2}\left[\frac{74.2}{79.3}\frac{\sigma}{\sigma}\right]u_G^{0.45}\left[\frac{A_{int}}{A_{ann}}\right]^{1.08}\mu_L^{1.38} \tag{8E1.3}$$

Holdup above baffle:

$$H_3 = 7.5 \times 10^{-3}u^{0.88} \tag{8E1.4}$$

Total column holdup:

$$H = 0.003u^{0.88}$$

where μ_L liquid viscosity at column temperature (cP)
μ_{H_2O} water viscosity at column temperature (cP)
σ gas-liquid surface tension (dyne/cm)
u superficial gas velocity (cm/s)
A_{int} cross-sectional area of draft tube (cm^2)
A_{ann} cross-sectional area of annulus (cm^2)

Laboratory-scale gas-lift column[1] in draft tube:

$$H_d = \frac{u_d}{1.065u_d + u_t} \quad \text{void fraction} \tag{8E1.5}$$

where u_d is the superficial gas velocity in draft tube and, using volumetric flows,

$$j = \frac{\text{gas flow rate}}{\text{gas + liquid flow rate}}$$

$$u_t = \begin{cases} 32\ \text{cm/s} & j < 0.43 \\ 257(j - 0.43) + 32 & j > 0.43 \end{cases}$$

Aerated tank[2] diameter ≈ height for $\text{Re}_i^{0.7}(N_i D_i^2/\nu)^{0.3} > 2 \times 10^4$

$$H = \sqrt{\frac{u}{u_t}}\,H + 0.015a_{to} \quad \text{and} \quad a_{to} = 1.44\frac{P^{0.4}\rho^{0.2}}{\sigma^{0.6}}\left(\frac{u}{u_t}\right)^{1.2}$$

For $\text{Re}_i^{0.7}(N_i D_i^2/\nu)^{0.3} < 2 \times 10^4$

$$H = \frac{a_t}{a_{to}}\sqrt{\frac{u}{u_t}}\,H + 0.015a_t$$

and

$$\log\frac{2.3a_t}{a_{to}} = 1.95 \times 10^{-5}\,\text{Re}_i^{0.7}\left(\frac{N_i D_i^2}{u}\right)^{0.3}$$

[1] M. Chakravarty, S. Begum, H. D. Singh, J. N. Barrah, and M. S. Iyengar, *Biotech. Bioeng. Symp.* 4: 373, 1973.
[2] R. T. Hatch, Ph.D. Thesis in Food Science and Nutrition, p. 150, Massachusetts Institute of Technology, Cambridge, Mass., 1973.
[3] P. H. Calderbank, *Trans. Inst. Chem. Eng.*, **36**: 443 1958.

where a_0, a_i interfacial area per unit volume of broth
Re_i impeller Reynolds number $\rho N_i D_i^2/\mu_l$
u superficial gas velocity (empty-tank basis)
u_t bubble rise velocity

and N_i, D_i, P, ρ, σ are as in the text (see Sec. 8.4).

Agitated vessels[1] For air in water Richards' data can be represented by

$$\left(\frac{P}{V}\right)^{0.4} u^{1.2} = 7.63H + 2.37$$

where P horsepower (hp)
V ungassed liquid volume, m^3
u superficial velocity, m/h
H volume void fraction (valid for $0.02 < H < 0.2$)

8.4 FORCED CONVECTIVE MASS TRANSFER

Vigorous mechanical mixing of air–liquid dispersions is often necessary to obtain economic rates of biomass increase, substrate consumption, or product formation. The concerns of this section are again relationships between appropriate variables allowing estimation of mass-transfer coefficients k_l and/or a or a', the interfacial area per appropriate volume.

8.4.1 General Concepts and Key Dimensionless Groups

The functions served by mechanical agitation augment (and in some cases dominate) the influences of convection driven by freely rising or falling dispersed phases:

1. The high dynamic pressure near the impeller tip or other mixer devices produce small bubbles, thereby increasing a' locally. Provided that the rate of bubble coalescence is not correspondingly increased elsewhere in the vessel, the result is an increased value of the volumetric average value of a'.
2. The fermentation fluid may contain a suspension of solid or other liquid phases which may tend to rise or fall in the vessel. Mechanical mixing provides a more uniform volumetric dispersion of these phases in the bulk liquid. For hydrocarbon dispersions, k_l contains a term proportional to the cube root of the phase-density difference $(\rho_{\mathrm{H_2O}} - \rho_{\mathrm{HC}})^{1/3}$ [recall Eq. (8.38)]; the resulting small mass-transfer coefficient for hydrocarbon-substrate-limited fermentations is increased by agitation.
3. For gas bubbles of given size in vigorously agitated vessels, k_l does not vary significantly with power input since the relative gas or fluid velocity is dominated by density differences. (Why is this true?) The agitator turbulence, however, will decrease D and thus increase a' for a given holdup; note that this result will change the size of the bubbles and thus k_l through the influence of D.
4. The maximum size of loosely aggregated mycelia, microbial slimes, mold pellets, etc., may be diminished by agitation, thus maintaining a smaller microbial Thiele modulus (Sec. 4.4) and again rendering the vessel more uniformly mixed with respect to the liquid phase. Examples of decreased yields of desired products have been reported at relatively high agitation rates; these may be due to cellular or extracellular enzyme damage, mixing interference with morphological development and differentiation, etc.
5. The liquid-cell suspension may be so viscous that only mechanical agitation provides any degree of bulk-liquid mixing (considered further in Sec. 8.8).

[1] J. W. Richards, *Prog. Ind. Microbiol.*, 3: 143, 1961.

In forced convection, the action of the applied mechanical work produces some characteristic velocity against which other motions can be scaled. For impeller agitation, two scales exist: the rms fluid velocity fluctuation u_{rms}, and the impeller tip velocity u_i, which is proportional to $N_i D_i$, where N_i is the impeller rotation rate in revolutions per unit time, and D_i is the impeller diameter.

Reduction of the forced-convection balances for total mass, species, and momentum produces the following dimensionless groups using u_{rms} as the characteristic velocity:

$$\text{Sherwood number} = \mathrm{Sh} = \frac{k_l D}{\mathscr{D}_{\mathrm{O_2}}} \tag{8.62a}$$

$$\text{Schmidt number} = \mathrm{Sc} = \mu_l/\rho_l \mathscr{D}_{\mathrm{O_2}} \tag{8.62b}$$

$$\text{Reynolds number} = \mathrm{Re} = \rho_l D u_{\mathrm{rms}}/\mu_l \tag{8.62c}$$

$$\text{Froude number} = \mathrm{Fr} = u_{\mathrm{rms}}^2/gD \tag{8.62d}$$

Alternately, in stirred systems, the characteristic dimension may be taken as the impeller diameter D_i, and the reference velocity is $N_i D_i$. The subscripts i remind us that the scaling is to the impeller rather than the gas, liquid, or solid particles present in the dispersion. In this case, the appropriate Reynolds and Froude numbers are given by

$$\mathrm{Re}_i = \frac{\rho_l D_i}{\mu_l} N_i D_i = \frac{\rho_l N_i D_i^2}{\mu_l} \quad \text{and} \quad \mathrm{Fr}_i = \frac{N_i^2 D_i}{g} \tag{8.63}$$

The Froude number has received other definitions. For mass transfer into a suspension of "neutrally buoyant" particles, the following relationship has been suggested:

$$\mathrm{Fr}_L = \frac{N_i^2 D_i^2}{gL} \tag{8.64}$$

where L is the reactor height. As the Froude number represents the contribution of free-surface dynamics vs. mechanical mixing, the distance of the surface from

the tank bottom could logically enter in its description. When the stirred volume refers to the mixing of two phases (continuous and dispersed) of different densities, e.g., hydrocarbon droplets in aqueous phases, the following definition of a modified Froude number may be useful:

$$\mathrm{Fr}_{\text{two phase}} = \frac{\rho N_i^2 D_i^2}{\Delta\rho\, gL} \tag{8.65}$$

It is clear that close attention should be paid to both the form of correlations and the definitions of the groups involved in literature reports; a correlation should never be used or cited without careful group definitions.

8.4.2 Correlations for Mass-Transfer Coefficients and Interfacial Area

The mass-transfer coefficient of gases depends largely on the hydrodynamics of the liquid film near the bubble; this in turn is dominated by the natural convection buoyancy forces and the turbulent Reynolds number during most of the bubble residence time; thus correlations for freely rising bubbles are most usefully associated with the Reynolds number of Eq. (8.62*c*).

In sufficiently large reactors fitted with baffles to maximize mixing rates within the continuous phase (Chap. 9), the influence of free-surface effects (Froude number) becomes unimportant. Free-surface gas exchange can be significant in bench-scale bioreactors, but this contribution fades to insignificance as reactor scale increases. In the absence of such surface influences, the dimensionless solutions for the velocity and concentration fields yield

$$\bar{c} = f(\bar{z}, \mathrm{Re}, \mathrm{Sc}, \mathrm{Sh}) \tag{8.66}$$

so that the dependence of the Sherwood number is

$$\mathrm{Sh} = \frac{k_l D}{\mathscr{D}_{O_2}} = g(\mathrm{Re}, \mathrm{Sc})$$

Data of Calderbank's [11] give the correlation

$$\mathrm{Sh}\ (\text{turbulent aeration}) = 0.13\,\mathrm{Sc}^{1/3}\mathrm{Re}^{3/4} \tag{8.67}$$

In terms of power input per unit reactor volume, using relation (8.52) we can show that the variation of $k_l(\mathrm{Sh})$ with P/V is

$$\mathrm{Sh} \propto \left(\frac{P}{V}\right)^{1/4} \tag{8.68}$$

Thus

$$k_l = 0.13\left(\frac{\alpha^3 \mu_l (P/V)}{\rho_l D}\right)^{1/4} \mathrm{Sc}^{-2/3} \tag{8.69}$$

Once turbulence has been achieved, so that the previous equation applies, the specific increase in k_l with P diminishes rapidly, as is seen by evaluation of

$$\frac{1}{k_l}\frac{dk_l}{dP} = \frac{1}{4P} \tag{8.70}$$

From the previous discussion of bubble breakup, we expect to be able to correlate the maximum stable bubble diameter D_c as a function of σ and the variables dominating dynamic stress. Since this value is closely related to the characteristic actual bubble diameter D_{sm} in many cases, it is not surprising that correlations for D_{sm} have a similar form. The inclusion of additional terms depending on the gas holdup H and dispersed phase viscosity μ_d in these correlations indicate important but not dominant contributions from other processes. The earlier caveat about comparing coalescence properties in the correlation basis experiment and the system of interest stands also in connection with the correlations in Example 8.2.

Example 8.2 Correlations for maximum (D_c) or Sauter mean (D_{sm}) bubble or droplet diameters

For freely rising bubbles, experimental values[†] are

$$D_c = \left(1.452 \times 10^{-2}\frac{\sigma}{\Delta\rho}\right)^{1/2} \quad \text{cm} \tag{8E2.1}$$

For agitated vessels, on a power-per-unit-volume basis we list the results of several experiments:

Experiment 1 liquid–liquid:[‡]

$$D_{sm} = 0.224\frac{\sigma^{0.6}}{\rho_l^{0.2}(P/V)^{0.4}} H^{0.5}\left(\frac{\mu_d}{\mu_c}\right)^{0.25} \tag{8E2.2}$$

Experiment 2 gas–liquid electrolyte:[‡]

$$D_{sm} = 2.25\frac{\sigma^{0.6}}{\rho_l^{0.2}(P/V)^{0.4}} H^{0.4}\left(\frac{\mu_g}{\mu_l}\right)^{0.25} \tag{8E2.3}$$

Experiment 3 gas in alcohol solutions:[¶]

$$D_{sm} = 1.90\frac{\sigma^{0.6}}{\rho_l^{0.2}(P/V)^{0.4}} H^{0.65}\left(\frac{\mu_g}{\mu_l}\right)^{0.25} \tag{8E2.4}$$

For gases in viscous liquids,[§]

$$D_{sm} = 0.7\frac{\sigma^{0.6}}{(P/V)^{0.4}\rho_l^{0.2}}\left(\frac{\mu_l}{\mu_g}\right)^{0.1} \tag{8E2.5}$$

[†] S. Hu and R. C. Kintner, "The Fall of Single Liquid Drops Through Water," *AIChE J.*, **1**: 42, 1955.

[‡] P. H. Calderbank, *Trans. Inst. Chem. Eng.*, **36**: 443, 1958.

[¶] J. A. McDonough, W. J. Tomme, and C. D. Holland, "Formulation of Interfacial Areas in Immiscible Liquids by Orifice Mixers," *AIChE J.*, **6**: 615, 1960.

[§] S. M. Bhavaraju, T. W. F. Russell, and H. W. Blanch, "Design of Gas Sparged Devices for Viscous Liquid Systems," *AIChE J.*, **24**: 454 (1978).

For agitated vessels, impeller variables [26]

$$\frac{P}{V} \approx \text{const}\,\frac{\rho_l N_i^3 D_i^5}{D_i^3} \qquad \text{for} \qquad \text{Re}_i \geq 10^4 \tag{8E2.6}$$

$$\frac{D_c}{D_i} = (\text{const})\left(\frac{\sigma}{N_i^2 D_i^3 \rho_l}\right)^{0.6} \tag{8E2.7}$$

For turbulent pipe flow [11]

$$\frac{D}{D_{\text{pipe}}} = (\text{const})(\text{We}_{\text{pipe}}^{-0.6}\text{Re}_{\text{pipe}}^{-0.1}) = (\text{const})\left(\frac{\sigma}{\rho_l \langle u^2\rangle D_{\text{pipe}}}\right)^{0.6} \cdot \left(\frac{\mu_l}{D_{\text{pipe}} u_{\text{rms}} \rho_l}\right)^{0.1} \tag{8E2.8}$$

where

$$\text{We}_{\text{pipe}} \equiv \left(\frac{\sigma}{\rho_l \langle u^2\rangle D_{\text{pipe}}}\right)^{-1} \qquad \text{and} \qquad \text{Re}_{\text{pipe}} = \frac{D_{\text{pipe}} u_{\text{rms}} \rho_l}{\mu_l} \tag{8E2.9}$$

For flow through an orifice in pipe flow (measured one foot downstream)†

$$\frac{D_{\text{pipe}}}{D} = 21.6\left(\frac{D_{\text{orifice}}}{D_{\text{pipe}}}\right)^{3.73} \text{H}^{0.121}\text{We}_{\text{pipe}}^{-0.722}\text{Re}_{\text{pipe}}^{-0.065} \tag{8E2.10}$$

where We_{pipe} and Re_{pipe} are as in Eq. (8E2.9).

Given D_c or D_{sm} and the holdup H, the value of a is calculated from Eq. (8.60). For complex situations like those applying to most of the macroscopic contactor situations in Fig. 8.2, H must be measured directly or obtained from correlations for similar configurations. A representative sampling of such correlations was given in Example 8.1.

8.5 OVERALL $k_l a'$ ESTIMATES AND POWER REQUIREMENTS FOR SPARGED AND AGITATED VESSELS

In this section we summarize different experimental findings on the volumetric mass transfer coefficient $k_l a'$. Experimental results are often reported in this form because of lack of knowledge of a' directly. Also, in some cases this combined parameter is used to account for other effects such as long residence times of small bubbles in highly viscous fermentations. These bubbles become depleted of oxygen and therefore contribute little to oxygen transfer. Thus, an optically determined a' value may not represent the interfacial area per unit volume of oxygen-containing bubbles.

We have already noted that increasing power input can reduce bubble size and thereby increase interfacial area. Here, we cite methods for calculating power input in terms of the gas sparging and agitation parameters. Also, we consider the common case of simultaneous gas sparging and mechanical agitation.

† J. A. McDonough, W. J. Tomme, and C. D. Holland, "Formulation of Interfacial Areas in Immiscible Liquids by Orifice Mixers," *AIChE J.*, 6: 615, 1960.

Many studies of gas-liquid mass transfer in low viscosity fluids in agitated vessels have been reviewed by Van't Riet [9]. Results of many experiments in many different vessels with different mixer configurations are all fit within 20 to 40 percent by the relationships

Stirred vessel, water, coalescing:

$$k_l a = 2.6 \times 10^{-2}\left(\frac{P}{V}\right)^{0.4} (u_{gs})^{0.5}\ (\text{s}^{-1}) \tag{8.71}$$

$$(V \leq 2600L;\ 500 < P/V < 10{,}000\ \text{W/m}^3)$$

Stirred vessel, water, noncoalescing:

$$k_l a = 2.0 \times 10^{-3}\left(\frac{P}{V}\right)^{0.7} (u_{gs})^{0.2}(\text{s}^{-1}) \tag{8.72}$$

$$(2 < V < 4400L;\ 500 < P/V < 10{,}000\ \text{W/m}^3)$$

Here u_{gs} is the superficial gas velocity which is equal to the gas feed volumetric flow rate divided by vessel cross section area times the gas holdup. The ranges of vessel volumes and volumetric power input considered in obtaining these correlations is indicated with each.

It is significant to note that, consistent with the concepts of turbulence discussed earlier, these correlations have been applied (within the indicated 20 to 40 percent) regardless of the type of stirrer (turbines, paddles, propellers, rods, self-inducing agitators) and the number of stirrers. Stirrer position also seems to be immaterial unless the stirrer is close to the bottom of the vessel (less than the stirrer diameter), which decreases dissipated power, or close to the surface, which results in air entrainment and lower power consumption.

Similar examination of mass transfer data from bubble columns shows:

Bubble column, water, coalescing:

$$k_l a = 0.32(u_{gs})^{0.7} \tag{8.73}$$

If noncoalescing conditions exist in a bubble column, no general correlation can be presented since sparger construction influences $k_l a'$.

As indications of the other types of correlations which have been proposed, and because *a priori* determination of power consumption or gas superficial velocity may not be simple, we summarize next several additional correlations. For gas transfer in a bubble column, Akita and Yoshida [12] reported

$$\frac{k_l(ad_t^2)}{D} = 0.6(\text{Sc})^{1/2}\text{Bo}^{0.62}\text{Ga}^{0.31}H^{1.1} \tag{8.74}$$

where the Bond number ($\text{Bo} \equiv gd_t^2\rho_c/\sigma$) and Galileo number ($\text{Ga} = gd_t^3/u_l^2$) are referred to the tower diameter d_t. This equation is found accurate for $d_t \leq 60$ cm, and also useful if, for $d_t > 60$ cm (0.6 m), the value of 0.6 m for d_t is used in Eq. (8.74).

In the same spirit, the volumetric mass transfer coefficient, $k_l a$, for an airlift column is given by Bello et al. [13] as Eq. (8.75)

$$k_l a = \frac{0.0005 \cdot (P/V)^{0.8}}{(1 + A_d/A_r)} \tag{8.75}$$

where A_d/A_r = ratio of areas of downcomer and riser sections and P/V = aeration power input/volume. This correlation is useful, but hides the fact that mass transfer, holdup, etc., are not the same in the riser headspace and downcomer portions of the air lift equipment.

All correlations have a limited range of applicability. For example, the strong dependence of $k_l a'$ on P/V indicated in Eq. (8.75) vanishes at sufficiently small P/V values ($P/V < 1$) since bubble fluid dynamics are here dominated by natural convection driven by bouyancy.

A motionless mixer may be used to subdivide and remix repeatedly the liquid phase, as well as to maintain the upward bubble flow and reduce or eliminate large bubbles or air "slugs." Wang and Fan [14] suggest the volumetric mass-transfer correlation

$$k_l a = 0.12 u_l^{0.624} \left(\frac{u_g}{1.99 u_g + 47.1} \right) (\mathrm{s}^{-1}) \tag{8.76}$$

where u_g, u_l are gas and liquid superficial velocities (cm/s).

A potential shortcoming of using any correlation is the frequent implicit assumption of uniformity of power dissipation and/or $k_l a'$ in the contactor in which data underlying the correlation was taken or in the vessel to be designed or analyzed. As an indication of potential difficulties in this connection, consider the variations in mean flow velocities measured in a standard agitated, baffled tank. The lines in Fig. 8.6 indicate circulation patterns and the numbers give local average velocities as a fraction of the impeller tip velocity.

Several studies of sparged column contactors vividly illustrate important spatial variations in $k_l a'$. Figure 8.7 shows experimental measurements of dissolved oxygen axial profiles in a bubble column and in a three phase fluidized bed containing particles of diameter 0.1 cm. In both cases, there is an entry zone near the sparger in which oxygen transfer rates are relatively large and a later zone of much smaller transfer rates. This may be due to a transition from bubble sizes dominated by sparger conditions to bubble sizes dictated by coalescence-breakup equilibrium. Other indicated points in Fig. 8.7 are calculated from a mathematical model which assumes plug flow of gas through the column through two zones with different volumetric mass-transfer coefficients for each zone. The interface between the two zones was estimated to be around 33 cm above the sparger. Decreasing $k_l a'$ values over the first 27.6 cm above the sparger, then constant $k_l a'$ were successfully employed in another model for a different bubble column contactor.

A clear pitfall exists here for scale-up. The entry region identified above will contribute significantly in small laboratory systems but will constitute only a small fraction of the vessel volume in a tall, large-scale column.

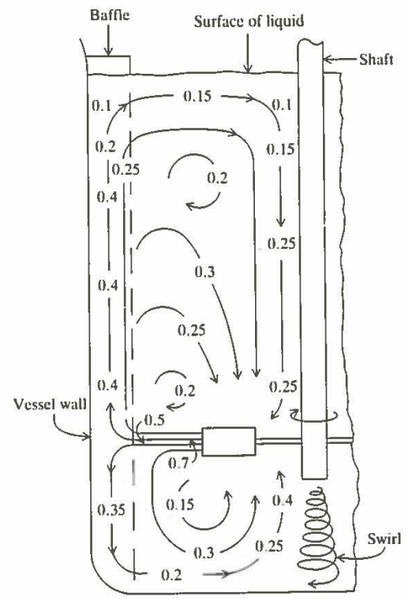

Figure 8.6 Average flow velocities (as fraction of impeller tip speed = 5.2 ft/s) and circulation patterns in water in a 12" high tank stirred at 200 rpm. *(W. L. McCabe and J. C. Smith, Unit Operations in Chem. Eng., 3d ed., 1976, p. 234, McGraw-Hill, New York.)*

Next we consider calculation of power requirements to achieve desired gas sparging and mechanical agitation rates. Our emphasis here is on important overall concepts and trends; more detailed treatments considering energy losses in process equipment components are available in the references. For gas sparging into a column, the power used in compression to sparge a gas volumetric flow rate F_0, at pressure p_1, is

$$P_g = \rho_g F_0 \left[\frac{RT}{(MW)} \ln \frac{p_1}{p_2} + \alpha \frac{u_0^2}{2} \right] \tag{8.77}$$

where p_2 is the pressure at the top of the vessel and u_0 is the gas velocity at sparger orifice. The fraction of gas kinetic energy transferred to the liquid, α, is typically about 0.06.

The power consumption for stirring nonaerated fluids depends upon fluid properties ρ_l and μ_l, the stirrer rotation rate N_i and diameter D_i, and the drag coefficient of the impeller C_{D_i}. The latter is expected to vary with impeller Reynolds number in a different manner for each flow regime: laminar, transition,

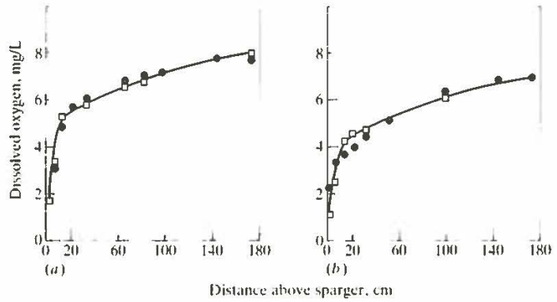

Figure 8.7 Experimental data (●) showing variation of dissolved oxygen content as a function of distance above the sparger for (*a*) a bubble column (u_l = 7.5 cm s^{-1}, u_g = 28 cm s^{-1}) and (*b*) a three-phase fluidized bed containing 0.1 cm diameter particles (u_l = 7.5 cm s^{-1}, u_g = 20 s^{-1}). The points (□) were calculated from a mathematical model. Lines drawn to show trends. *(Reprinted by permission from M. Alvarez Cuenca and M. A. Nerenberg, Adv. in Biotechnol. vol. 1, p. 477 (1980), M. Moo Young (ed.), Pergamon Press, p. 477.)*

or turbulent. A well-known study by Rushton, Costich, and Everett [26] is summarized in Fig. 8.8*a* for three impeller geometries. The data are plotted as a dimensionless power input, the power number P_{no}, vs. impeller Reynolds number Re_i:

$$P_{no} \equiv \frac{Pg}{\rho_l N_i^3 D_i^5} \tag{8.78}$$

In the turbulent regime, the power input is independent of Re_i,

$$P \propto N_i^3 D_i^5 \qquad P_{no} = \text{const}$$

whereas in laminar flow, the relation is more nearly given by

$$P \propto N_i^2 D_i^3 \qquad \text{or} \qquad P_{no} \propto \frac{1}{Re_i}$$

The proportionality constant in each case depends on the impeller geometry. It is interesting to note the strong similarity between this figure and the plot of the friction factor in tube flow. In the latter case, the friction factor varies as 1/Re in laminar flow (as does the power number vs. Re_i), and, in turbulent flow, f tends to a nearly constant value which has a larger magnitude for pipes with rough walls. Similarly, as the agitator geometry becomes less "smooth," Fig. 8.8*a*, the power number reaches a higher turbulent plateau value. The latter case is more complicated since the presence of the tank walls and baffles will also exert an effect on the measured power input P.

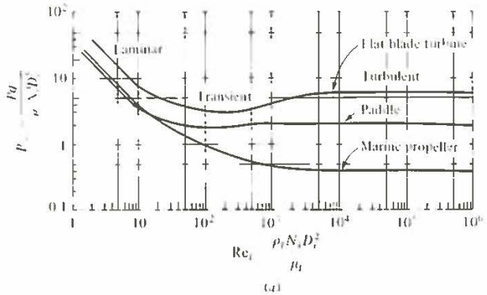

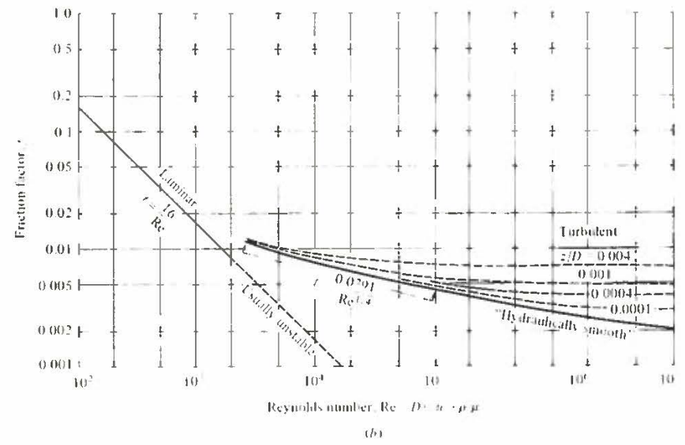

Figure 8.8 (*a*) Power number vs. Reynolds number (impeller) for various impeller geometries. (*b*) Pipe friction factor f vs. Reynolds number, Re. ε equals height of surface roughness peaks. *[(a) Reprinted from S. Aiba, A. E. Humphrey and N. F. Millis, "Biochemical Engineering" 2d ed., p. 174, Univ. Tokyo Press, Tokyo, 1973, modified from J. H. Rushton, E. W. Costich, and H. J. Everett, "Power Characteristics of Mixing Impellers, part 2," Chem. Eng. Prog., vol. 46, p. 467, 1950. (b) Reprinted by permission from W. L. McCabe and J. C. Smith "Unit Operations of Chemical Engineering" McGraw-Hill, New York, 1954 (original curves from L. F. Moody, Trans. ASME, vol. 66, p. 671, 1944).]*

When the agitated vessel is simultaneously aerated, the power requirements for agitation decrease. The ratio of power requirements in aerated vs. nonaerated vessels, P_a/P vs. a dimensionless aeration rate N_a

$$N_a = \frac{F_g}{N_i D_i^3} \tag{8.79}$$

(where F_g is volumetric gas rate) has been correlated, as shown in Fig. 8.9.

Except for the most rapidly changing part of the curve, these forms can be fitted to

$$\frac{P_a(N_a) - P_a(N_a = \infty)}{P - P_a(N_a = \infty)} = e^{-mN_a} \tag{8.80}$$

where m = const. An alternative form which is also useful in turbulent aeration of non-Newtonian fluids is due to Michel and Miller [28]:

$$P_a = m'\left(\frac{P^2 N_i D_i^3}{F_g^{0.56}}\right)^{0.45} = m'\left(\frac{P^2 (N_i D_i^3)^{0.44}}{N_a^{0.56}}\right)^{0.45} \tag{8.81}$$

where m' = const. In both the above correlations, P is the nonaerated power input of the earlier chapter formulas.

From the relations of the previous paragraph, at constant N_i and D_i, the power input diminishes with increased N_a, that is, increased air flow F_g. This effect appears partially due to the decrease in average density of the fluid being agitated. Uniformity of bulk mixing diminishes with increasing N_a.

In several bioreactor designs, mixing is provided by injection of a liquid jet into the vessel. In this case the power dissipation may be estimated from (see Ref. 29)

$$P = \frac{8\rho_l F_l^3}{\pi^2 D_j^{0.4}} \tag{8.82}$$

where D_j is the jet diameter.

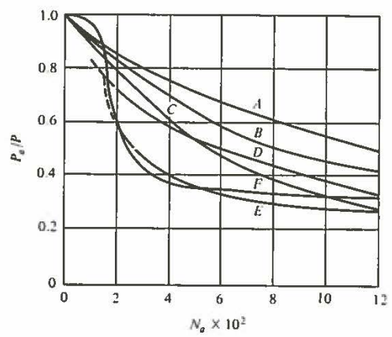

Figure 8.9 Ratio of power requirement for aerated vs. nonaerated systems as a function of N_a (see text): *A*, flat blade turbine (8 blades); *B*, vaned disc (8 vanes); *C*, vaned disc (6 vanes); *D*, vaned disc (16 vanes); *E*, vaned disc (4 vanes); *F*, paddle. *(Reprinted by permission from Y. Ohyama and K. Endoh, "Power Characteristics of Gas-Liquid Contacting Mixers," Chem. Eng., Japan, vol. 19, p. 2, 1955.)*

8.6 MASS TRANSFER ACROSS FREE SURFACES

Gas transfer through gas-liquid free surfaces (Fig. 8.10) plays a major role in oxygen supply and CO_2 removal from animal cell cultures. Surface mass transfer is also important in shake flask and small-scale stirred bioreactors for microbial cultivations. Transport across free liquid surfaces is essential for stream reaeration and respiration of aerobic life near the sea surface and in lake communities. Free-surface mass transfer is also important in many industrial microbial processes employing trickle-bed reactors, e.g., wine-vinegar manufacture and wastewater treatment. In the former cases, the depth of oxygen transfer depends on the scale of eddy motions near the liquid surface. Mass transfer into or out of falling-liquid films has been studied frequently, though not often under conditions appropriate to microbial processes. This circumstance is considered first.

The area-integrated absorption rate for a falling laminar liquid film of thickness h, length L, and width W and with zero initial concentration of dissolved gas is given by

$$\text{Integrated absorption rate (moles/unit time)} = WLc_i^*\left(\frac{4\mathscr{D}_{O_2} u_{max}}{\pi L}\right)^{1/2} \tag{8.83}$$

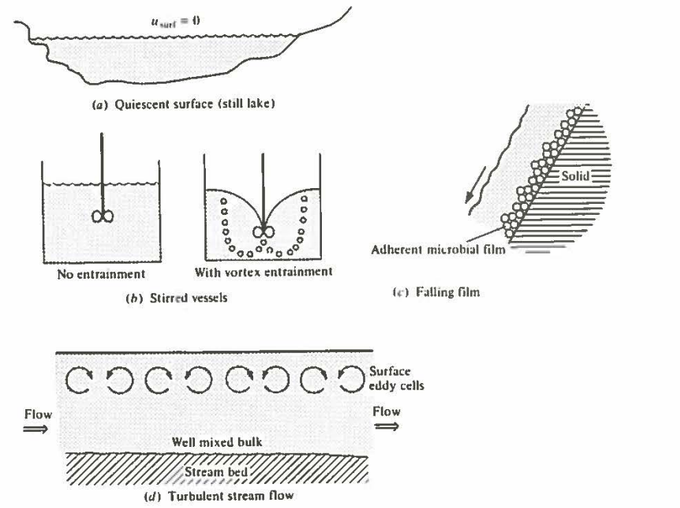

Figure 8.10 Free surface operation configurations: (*a*) quiescent surface, (*b*) stirred vessels, (*c*) falling film, (*d*) turbulent stream flow.

When the agitated vessel is simultaneously aerated, the power requirements for agitation decrease. The ratio of power requirements in aerated vs. nonaerated vessels, P_a/P vs. a dimensionless aeration rate N_a

$$N_a = \frac{F_g}{N_i D_i^3} \tag{8.79}$$

(where F_g is volumetric gas rate) has been correlated, as shown in Fig. 8.9.

Except for the most rapidly changing part of the curve, these forms can be fitted to

$$\frac{P_a(N_a) - P_a(N_a = \infty)}{P - P_a(N_a = \infty)} = e^{-mN_a} \tag{8.80}$$

where m = const. An alternative form which is also useful in turbulent aeration of non-Newtonian fluids is due to Michel and Miller [28]:

$$P_a = m'\left(\frac{P^2 N_i D_i^3}{F_g^{0.56}}\right)^{0.45} = m'\left(\frac{P^2 (N_i D_i^3)^{0.44}}{N_a^{0.56}}\right)^{0.45} \tag{8.81}$$

where m' = const. In both the above correlations, P is the nonaerated power input of the earlier chapter formulas.

From the relations of the previous paragraph, at constant N_i and D_i, the power input diminishes with increased N_a, that is, increased air flow F_g. This effect appears partially due to the decrease in average density of the fluid being agitated. Uniformity of bulk mixing diminishes with increasing N_a.

In several bioreactor designs, mixing is provided by injection of a liquid jet into the vessel. In this case the power dissipation may be estimated from (see Ref. 29)

$$P = \frac{8\rho_l F_l^3}{\pi^2 D_j^{0.4}} \tag{8.82}$$

where D_j is the jet diameter.

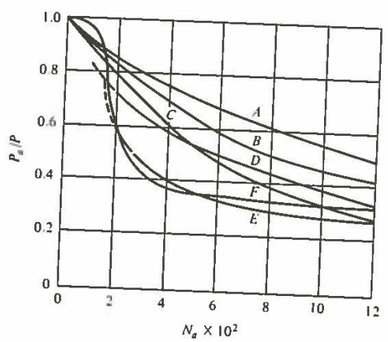

Figure 8.9 Ratio of power requirement for aerated vs. nonaerated systems as a function of N_a (see text): *A*, flat blade turbine (8 blades); *B*, vaned disc (8 vanes); *C*, vaned disc (6 vanes); *D*, vaned disc (16 vanes); *E*, vaned disc (4 vanes); *F*, paddle. *(Reprinted by permission from Y. Ohyama and K. Endoh, "Power Characteristics of Gas-Liquid Contacting Mixers," Chem. Eng., Japan, vol. 19, p. 2, 1955.)*

8.6 MASS TRANSFER ACROSS FREE SURFACES

Gas transfer through gas-liquid free surfaces (Fig. 8.10) plays a major role in oxygen supply and CO_2 removal from animal cell cultures. Surface mass transfer is also important in shake flask and small-scale stirred bioreactors for microbial cultivations. Transport across free liquid surfaces is essential for stream reaeration and respiration of aerobic life near the sea surface and in lake communities. Free-surface mass transfer is also important in many industrial microbial processes employing trickle-bed reactors, e.g., wine-vinegar manufacture and wastewater treatment. In the former cases, the depth of oxygen transfer depends on the scale of eddy motions near the liquid surface. Mass transfer into or out of falling-liquid films has been studied frequently, though not often under conditions appropriate to microbial processes. This circumstance is considered first.

The area-integrated absorption rate for a falling laminar liquid film of thickness h, length L, and width W and with zero initial concentration of dissolved gas is given by

$$\text{Integrated absorption rate (moles/unit time)} = WLc_l^*\left(\frac{4\mathscr{D}_{O_2} u_{max}}{\pi L}\right)^{1/2} \tag{8.83}$$

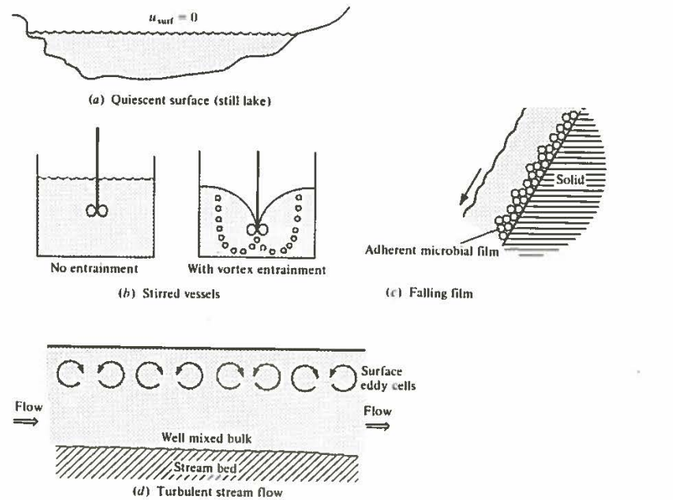

Figure 8.10 Free surface operation configurations: (*a*) quiescent surface, (*b*) stirred vessels, (*c*) falling film, (*d*) turbulent stream flow.

where u_{max} is the free-surface velocity. In the derivation, it is assumed that the solute concentration near the solid boundary never departs from zero; i.e., the diffusing solute does not "penetrate" the entire film thickness during the falling-time interval [5].

We define the Reynolds number for the situation as

$$\mathrm{Re} = \frac{u_{max} R_h \rho}{\mu_l}$$

where the hydraulic radius R_h is used as the length scale

$$R_h = \frac{Wh}{2W + 2h} \approx \frac{h}{2} \qquad \text{if } h \ll W$$

From the definition for the mass-transfer coefficient

$$\text{Integrated absorption rate} = k_l(c_l^* - c_l)WL \tag{8.84}$$

For c_l approximately zero relative to c_l^*, Eqs. (8.83) and (8.84) can be rewritten in the form $\mathrm{Sh} = f(\mathrm{Sc}, \mathrm{Re})$:

$$\mathrm{Sh} = \frac{k_l h}{\mathscr{D}_{O_2}} = 2b(\mathrm{Sc}\,\mathrm{Re})^{1/2} \tag{8.85}$$

where h is the length scale for the Sherwood number and $b = (L/h)^{1/2}$. Thus, Sh varies as $\mathrm{Re}^{1/2}$.

Livansky et al. [18] studied CO_2 absorption into aqueous films moving down a slope of known area using water, algal suspensions, and nutrient medium as absorbing fluids. The value of k_l at $\mathrm{Re} = 7$ to 8×10^3 was the same for all three fluids; only the algal suspensions were studied at different Reynolds numbers. (These films may have been turbulent.) Their results can be described by

$$k_l = 4 \times 10^{-5}\,\mathrm{Re}^{2/3} \qquad \text{for } 2000 \le \mathrm{Re} \le 8000$$

In turbulent flowing streams, the scale of circulation is important since this scale determines the depth to which fluid carries fresh, nearly saturated liquid from the surface into the bulk liquid. If we imagine a circulating eddy of length and depth Λ, as shown in Fig. 8.11, the average Sherwood number for mass transfer under turbulent conditions can be defined analogously to Eq. (8.28) as

$$\overline{\mathrm{Sh}} = \frac{\bar{k}_l \Lambda}{\mathscr{D}_{O_2}} = \int_0^{\Lambda} \left(\frac{\partial c}{\partial \bar{z}}\right)_{\bar{z}=0} d\bar{w}$$

where $\bar{z}$ and $\bar{w}$ are dimensionless coordinates scaled by Λ, and $\bar{k}_l$ is the average value over the eddy length.

The rate of mass transfer is ultimately dependent on $\mathscr{D}_{O_2}$ locally and on the rate at which fluid near the surface is renewed by the circulation pattern. An

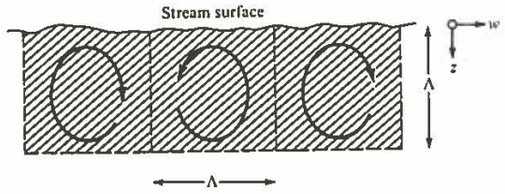

Figure 8.11 Sketch of circulating eddies near a free liquid surface.

early derivation due to Higbie† argued that for fluid elements with identical residence times τ at the gas-liquid surface the mass-transfer coefficient k_l should be

$$\bar{k}_l = \left[\frac{\mathscr{D}_{O_2}}{\pi\tau}\right]^{1/2} \tag{8.86}$$

This form has been extended by Danckwerts for distributions of surface residence times, the result still giving $\bar{k}_l \propto (\mathscr{D}_{O_2})^{1/2}$. A flowing turbulent stream of average flow velocity $\langle u_w \rangle$ has been suggested to have a renewal time τ equal to the ratio of stream depth h to average velocity $\langle u_w \rangle$:

$$\tau_{stream} = \frac{h}{\langle u_w \rangle}$$

thus predicting

$$k_l = \left(\frac{\mathscr{D}_{O_2}}{\pi} \frac{\langle u_w \rangle}{h}\right)^{1/2}$$

If the stream has width W, the interfacial area a per stream volume is

$$\frac{W(1)}{W(1)(h)} = \frac{1}{h}$$

Thus

$$k_l a = \left(\frac{\mathscr{D}_{O_2}}{\pi} \frac{\langle u_w \rangle}{h^3}\right)^{1/2} \qquad \text{(O'Connor-Dubbins)} \tag{8.87}$$

a form which has had reasonable success for describing reaeration of oxygen-deficient lakes and streams. Another treatment accounting for the variation of k_l with position w in the eddy provides

$$\bar{k}_l = 1.46\left(\frac{\mathscr{D}_{O_2} u_{rms}}{\Lambda}\right)^{1/2} \tag{8.88}$$

† R. Higbie, *Trans. AIChE*, 35: 365 (1935).

where u_{rms} is the rms velocity in the eddy circulation. In general, it appears reasonable to take Λ and u_{rms} proportional to mean stream depth and mean stream velocity, respectively:

$$\gamma \times \text{depth} = \Lambda \qquad \gamma \times \text{mean stream velocity} = u_{rms}$$

with the same constant of proportionality γ.

The motion of waves at air-water interfaces is known to influence gas transfer strongly. Here, in contrast to the preceding treatments, the gas-flow patterns, e.g., average and turbulent velocity components of wind which drives ocean waves, are of major importance. However, the general topic is too complex for this text (see the references).

8.7 OTHER FACTORS AFFECTING $k_l a'$

From the definitions of k_l and a' and consideration of the factors responsible for the thickness of the mass-transfer resistance zone near bubble and droplet surfaces, k_l and a' will be influenced by alteration of the values of liquid-phase solute diffusivity $\mathscr{D}_{O_2}$, continuous-phase viscosity μ_c, and the gas-liquid interfacial resistance. The liquid "viscosity" may vary with shear rate; this non-Newtonian behavior is of sufficient importance to be discussed separately (Sec. 8.8). The remaining influences are summarized in this section.

8.7.1 Estimation of Diffusivities

The Wilke-Chang correlation is a useful means of estimating (usually to better than 10 to 15 percent) the diffusion coefficient of small molecules in low-molecular-weight solvents:

$$\mathscr{D} = 7.4 \times 10^{-8} \frac{T(x_a M)^{1/2}}{\mu_l V_m^{0.6}} \quad \text{cm}^2/\text{s} \tag{8.89}$$

where M = solvent molecular weight
V_m = molecular volume of solute at normal boiling point, $\text{cm}^3/\text{g mol}$
μ_l = liquid viscosity (cp)

The parameter x_a represents the association factor for the solvent of interest; some values for x_a are 2.6 (H_2O), 1.9 (methanol), 1.5 (ethanol), and 1.0 (benzene, ether, and heptane).

The diffusion coefficient will vary with ionic strength (as does solubility, Table 8.1) and with concentration of solutes which change the solution viscosity. Provided that the solute-solvent interactions are not altered in the latter case, the relation

$$\mathscr{D}_1 \mu_{c1} = \mathscr{D}_{\text{ref}} \mu_{c,\text{ref}}$$

provides a useful scale to correct for changes in solution viscosity from a reference point, say that of pure water, with temperature held constant.

Table 8.4 Diffusion coefficients in microbial film

Biomass	Reactor	$\mathscr{D}_{meas}$, $\text{cm}^2/\text{s} \times 10^5$	% of H_2O value
Bacterial slimes	Rotating tube	1.5	70
	Submerged slide	0.04	2
Zoogloea ramigera	Fluidized reactor	0.21	8

The diffusion coefficient in microbial aggregates is usually less than that in pure water ($2.25 \times 10^{-5}\ \text{cm}^2/\text{s}$), as summarized in Table 8.4 for oxygen. A recent study examining other variables concluded that the O_2 diffusion coefficient in waste-treatment microbial aggregates decreases from the pure H_2O value in the range 20:1 to 5:1 with increased aggregate lifetime in the reactor and with increased C/N ratio of the entering wasted substrates.

8.7.2 Ionic Strength

The precise resolution of ionic-strength influences into all pertinent factors appears difficult. An examination of Newtonian fluids gives the physical-absorption result

$$K_l a = \lambda \left(\frac{P_a}{V_l}\right)^n \left(\frac{F_g}{A}\right)^m \left(\frac{\rho_l^{0.533} \mathscr{D}_{O_2}^{2/3}}{\sigma^{0.6} \mu_l^{1/3}}\right) \tag{8.90}$$

where M = solvent molecular weight
V_m = molecular volume of solute at normal boiling point, $\text{cm}^3/\text{g mol}$
μ_l = liquid viscosity (cp)

An empirical fit for λ, n, and m vs. ionic strength $I(=\frac{1}{2}\sum Z_i^2 c_i$, i = species, Z_i = species charge) is possible:

$$\lambda = 18.9 - \frac{28.7I'}{0.276 + I'} \qquad I' = \begin{cases} I & \text{if } 0 \le I \le 0.40 \text{ g ion/L} \\ 0.40 & \text{if } I > 0.40 \text{ g ion/L} \end{cases}$$

$$n = \begin{cases} 0.40 + \dfrac{0.862I'}{0.274 + I'} & I' = I \le 0.4 \\ 0.90 & I > 0.4 \end{cases}$$

$$m = \begin{cases} \text{monotonic increasing} & \\ \text{from 0.35} & I = 0 \\ \text{to 0.39} & I \ge 0.4 \end{cases}$$

for $K_l a$ in s^{-1}, P_a in $\text{ft-lb}_f/\text{min}$, V_l in ft^3, F_g in ft^3/s, A in ft^2, and physical properties in cgs units.

8.7.3 Surface-Active Agents

As discussed in Chap. 2, many biochemicals are amphipathic, i.e., contain strongly hydrophobic and hydrophilic moieties which tend to concentrate at gas–liquid and liquid–liquid interfaces. In various phases of fermentations, cells secrete species such as polypeptides which may behave like surfactants, at times leading to foaming tendencies in aerated vessels. Addition of chemical antifoams also affects interfacial resistances to mass transfer, though typically in a manner opposing that of surfactants.

Adsorption of surfactants at the phase interface is a spontaneous process; the interfacial free energy and thus the surface tension σ is reduced relative to the original value. From the correlations in Example 8.2 the values of D_{Sauter} and D_c are expected to decrease, leading to higher values of the interfacial area per volume a'.

This tendency for a' to increase is countered by the effect of surfactant films on the mass-transfer coefficient k_l. The adsorption of a macromolecular film results in a stagnant, rigid interface. The decreases in k_l discussed below are thought to be due to either or both of two mechanisms: (1) the ease of liquid movement near the interface is reduced due to the decreased mobility of the interface; thus, the variety of mass-transfer theories based on estimating exchange rates of small fluid elements between the surface and the bulk will predict a decreased mass-transfer coefficient (see Refs. 3 and 4 for further discussion); (2) like the cell membrane itself, the molecular film is expected to contribute a resistance of its own, which may cause a departure from the presumed gas–liquid equilibration in the plane of the interface.

Addition of 10 ppm sodium lauryl sulfate (SLS) reduced k_l for oxygen transfer by 56 percent versus pure water. A constant or plateau value of k_l was observed at all higher surfactant concentrations. The surface area per volume a' increased slowly throughout the range of SLS concentrations from 0 to 75 ppm, with a minimum of $k_l a'$ at about 10 ppm surfactant.

The product $k_l a'$ has been observed to increase continuously with surfactant addition in a turbine aerator. Inspection of the data for the reported ratio of a' (surfactant)/a' (no surfactant) and the corresponding ratio for the product $k_l a'$ shows that while a' increased 400 percent for addition of 4.0 ppm sodium dodecyl sulfate, $k_l a'$ increased only about 15 percent, implying a decrease of about 71 percent in the value of k_l.

This reduction observed in both sets of data is in agreement with results of others. For a variety of sparingly soluble gases, the average plateau values of k_l upon surfactant addition correspond to reductions of k_l by a factor of 60 percent. The sodium dodecyl sulfate data of Benedek and Heideger [33] suggest that turbine-agitated aeration corresponds to the transition region between the two correlations presented earlier in Eqs. (8.35) and (8.36); a similar result appears to be the case for aeration with sieve trays (Danckwerts). This serves to warn the reader that such correlations are useful estimates but should be replaced by experimental values from more pertinent equipment when possible.

8.8 NON-NEWTONIAN FLUIDS

For fluids, the ratio of shear stress τ_s to the velocity gradient du/dy is defined as the viscosity η_v (the subscript v distinguishes the viscosity from the earlier effectiveness factor η). Thus,

$$\tau_s = -\eta_v \frac{du}{dy} \tag{8.91}$$

A plot of τ vs. du/dy for a Newtonian fluid is linear and passes through the origin. A variety of non-Newtonian behaviors has been observed in steady flows for liquid solutions of polymers and/or suspensions of dispersed solids or liquids; the features of the more common of these are summarized in Fig. 8.12, where shear rate $\dot{\gamma}$ is used rather than du/dy.

8.8.1 Models and Parameters for Non-Newtonian Fluids

The dilatant, Newtonian, and pseudoplastic behaviors are examples of the general Ostwald-de Waele or power-law formulations for fluids

$$\tau_s = -\eta_0 |\dot{\gamma}|^{n-1}\dot{\gamma} = -(\text{apparent viscosity})(\dot{\gamma}) = -\eta_v \dot{\gamma} \tag{8.92}$$

where n { $> 1 \rightarrow$ dilatant; $= 1 \rightarrow$ Newtonian; $< 1 \rightarrow$ pseudoplastic

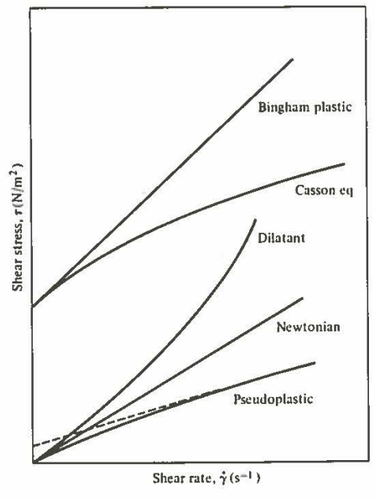

Figure 8.12 Stress vs. shear-rate behavior of Newtonian and common non-Newtonian fluid models. *(Reprinted from J. A. Roels, J. van den Berg, and R. M. Voncken, "The Rheology of Mycelial Broths," Biotech. Bioeng., vol. 16, p. 181, 1974.)*

Some systems appear not to produce a motion until some finite yield stress τ_0 has been applied. For Bingham plastic fluids, the form

$$\tau_s = \tau_0 - \eta_0|\dot{\gamma}|^{n-1}\dot{\gamma} \qquad \text{where} \qquad n = 1,\ \tau_0 \neq 0,\ \tau_s > \tau_0 \tag{8.93}$$

is useful.

The last form with finite τ_0 and n less than unity would give a curve similar to the Casson equation, which is given by

$$\tau_s^{1/2} = \tau_0^{1/2} - K(\dot{\gamma}^{1/2}) \tag{8.94}$$

In the subsequent discussion of mass-transfer coefficients, power input, mixing, etc., we shall refer to various fermentation or other fluid systems of interest as being (apparently) pseudoplastic, Newtonian, etc., and indicate correlations between the fluid-model parameters and the former quantities of interest. The fluid descriptions in Fig. 8.12 refer to behavior in steady shear flows. Under unsteady-state conditions, such as follow a step change in the applied shear rate, time-dependent responses in apparent viscosity η_a are often observed, thus demanding a more structured fluid model (in the same sense as the Chap. 7 cell kinetics models) to describe transient situations. Such transient states may more accurately apply to turbine agitation and turbulent mixing in non-Newtonian systems. These more structured models are a relatively difficult and undeveloped area of mechanics; we simply insert the caveat here that our understanding of the factors responsible for non-Newtonian behavior and their description is weaker than the theories for the previous sections of this chapter.

Non-Newtonian behavior may arise in at least two distinct cases: (1) suspensions of small particles and (2) solutions of macromolecules. It is apparent that the two cases become similar as molecular diameters increase above 50 to 100 Å or as particle diameters fall from the order of micron sizes.

8.8.2 Suspensions

Various theories predict that a dilute suspension of spheres should remain Newtonian, the effective viscosity $\eta_{s,\text{eff}}$ of the suspensions being given by

$$\frac{\eta_{s,\text{eff}}}{\eta_{\text{solvent}}} = 1 + \tfrac{5}{2}\phi + b\phi^2 + \cdots \tag{8.95}$$

where ϕ is the volume fraction solids and b is of the order of 6 to 8. For a bacterial density as high as 10^9 cells per milliliter and a cell diameter of 3×10^{-4} cm, the value of ϕ is about 5×10^{-3}: the effect of the cells is apparently negligible. Higher volume fractions occur in filtration operations such as dewatering (in product recovery from cell broths) and in fermentations producing the mold pellets or mycelia of previous discussions.

At higher volume fractions, solid suspensions may exhibit a yield stress; e.g., aqueous slurries of nuclear fuel particles with diameters in the micrometer range appear usefully modeled by the Bingham plastic model. Mycelial fermentations of *Streptomyces griseus* appear to follow a Bingham form except at very low shear rates; this may be important in aeration. From Eq. (8.50) note that the maximum stress for a rising bubble is associated with the terminal rise velocity. Thus, in Bingham fluids, a sufficiently small bubble will not exert the yield stress on the surrounding fluid and it will remain fixed in the same fluid element for long times; i.e., it would be expected to circulate in the vessel with the fluid rather than following the usually rising path of larger bubbles.

The Casson equation has been fruitfully applied to descriptions of blood flow. Red blood cells form aggregates, the size of which diminishes with increasing shear forces. The apparent viscosity η_a diminishes with increased shear, as seen from Fig. 8.12 for the Casson equation. In floc-forming fermentations, we may expect stirrer shear forces to control the average size of the microbial flocs; hence the Casson equation may be useful in some such fermentations.

A study of rheology of penicillin broths vs. time over a large range of shear rates used a turbine impeller for viscometry studies rather than a rotating cylinder, the two cited advantages being (*a*) the stirring prevents phase separation, which otherwise would affect the reliability of the measurement: without stirring a thin "cell-free" layer of liquid is formed at the wall of the cylinder, and (*b*) the shear rate of the impeller is a simple function of the impeller speed and is independent of the rheology of the liquid as has been shown previously [38, pp. 188 189]. This research revealed that the Bingham and power-law models were inadequate to represent the results over the full range of shear rates investigated. A reasonable modification of the Casson equation was derived:

$$(M_\tau)^{1/2} = (M_{\tau_0})^{1/2}\left(1 + \frac{0.69(M_{\tau_0})^{1/2} - 1.1}{(M_{\tau_0})^{1/2}}(N_i)^{1/2}\right) \tag{8.96}$$

where M_τ is proportional to stress: $M_{\tau_0} = 64D_i^3/2\pi K$, N_i is the impeller rotation rate (revolutions per second) and K is the ratio of shear rate to impeller speed (constant). The data agreed well with the above equation though a slightly better fit resulted if the second term on the right-hand side was modified to

$$\frac{0.193(M_{\tau_0})^{0.75} + 0.1}{(M_{\tau_0})^{1/2}}(N_i)^{1/2}$$

The importance of the result is threefold: (1) The rheological data were taken over a sufficient range of shear rates to *discriminate* between models which are similar over restricted shear-rate ranges. (2) The results showed that the power and Bingham laws were most inadequate at low shear rates; this range is likely to be important in determining tank-mixing uniformity; i.e., extrapolation of the Bingham and power laws to this situation would lead to large errors (mixing problems in vessels are discussed in Chap. 9 in connection with fluid circulation-time and residence-time distributions). (3) The modified Casson equation was shown to predict a factor dependent on the mold *morphology* (shape) through the ratio of length to diameter of the filaments. This result (and other theories for nonspherical particles) provide an important potential connection between reactor-design calculations (analysis) and morphology (observation) since the latter subject has been examined for a range of species and conditions in the literature.

The power-law model appears to fit data for mold filaments over the higher range of shear rates. It also describes suspensions of paper pulp; 4 percent paper pulp in water suspensions have power-law parameters $n = 0.575$ and $\eta_0 = 0.418\ \text{lb}_f \cdot \text{s}^n/\text{ft}^2$. Investigations of oxygen transfer with pulp suspensions have been used to simulate some fermentation conditions: if the overall oxygen uptake is determined by mass-transfer limitations in high shear regions, this may be useful. The previous paragraph casts more doubt on such simulation studies where bulk mixing influences O_2 uptake by the microorganism(s).

In continuous-flow systems with several reactors in series (Chap. 9), the tank number replaces time as an indication of population growth phase, and changes in rheology with tank number may be encountered. For example, two-stage cultivation of *Candida utilis* [41] at large flow rates led to second-tank conditions such that the specific biomass growth rate became so much larger than specific rate of cell multiplication that an increase in average cell size occurred. A change of cell and aggregate morphology was also noted, indicating again a possible connection between morphology and rheology.

8.8.3 Macromolecular Solutions

A number of microbes secrete extracellular polysaccharides and related biopolymeric derivatives. Examples include xanthan gum, polyalginic acid, and pullulan. The first is widely used in modifying viscosity of processed foods, in stabilizing suspensions, and as a major candidate for oil field recovery operations. These secreted biopolymers render the fermentation fluid non-Newtonian; the fluids are characteristically described by a simple power law behavior [Eq. (8.92)] where $n < 1$ (pseudoplastic).

The time-varying biopolymer concentration in a batch fermentation gives rise to time-varying fluid and hence transport properties (mass and heat transfer). As correlations for transport coefficients in non-Newtonian fluids are typically expressed in terms of the power law parameters, n and η_0, we seek a relation between biopolymer concentration and rheological parameters.

For xanthan gum, the polymer concentration, $[P]$, and the power law parameter, η_0, are related by a correlation of the form

$$\eta_0 = A \cdot [P]^B \tag{8.97}$$

where $B \sim 2.5$.

For a number of microbial exobiopolymers, the time-varying power law exponent n and consistency η_0 do not vary independently in a fermentation but are related by a correlation of the form

$$\ln \eta_0(t) = C + D \cdot n(t) \tag{8.98}$$

With $[P(t)]$ available from a biological kinetic model, Eqs. (8.97) and (8.98) provide a simple description of the time evolution of $n(t)$ and $\eta_0[P(t)]$. These values can then be used to predict heat and mass transfer coefficients, as well as mixing and power consumption characteristics [39, 40].

8.8.4 Power Consumption and Mass Transfer in Non-Newtonian Fermentations

An instantaneous impeller Reynolds number Re_i' may be defined according to Calderbank [11]:

$$\text{Re}_i' = \frac{D_i^2 N_i^{2-n} \rho}{0.1 K_c} \left(\frac{n}{6n+2} \right)^n \tag{8.99}$$

where K_c, the consistency index, equals the shear stress τ at a shear rate of $1\ \text{s}^{-1}$.

For the nonaerated non-Newtonian broths of *Endomyces*, the power number [Eq. (8.78)] was correlated with the Reynolds number Re_i' as shown in Fig. 8.13. The curves plotted there can be represented by the relationship

$$P_{no} = k(\text{Re}_i')^x \left(\frac{D_i}{D_T} \right)^y \left(\frac{W}{D_T} \right)^z \tag{8.100}$$

where D_i = impeller diameter
D_T = tank diameter
W = impeller width

and k, y, and z depend on the range of Re_i':

	Re_i'		
	<10	10–50	>50
k	32	11	9
x	−0.9	−0.4	−0.05
y	−1.7	−1.7	−1.2
z	0.4	0.5	0.9

The similarity of Fig. 8.13 to Rushton's data and the pipe friction factor in Fig. 8.8*a*, *b* is clear.

In aeration studies by the same group, the correlation of Michel and Miller (used earlier for Newtonian fluids) fitted the results in the turbulent regime ($\text{Re}_i' > 50$):

$$P_g \propto \left(\frac{P^2 N_i D_i^3}{F_g^{0.56}} \right)^{0.45} \tag{8.101}$$

The laminar and second regimes ($\text{Re}_i' < 50$) appear reasonably approximated by use of a smaller exponent:

$$P_g \propto \left(\frac{P^2 N_i D_i^3}{F_g^{0.56}} \right)^{0.27} \tag{8.102}$$

The two curves meet at a value of $P^2 N_i D_i^3 / F_g^{0.56} = 2 \times 10^{-2}$, and slightly different proportionality coefficients result for the different impellers used.

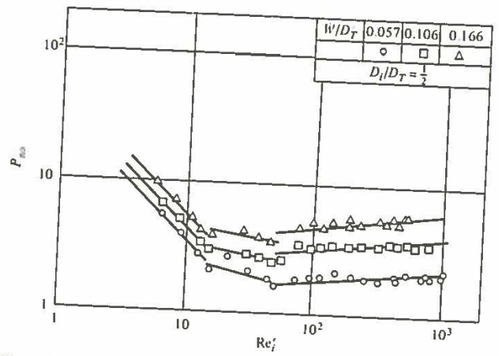

Figure 8.13 Power number vs. impeller Reynolds number, Re_i' (see text) for three different impellers in nonaerated systems. *(Reprinted from H. Taguchi and S. Miyamoto, "Power Requirements in Non-Newtonian Fermentation Broth," Biotech. Bioeng., vol. 8, p. 43, 1966.)*

The dilution of mycelial cultures by small volume percents of water (10 to 25 percent) produces marked changes in k_l and power-number parameters. The implications for power-input variations with dilution rate in continuous culture may be significant.

The influence of the microbial population depends on the physical situation which applies (floating single cells, cell aggregates, cells localized near particle or bubble surface, etc.) and the influence of the microbial particles on the fluid properties. The value of k_la has been observed to diminish 90 percent as the concentration of mycelial *Aspergillus niger* increased from 0.02 to 2.5 percent. Enhancement of O_2 mass transfer is observed in the presence of suspensions of *Candida intermedia*, *Pseudomonas ovalis*, or 0.3-μm alumina particles. Not only do cells and alumina give similar results, but through use of oxidative phosphorylation (Chap. 5) inhibitors, it is established that the enhancements are typically 40 percent vs. water and are independent of cell viability. It has been recently shown that the effect of the particles is to alter the hydrodynamics near the gas-liquid interface in such a way as to decrease the mass transfer resistance of the adhering fluid film near the bubble [44].

At the high shear rates needed to mix phases and promote mass transfer, diminutions in microbial activity have frequently been observed. For example, the viability of a relatively large cell, the protozoon *Tetrahymena*, began to be seriously altered by disruption at shear rates $>1200\ s^{-1}$. In these experiments the maximum shear rate characterized by the impeller tip speed appeared to be a more important variable than the turbulent Reynolds number or power input per unit volume.

The impeller can have other effects: the size of the extant microbial aggregates may be reduced, as mentioned earlier. Taguchi and Yoshida† divided the experimentally observed reduction of mycelial pellet size into two phenomena: (1) chipping small pellicules off the larger pellet and (2) directly rupturing the spherical shape of the pellet. The time evolution of particle diameter D due to the first process appeared to be governed by

$$\frac{dD}{dt} = -k_i(N_iD_i)^{5.5}D^{5.7} \tag{8.103}$$

while the second process could be described as a first-order decay

$$\frac{dN_p}{dt} = -k_rN_p \tag{8.104}$$

where N_p is the number of nondisrupted pellets remaining. The rate coefficient k_r was correlated with D, N_i, and D_i to give

$$k_r = +(\text{const})(D^{3.2}N_i^{6.65}D_i^{8.72}) \tag{8.105}$$

Assuming that the turbulent Reynolds stress rather than the viscous stress is responsible for pellet rupture and that the pellet resistance depends directly on the measurable tensile strengths of the pellets, Taguchi et al. argue that the last equation may have some theoretical basis.

Regarding the oxygen transfer rate in paper-pulp suspensions, impeller and tank geometry were found to be important, in agreement with the earlier results of Taguchi and Miyamoto [42] for aerated and nonaerated *Endomyces* suspensions. In 1.6 percent pulp suspensions, the product k_la was described by

$$\frac{k_la}{N_i} = 0.113\left(\frac{D_T^2h}{WL(D_i - W)}\right)^{1.437}(N_it)^{-1.087}\left(\frac{D_i}{D_T}\right)^{1.021} \tag{8.106}$$

where t = characteristic mixing time of vessel
h = liquid height
W = impeller width

and D_i, D_T, and L are as before.

In summary, a number of factors including bubble and cell dimensions, fluid properties and rheology, agitator and tank geometry, and power input determine mass-transfer coefficients and surface area per unit volume. The combination of these estimates with cell kinetics of the previous chapter and notions of mixing and macroscopic reactor configurations of Chap. 9 is important in assembling a complete reactor design. This state of knowledge is obviously wishful; the previous relations in this section are but the beginning of work needed to design confidently such reactors from first principles. As a closing example of some of the complexities yet to be unraveled, we note the time changes of the relations between bubbles, particulate substrate, and cells that accompany the fermentation of *Candida petrophilum* on *n*-hexadecane, as shown in Fig. 8.14. The description of this gas-liquid-liquid-cell system by the authors† is illuminating:

> During the first period of fermentation, oil droplets are relatively large and cells attach to oil droplets rather than to air bubbles. Air bubbles are unstable and easily renewed. The k_la value can be kept at the maximum level associated with the fermentor. During the second phase, oil

† H. Taguchi and T. Yoshida, *J. Ferment. Technol.*, 46:814, 1968.

† A. Mimura, I. Takeda, and R. Wakasa, "Some Characteristic Phenomena of Oxygen Transfer in Hydrocarbon Fermentation," *Biotechnol. Bioeng. Symp. 4*, pt. 1, p. 467, 1973.

droplets become smaller and cells are adsorbed onto the surface of the oil droplets, forming dense flocs. The flocs tend to attach to the surface of the air bubbles, but they can be easily separated with agitation.

The $k_l a$ value is decreased continuously as fermentation proceeds. The third phase is the last half period of the logarithmic growth phase, in which yeast is growing rapidly, although we cannot observe any oil droplets microscopically in the culture liquid. At this point the $k_l a$ value reaches its minimum throughout the fermentation.... [Air] bubbles are covered with yeast cells, and the bubbles come together with cells as an intermedium. They are very stable and float on the surface of the culture liquid. *n*-Paraffin is completely exhausted in the fourth phase. The cells are dispersed uniformly throughout the culture liquid. In this period the nature of the culture liquid may be similar to that in a carbohydrate fermentation, and $k_l a$ recovers its initial levels.

An analytical model including a few of the features of this fermentation type is considered in Chap. 9 (Example 9.2).

8.9 SCALING OF MASS-TRANSFER EQUIPMENT

As discussed by Oldshue,† the various quantities which may influence the product $k_l a$ in an agitated industrial reactor do not scale in the same way with reactor size or impeller rate.

1. The turbulent Reynolds number Re_t determines u_{rms} and thus bubble mass-transfer coefficients k_l

$$\mathrm{Re}_t = \frac{\rho u_{\mathrm{rms}} D}{\mu} \propto \frac{\rho D}{\mu}\left(\frac{D\,P}{\rho\,V}\right)^{1/3} \tag{8.107}$$

2. The impeller tip velocity $\pi N_i D_i$ determines the maximum shear rate $\dot{\gamma}$, which in turn influences both maximum stable bubble or microbial floc size (Sec. 8.3) and damage to viable cells (Sec. 8.8.4).
3. The power input per unit volume P/V through Re_t determines mass-transfer coefficients and particulate sizes. In laminar and transition regimes of aerators

$$P \propto N_i^2 D_i^3 \qquad \text{from Fig. 8.8}b$$

For turbulent regimes, the power number is constant; thus

$$P \propto N_i^3 D_i^5$$

Then taking V_{reactor} to scale with D_i^3 gives

$$\frac{P}{V} \propto \begin{cases} N_i^2 & \text{laminar, transition aeration} \\ N_i^3 D_i^2 & \text{turbulent aeration} \end{cases}$$

† J. Oldshue, *Biotech. Bioeng.*, **8**:3, 1966.

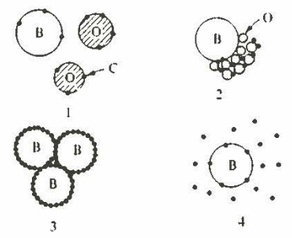

Figure 8.14 Different relationships among air bubbles (B), *n*-hexadecane droplets (O), and yeast cells (C) at different stages of batch culture of the yeast *Candida petrophilum* (1 log phase, 2 first half of exponential phase, 3 second half of exponential phase, 4 after n-hexadecane exhaustion). (*Reprinted from A. Mimuro, I. Takeda, and R. Wakasa, "Some Characteristic Phenomena of Oxygen Transfer in Hydrocarbon Fermentation," in B. Sikyta, A. Prokop, and M. Novak (eds.), Adv. Microbial. Eng., part 7, p. 467, Wiley-Interscience, New York, 1973.*)

4. The power input *during* aeration is

$$P_a = m'\left[\frac{P^2 (N_i D_i^3)^{0.44}}{N_a^{0.56}}\right]^{0.45} \tag{8.108}$$

Thus,

$$\frac{P_a}{V} \approx m'\left[\frac{P^2}{V^{2.22}}\,\frac{(N_i D_i^3)^{0.44}}{N_a^{0.56}}\right]^{0.45} \tag{8.109}$$

which will determine the motor size needed during fermentation.

5. If the vessel liquid is well mixed internally, a characteristic circulation time exists. The liquid recirculation flow rate F_l through the impeller region varies as a cross-sectional area πD_i^2 and tank average impeller velocity varies as $N_i D_i$. Thus

$$\frac{F_l}{V} \propto \frac{N_i D_i^3}{D_i^3} = N_i \qquad \text{time}^{-1}$$

a quantity of importance since it is inversely proportional to the time that fluid may spend away from the homogenizing influence of the impeller.

Given all these different quantities which can influence the process and which have different dependencies on agitation parameters, which one(s) should be used as the basis for scale-up? Here by "basis for scale-up" we mean the quantity which, by choice of operating conditions in the larger unit, will be maintained at the same value as in the smaller scale unit. For example, if we scale-up on the basis of constant power per unit volume, for mechanical agitators in the turbulent regime this means

$$N_{i1}^3 D_{i1}^2 = N_{i2}^3 D_{i2}^2 \tag{8.110}$$

where 1 and 2 denote the values in the small and large scale vessel, respectively. In scale-up of the early penicillin bioreactors, maintaining constant power input per unit volume (around 1 hp per 100 gal) plus vessel geometric similarity were used. As indicated in Fig. 8.15*a* this gives very similar yields of penicillin for vessels from 5 liters to 200 gallons. However, from the curves in Fig. 8.15*a*, we see

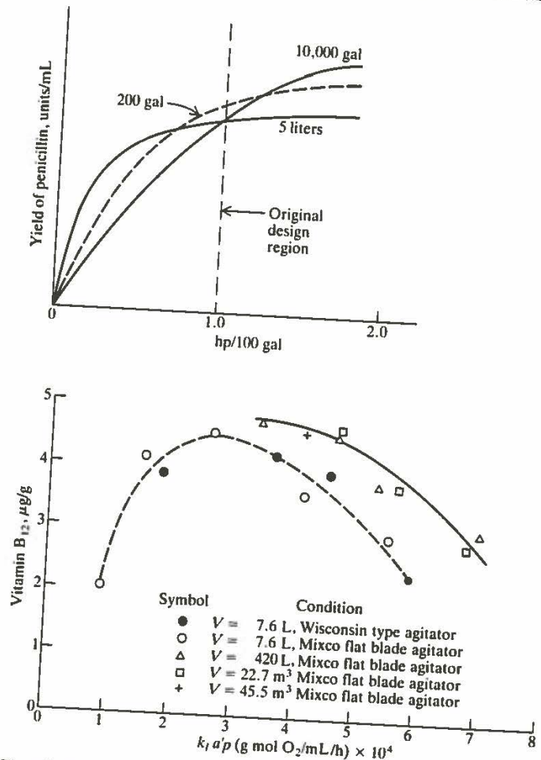

Figure 8.15 (*a*) Penicillin yields vs. power input in various sized vessels *(After E. Gaden, Sci. Rep. Ist Super. Sanita, vol. 1, p. 61, 1961)*. (*b*) Vitamin B_{12} yield (μg/g) vs. mass-transfer group ($k_l ap$) (see text) *(After W. H. Bartholomew, Adv. Appl. Microbiology, vol. 2, p. 289, 1960)*.

that, at different P/V values, there are significant differences in yield at different scales.

Another frequently applied basis for scale-up is constant volumetric transfer coefficient $k_l a$. Fig. 8.15*b* shows vitamin B_{12} yields from bacterial fermentations at different scales versus corresponding values of ($k_l ap$). The total pressure is included here to correct for the greater driving force for oxygen transfer at higher pressures which are encountered in large-scale bioreactors. The correlation between yield and $k_l ap$ is good, although data for the benchtop unit lie generally

below those for fermentation in larger vessels. Notice also that, in contrast to earlier discussions emphasizing oxygen transport limits on growth and the need for large $k_l a$ values, these data show a distinct maximum with respect to $k_l ap$. This probably occurs because at the same $k_l a$ value, other mixing and flow characteristics such as maximum shear rate or circulation time are generally *not* the same in vessels of different scale.

Therefore, if we scale up on one basis, we must be aware that other mixing and flow properties are different. This point is dramatically illustrated in an example of Oldshue† which considers scale-up from an 80 L to a 10,000 L agitated bioreactor. Here, D_i increases fivefold and V increases by a factor of 125. The 1.0 in each column of Table 8.5 indicates the property which is kept the same in the large tank as in the small tank. Values for each property have been normalized by the values for the 80-L tank, so the "small-scale" column shows all 1.0s. For example, scale-up based on constant P/V will increase the maximum shear rate by 70 percent ($N_i D_i = 1.7$) and increase the circulation time about threefold. On the other hand, scale-up based on circulation time (that is, F_l/V) requires 3125 times more power in the large tank!

The different dependencies of important transport properties on agitator design makes scale-up of agitated vessels something of an art. We must try to select as a scale-up basis the transport property most critical to the performance of the bioprocess. This is not easy given the potentially sensitive and diverse responses of cells to each of the transport phenomena influenced by the mixer size and rotation speed.

The total oxygen consumption rate of the vessel is found by combining $k_l a$ with an appropriate macroscopic description of the vessel. If the bulk liquid composition is uniform and the bubbles are uniformly dispersed throughout the vessel, the mass-transfer rate is simply

$$Vk_l a(c^* - c_{liq})_e = \text{oxygen consumption rate, mol } O_2/\text{s} \qquad (8.111)$$

Table 8.5 Relationship between properties for scale-up†

Property	Small scale, 80 L	Large scale, 10^4 L			
P	1.0	125	3125	25	0.2
P/V	**1.0**	**1.0**	25	0.2	0.0016
N_i	1.0	0.34	1.0	0.2	0.04
D_i	1.0	5.0	5.0	5.0	5.0
F_l	1.0	42.5	125	25	5.0
F_l/V	**1.0**	0.34	**1.0**	0.2	0.04
$N_i D_i$	**1.0**	1.7	5.0	**1.0**	0.2
Re_i	**1.0**	8.5	25	5.0	**1.0**

† S. Y. Oldshue: Fermentation Mixing Scale-up Techniques, *Biotech. Bioeng.*, 8: 3, 1966.

where subscript e refers to gas exit compositions (a consequence of the perfect mixing assumption is that exit-stream compositions equal reactor compositions, Chap. 9).

When the bubbles rise in plug flow through the vessel but the impeller still maintains perfect mixing in the liquid phase, c^* varies with position. Over a differential reactor height dz, the instantaneous loss of oxygen from the bubble is

$$HA\,dz\,\frac{dp_{O_2}}{dt}\,\frac{1}{RT} = \frac{\text{gas vol}}{\text{reactor vol}}\left(\begin{matrix}\text{differential}\\ \text{reactor volume}\end{matrix}\right)\left(\begin{matrix}\text{conc. rate of}\\ \text{change in bubble}\end{matrix}\right) \tag{8.112}$$

which equals

$$-k_l a(c_l^* - c_b)A\,dz \tag{8.113}$$

the mass transfer rate into the liquid. Since $p_{O_2} = Mc_l^*$ (M is Henry's law constant), we have

$$\frac{H}{RT}\frac{dp_{O_2}}{dt} = \frac{HM}{RT}\frac{dc_l^*}{dt} = -k_l a(c_l^* - c_b) \tag{8.114}$$

For constant bubble-rise velocity u_b, $dt = dz/u_b$, and the z variation of c^* is seen to be

$$\ln\frac{(c_l^* - c_b)z}{(c_l^* - c_b)_{\text{inlet}}} = \frac{k_l aRT}{HM}\frac{z}{u_b} \tag{8.115}$$

or

$$(c_l^* - c_b)_z = (c_l^* - c_b)_{\text{inlet}}\exp\left(-\frac{k_l aRTz}{HMu_b}\right) \tag{8.116}$$

The overall mass-transfer rate in the volume Ah is therefore

$$\int_0^h k_l a(c_l^* - c_b)(z)A\,dz = \frac{HMu_b}{RT}(c_l^* - c_b)_{\text{inlet}}A\left[1 - \exp\left(-\frac{k_l aRTh}{HMu_b}\right)\right] \tag{8.117}$$

The interaction of mixing, fermentation kinetics, and mass transfer is considered in the remaining text chapters.

8.10 HEAT TRANSFER

In biological reactors, heat may be added or removed from a microbial fluid for the following reasons:

1. It is desired to sterilize a liquid reactor feed by heating in a batch or continuous-flow vessel. Thus, the temperature desired must be high enough to kill essentially all organisms in the total holding time (Sec. 9.9.4).
2. If the heat generated in substrate conversion is inadequate to maintain the desired temperature level, heat must be added. For example, the reactor is an anaerobic sewage-sludge digestor which operates best between, say, 55 and 60 C (Sec. 14.4.7).
3. The conversion of substrate generates excess heat with respect to optimal reactor conditions for, e.g., maintenance of viable cells, so heat must be removed, as in most microbial fermentation processes.
4. The water content of a cell sludge is to be reduced by drying.

The first three relate to cell viability and metabolism and will therefore be of concern here. The last example is a unit operation, drying, which is covered in most texts on engineering unit operations.

The heat is transferred between the bioprocess fluid to or from a second fluid in several ways, i.e., with externally jacketed vessels, coils inserted in a larger vessel, flow through a heat exchanger, or by evaporation or condensation of water and other volatile components of the cell-containing fluid. Examples of such configurations are shown in Fig. 8.16. Temperature fluctuations between atmosphere and thermally stratified lakes and land also clearly involve heat transfer, the resulting temperatures determining the habitable niches for species. The present section focuses on heat transfer in process reactors.

Assuming that transfer rates and changes in other forms of energy are negligible, the fundamental steady-state equation in heat transfer relates the total

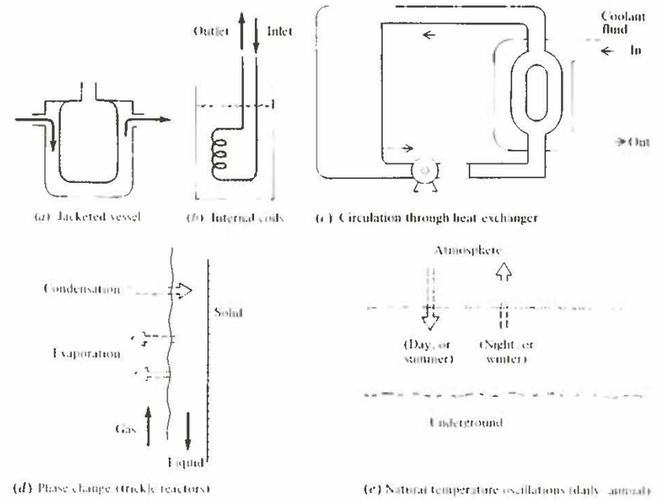

(a) Jacketed vessel (b) Internal coils (c) Circulation through heat exchanger

(d) Phase change (trickle reactors) (e) Natural temperature oscillations (daily, annual)

Figure 8.16 Examples of heat-transfer configurations: (*a*) jacketed vessel, (*b*) internal coils, (*c*) heat exchanger, (*d*) phase change of mass, and (*e*) natural temperature oscillations.

rate at which heat is generated to its rate or removal through some heat-transfer surface; thus

$$\text{Net generation rate} = \text{removal rate} = \bar{h}A\,\Delta T \tag{8.118}$$

where ΔT = characteristic temperature difference between bioprocess and cooling or heating fluid
A = heat-transfer surface area
$\bar{h}$ = overall heat-transfer coefficient

As with mass transfer, most of the resistance to heat transfer resides in a relatively quiescent thin fluid near the solid heating-cooling boundary, the bulk fluid being frequently well mixed and thus approximately isothermal. Our main concerns in this chapter are development of an overall energy balance and review of useful predictive formulas for $\bar{h}$ for various heater-cooler-sterilizer systems of interest. Methods for estimation of the heat load accompanying microbial growth have already been considered in Chap. 5.

The heat-transfer coefficients (Table 8.6) for boiling water and condensing vapors (steam, typically) make such fluids convenient in sterilization "reactors" (Sec. 9.9.4). Where lower temperatures are needed, as in heated anaerobic sludge digestors, a nonboiling water stream is useful. Viscous liquids exhibit greater heat-transfer resistances than water; as with mass transfer, this is due to lesser degree of bulk-fluid interchange with wall fluid and also to reduced thermal conductivity (analogous to $\mathscr{D}_{O_2}$).

Inspection of Fig. 8.16 reveals several design problems associated with heat transfer in biochemical reactors. The externally jacketed system has a heat-transfer area A which varies as the tank diameter (say impeller diameter) D_i^2. The volumetric heating or cooling demand of a reactor scales as D_i^3 if the overall

Table 8.6 General magnitude of heat-transfer coefficient h†

	h, kcal/(m² · h · °C)‡
Free convection:	
Gases	3–20
Liquids	100–600
Boiling water	1000–20,000
Forced convection:	
Gases	10–100
Viscous liquids	50–500
Water	500–10,000
Condensing vapors:	1000–100,000

† Data from H. Gröber, S. Erk, and U. Grigull, *Wärmeübertragung*, 3d ed., p. 158, Springer-Verlag, Berlin, 1955.

‡ Multiplication by 0.204 gives h in units of Btu/(ft² · h · °F).

microbial reaction rates and power input per unit volume are unchanged. Thus, jacketed vessels, sufficient in rendering laboratory reactors isothermal, must frequently be replaced by reactors with internal or external coils in heating, e.g., anaerobic sludge digestion, or cooling (e.g., hydrocarbon fermentation for single-cell protein production) of large-scale reactors.

The presence of such internal piping clearly alters mixing patterns, fluid velocities, and perhaps bubble-coalescence rates. The complexity of such a situation reminds us of the need to perform measurements in reactors approximating the desired configurations, as we may expect *a priori* design of such reactors to be more uncertain than for simpler systems. (Problems of vessel mixing patterns are discussed in the text and problems of Chap. 9). For example, the correlations in Sec. 8.10.1 indicate that the heat-transfer coefficient h[Btu/(ft² · h) or kcal/(m² · h)] changes as we shift configurations from a single cooling coil perpendicular to fluid flow to a set of staggered rows of coils in a tube coil perpendicular to the fluid-flow direction. Thus, the presence of the first row of coils alters the flow pattern past subsequent tube rows.

In very large scale systems with large heat loads, such as bacterial growth on methanol in a 1500 m³ reactor, internal coils become inadequate for cooling. Then, circulation through an external heat exchanger, or through an exchanger integral to a loop vessel configuration, is necessary. Here is an example where cooling loads, in concert with other considerations such as required power input for aeration and mixing, dictate a need for bioreactor designs substantially different from traditional agitated tank configurations. Several alternative vessel, contacting, and mixing configurations are summarized in Chap. 9.

Heat generation and removal rates are known with sufficient accuracy for some detailed heat-balance considerations to be possible, provided we clearly understand the basis on which such calculations are made and take appropriate precautions in terms of overdesign to allow for some uncertainty. The following section discusses the estimation of the heat-transfer demand (analogous to an oxygen demand); the subsequent sections discuss the conductance h.

Determination of the process heat transfer requirements begins with consideration of an overall energy balance. In a constant pressure system with negligible changes in potential and kinetic energies, the energy balance can be cast in terms of enthalpy changes, i.e., the heats of chemical transformation or phase transformation (e.g., evaporation, condensation), the sensible-heat flow in mass streams, and the heat transfer to or from second fluids acting as heating or cooling devices. Let

Q_{met} = heat-generation rate from cell growth and maintenance
Q_{ag} = heat-generation rate due to reactor mechanical agitation
Q_{gas} = heat-generation rate from aeration power input
Q_{acc} = heat-accumulation rate
Q_{exch} = heat-transfer rate to surroundings or exchanger
Q_{evap} = rate of heat loss by evaporation
Q_{sen} = rate of sensible-ethalpy gain of streams (exit − entrance)

Then

$$Q_{met} + Q_{ag} + Q_{gas} = Q_{acc} + Q_{exch} + Q_{evap} + Q_{sen} \tag{8.119}$$

Cooney, Wang, and Mateles [52] have utilized such a balance to calculate Q_{met} from measurement of Q_{acc} through monitoring the initial transient temperature rise of a nearly isolated fermentor. Under such an experiment, Q_{evap} and Q_{sen} are quite small, and Q_{exch} represents an important term compared with the difference of the larger individual rates $Q_{acc} - Q_{ag}$. As just mentioned, Q_{acc} was monitored calorimetrically, while Q_{ag} was calculated at each gas flow and impeller rate from the correlation of Michel and Miller (Eq. (8.81)].

In a fermentor design, $Q_{acc} = 0$ for a steady-state system [although temperature programming a batch reactor for optimal product yields (Sec. 10.7) may provide an additional complication]. Q_{ag} is estimated for ungassed or gassed systems using the appropriate power correlation presented earlier.

Neglecting Q_{evap} (which may be an important mechanism in trickle reactors) and Q_{sen} for the moment, the important remaining quantity is Q_{met}. Methods for estimating or measuring Q_{met} were presented in Chap. 5. In design of larger-scale reactors, the choice of an operating temperature and flow conditions will determine Q_{evap} and Q_{sen}, as the choice of agitator speed and diameter will determine Q_{ag} (corrected for the chosen aeration rate). Sparger design and gas flow rate will determine Q_{gas}. The remaining terms are Q_{acc} and Q_{exch}. Whether or not the reactor is operated isothermally, at each instant

$$\underset{\substack{\text{Heater}\\ \text{or cooler}\\ \text{duty}}}{Q_{exch}} = \underbrace{Q_{met} + Q_{ag} + Q_{gas}}_{\text{Generation}} - \underbrace{Q_{acc}}_{\text{Accumulation}} - \underbrace{(Q_{sen} + Q_{evap})}_{\substack{\text{Removal by other}\\ \text{than a solid heat}\\ \text{exchange surface}}} \tag{8.120}$$

This last equation sets the heat-transfer magnitude needed to maintain the desired temperature and rate of heat accumulation, if any.

We can use Eq. (7.35*a*) to represent the instantaneous mass-generation rate per unit volume in a batch reactor

$$\frac{dx}{dt} = \mu x \tag{7.35a}$$

and the corresponding instantaneous microbial heat-generation rate Q_{met} (heat/time) is evidently given by

$$Q_{met} = V_{reactor}\mu x \frac{1}{Y_\Delta} \tag{8.121}$$

where Y_Δ is the heat generation coefficient (g cell/kcal) considered in Sec. 5.10.4. Methods for estimating Y_Δ are presented there as are illustrative data showing greater metabolic heat generation for utilization of more reduced substrates (Table 5.12).

Table 8.7 Effect of substrate and yield coefficients on operating costs of fermentation

	Cost, cents per pound of cells			
Substrate	Substrate	O_2 transfer	Heat removal	Total
Maleate (as waste)	0	0.46	0.75	1.2
Glucose equivalents (molasses)	3.9	0.23	0.54	4.7
Paraffins	4.0	0.97	1.4	6.4
Methanol	5.0	1.2	1.9	8.1
Methane	1.6	3.3	3.7	8.6
Ethanol	8.8	0.75	1.3	11.0
Isopropanol	11.6	2.7	3.1	17.4
Acetate	16.7	0.62	1.1	18.4

† B. J. Abbott and A. Clamen, The Relationship of Substrate, Growth Rate, and Maintenance Coefficient to Single Cell Protein Production, *Biotech. Bioeng.*, **15**: 117, 1973.

The corresponding equation for a continuous-flow isothermal reaction at steady state is

$$Y_\Delta Q_{met} = V_{reactor}\mu x = (s_0 - s)Y_{X/S}F - xk_e \tag{8.122}$$

$$\frac{Q_{met}}{V_{reactor}} = \left[(s_0 - s)Y_{X/S}D - \frac{xk_e}{V_{reactor}}\right]\Big/ Y_\Delta \tag{8.123}$$

Recall that, as before, $Y_{X/S}$ may depend on the culture age in a batch reactor and upon dilution rate D in a continuous-flow system. The dependence of $Y_{X/S}$ (and thus Y_Δ) on a cell maintenance appears in Eq. (7.26).

Some economic estimates from Abbott and Clamen [43] as of 1973 indicate that both heat-transfer and mass-transfer (oxygen) operating costs of bacterial cell production from the substrates in Table 8.7 are appreciable fractions of total costs.

8.10.1 Heat-Transfer Correlations

From Eq. (8.118) and the overall heat balance [Eq. (8.119)] for heating, cooling, or sterilizing, the general working equation for heat-transfer design is

$$Q_{exch} = \bar{h}A\,\Delta T \tag{8.118a}$$

An expression for the overall heat-transfer coefficient $\bar{h}$, analogous to the earlier overall coefficient K_l for gas-liquid mass transfer, is required. For steady-state heat transfer through a flat wall of thickness L_w separating the fermentation fluid at $T_{bulk,1}$ from heating or cooling fluid at $T_{bulk,2}$ continuity of heat flux demands

$$h_{w1}(T_{bulk,1} - T_{wall,1}) = k_s\left(\frac{T_{wall,1} - T_{wall,2}}{L_w}\right)$$
$$= h_{w2}(T_{wall,2} - T_{bulk,2}) \quad \text{kcal/(cm}^2\cdot\text{h)} \tag{8.124}$$

where k_s is the thermal conductivity of the wall in kilocalories per centimeter per second per Celsius degree. In terms of an overall heat-transfer coefficient $\bar{h}$, defined by

$$\text{heat flux} = \bar{h}(T_{\text{bulk},1} - T_{\text{bulk},2}) \tag{8.125}$$

rearrangement of the previous equations yields:

$$\frac{1}{\bar{h}} = \frac{1}{h_{w1}} + \frac{1}{k_s} + \frac{1}{h_{w2}} \qquad \text{(planar wall)} \tag{8.126}$$

In clear analogy with our mass-transfer discussions, the overall resistance $1/\bar{h}$ is the sum of three resistances in series. For heat transfer across a cylindrical-tube wall in heating or cooling coils, the cross-sectional area for heat transfer changes continuously through the wall. In this instance the appropriate equation for $\bar{h}$ is

$$\frac{1}{\bar{h}_o d_o} = \frac{1}{h_o d_o} + \frac{\ln (d_o/d_i)}{2k_s} + \frac{1}{h_i d_i} \qquad \text{(tube wall)} \tag{8.127}$$

where d_i and d_o are the tube inside and outside diameters, respectively. Note the use of subscript o for $\bar{h}_o$ since it reminds us to use the outside tube surface as the basis for a heat-transfer area. The thermal conductivity k_s of the solid depends on the material; e.g., at 100°C, $k_s = 0.908$ cal/(s·cm·K) (copper) and 0.107 cal/(s·cm·K) (steel): k_s increases slowly with diminishing temperature. Appropriate values for different heat exchanger materials are found in standard engineering handbooks.

The analysis of momentum and heat transfer at either fluid-solid interface gives the individual-side heat-exchange coefficients (h_{w1}, h_{w2}) or (h_o, h_i) in Eq. (8.126) and (8.127). Where such individual coefficients vary along the heat-transfer surface, an overall local heat-transfer coefficient is defined by equations such as (8.126) and (8.127), and a detailed integration over the heat-transfer area is needed to calculate the total heat transferred.

For fluid-wall heat transfer, the important dimensionless groups are the following:

$$\text{Nusselt number} = \text{Nu} = \frac{hd}{k_f} \tag{8.128a}$$

$$\text{Prandtl number} = \text{Pr} = \frac{C_p \mu}{k_f} \tag{8.128b}$$

$$\text{Brinkman number} = \text{Br} = \frac{\mu u^2}{k_f(T_{\text{bulk}} - T_{\text{wall}})} \tag{8.128c}$$

$$\text{Froude number} = \text{Fr} = \frac{u^2}{gd} \tag{8.128d}$$

and

$$\text{Reynolds number} = \text{Re} = \frac{\rho u d}{\mu} \tag{8.128e}$$

where k_f = thermal conductivity of fluid, cal/(s·cm·°C)
C_p = heat capacity, cal/(g·°C)
d = distance (tube diameter or spacing, cm)
μ = viscosity (poise)
u = velocity (cm/s)
g = gravitational constant (g·cm/s²)

As discussed elsewhere [5], the Brinkman number represents heat production by viscous dissipation divided by heat transport by conduction and may usually be neglected at the heat-exchanger surface for our purposes. (In the impeller-tip vicinity, this number becomes important.) Similarly, in a baffled vessel or one with an off-center stirrer, the Froude number is usually negligible.

The heat-transfer coefficient h, rendered dimensionless as Nu, is a function of Pr and Re:

$$\text{Nu} = f(\text{Pr}, \text{Re}) \tag{8.129a}$$

As hydrodynamics may vary with the aspect of the exchange surface, i.e., the length L to diameter d ratio, L/d, correlations are also available in the form

$$\text{Nu} = f'\left(\text{Pr}, \text{Re}, \frac{L}{d}\right) \tag{8.129b}$$

Temperature variations induce variations of fluid properties at different points near the heat-transfer surface. As liquid viscosity is the most important of these, the ratio

$$\mu_b/\mu_0 = \text{viscosity}\ (T_{\text{bulk fluid}})/\text{viscosity}(T_{\text{wall}})$$

is a useful correlating variable:

$$\text{Nu} = f''\left(\text{Pr}, \text{Re}, \frac{L}{d}, \frac{\mu_b}{\mu_0}\right) \tag{8.129c}$$

As h (and therefore Nu) may be defined as a local transfer coefficient or as one which has been averaged over the surface in several possible ways, care must be taken to use the appropriate ΔT_{loc} or ΔT_{av} with Nu_{loc} or Nu_{av} from literature correlations.

For fluids of viscosity near that of water, a useful correlation in turbulent flow (heating or cooling) is†

$$\text{Nu} = \frac{hd}{k} = 0.023\ \text{Re}^{0.8}\text{Pr}^{0.4} \tag{8.130}$$

† W. H. McAdams, *Heat Transmission*, 3d ed., p. 152. McGraw-Hill Book Company, New York, 1954.

which appears valid when

$10^4 \le \text{Re} \le 1.2 \times 10^5$	turbulent
$0.7 \le \text{Pr} \le 120$	valid for all liquids except molten metals
$\frac{L}{d} \ge 60$	long tubes

A modification due to Seider and Tate† incorporates an allowance for larger temperature differences; it appears useful for estimating heat transfer with viscous fluids (such as oils):

$$\text{Nu} = \frac{hd}{k} = 0.027\,\text{Re}^{0.8}\text{Pr}^{0.33}\left(\frac{\mu_b}{\mu_0}\right)^{0.14} \tag{8.131}$$

When natural convection is also important due to the presence of nonuniform fluid density, the Grashof number

$$\text{Gr} = \frac{d^3 g\,\Delta\rho\,\rho_{av}}{\mu^2} \tag{8.132}$$

appears in the correlation‡ for the liquid flowing in horizontal tubes:

$$\text{Nu} = 1.75\left[\frac{d}{L}\cdot\text{Pr Re} + 0.04\left(\frac{d}{L}\,\text{Gr Pr}\right)^{0.75}\right]^{1/3}\left(\frac{\mu_b}{\mu_0}\right)^{0.14} \tag{8.133}$$

(For vertical tubes, the viscosity ratio is replaced by 1.0 and the constant 0.04 by 0.0722.)

When the fluid is known to be non-Newtonian, the forms change. Two equations§ which have been used for pseudoplastic fluids (Sec. 8.8) are

$$\text{Nu} = \frac{hd}{k} = 2.0\left(\frac{d}{L}\,\text{Re Pr}\right)^{1/3}\left[\frac{\eta_b(\text{bulk})}{\eta_b(\text{wall})}\left(\frac{3+1/n}{4}\right)\frac{1}{2}\right]^{0.14} \tag{8.134a}$$

or

$$\text{Nu} = \frac{hd}{k} = 1.75\left(\frac{d}{L}\,\text{Re Pr}\right)^{1/3}\left(\frac{3n+1}{4n}\right)^{1/3} \tag{8.134b}$$

where η_b is the apparent viscosity (Eq. 8.92) evaluated at the bulk fluid or wall temperature. Note that for a Newtonian fluid ($n = 1$) without large bulk-wall temperature differences, Eq. (8.134*b*) reduces to Eq. (8.133). The viscosity variations with temperature, however, are explicitly represented in Eq. (8.134*a*) in the same form as Eq. (8.133).

A wide variety of reactor heat-transfer surface and flow configurations are possible. Some correlations for several of these are given in Example 8.3; others

† F. E. N. Seider and G. E. Tate, "Heat Transfer and Pressure Drop of Liquids in Tubes," *Ind. Eng. Chem.*, **28**:1429, 1936.

‡ R. C. Martinelli and L. M. Boelter, *AIChE Mtg.*, 1942 (cited in McAdams, op. cit.).

§ S. E. Charm and E. W. Merrill, "Heat Transfer Coefficients in Straight Tubes for Pseudoplastic Food Materials in Streamline Flow," *Food Res.*, **24**:319, 1959.

can be found in standard heat-transfer texts and in Chap. 3 of Charm (ref. 30 of Chap. 9). Some example calculations for heat-transfer coefficients and heat-exchanger duties are considered in the problem section. Microbial fluids occasionally deposit a residue on the heater surface leading to fouling (time-varying wall heat-transfer coefficient) and a decrease in h for the fluid-side.

Example 8.3 Heat transfer correlations

Natural convection from vertical plane or cylinder:†

$$\text{Nu} \equiv \frac{hL}{k} = c(\text{Gr Pr})^a \tag{8E3.1}$$

where L is the plate length or cylinder diameter, all parameters are evaluated at $(T_{\text{bulk}} + T_{\text{wall}})/2$, and

$3.5 \times 10^7 \le \text{Gr Pr} \le 10^{12}$ $\quad c = 0.13,\ a = \frac{1}{3}$ (turbulent)

$10^4 \le \text{Gr Pr} \le 3.5 \times 10^7$ $\quad c = 0.55,\ a = \frac{1}{4}$ (laminar)

Heat transfer in concentric annuli:‡

Streamline flow:

$$\text{Nu} \equiv \frac{hd}{k} = \left(\frac{d_o}{d_i}\right)^{0.8}(\text{Re Pr})^{0.45}\left(\frac{d}{L}\right)^{0.45}\text{Gr}^{0.5} \tag{8E3.2}$$

where d_o, d_i = outside and inside diameters

Turbulent flow:

$$\frac{h}{c_p G} = \begin{cases} \dfrac{0.23\,\text{Pr}^{-2/3}(\mu_b/\mu_0)^{0.14}}{[(d_o - d_i)/\mu_b]^{0.2}} & \text{outer wall} \\ \dfrac{(0.023)(0.87)(d_o/d_i)^{0.53}}{[(d_o - d_i)G/\mu_b]^{0.2}} & \text{inner wall} \end{cases} \tag{8E3.3}$$

Gravity flow over horizontal tube surfaces:

$$h = 65\left(\frac{w}{\mu_t L d_o}\right)^{1/3} \quad \text{Btu/(h·ft·°F)} \quad \text{if } \frac{w}{2\mu_c L} < 525 \tag{8E3.4}$$

where w = liquid flow rate
L = tube length
d_o = outside diameter

Turbulent flow in tubes:§

$$\text{Nu} = \frac{hd}{k} = 0.023\,\text{Re}^{0.8}\,\text{Pr}^b \tag{8E3.5}$$

$$b = \begin{cases} 0.4 & \text{for heating} \\ 0.3 & \text{for cooling} \end{cases}$$

† W. J. King, "Free Convection," *Mech. Eng.*, **54**:347, 1932.

‡ C. C. Monrad and J. F. Pelton, in W. H. McAdams, "Heat Transmission," McGraw-Hill Book Company, New York, 1954.

§ F. W. Dittus and C. M. K. Boelter, *Univ. Calif. Publ. Eng.*, **2**:443, 1930 (see McAdams, *Heat Transmission*).

Flow perpendicular to isolated cylinder:†

$$\mathrm{Nu} = \frac{hd}{k} = (\mathrm{Pr})(0.35 + 0.56\ \mathrm{Re}^{0.52}) \tag{8.E3.6}$$

Flow perpendicular to one row of tubes centered 2d apart:†

$$\mathrm{Nu} = \frac{hd}{k} = 0.21\ \mathrm{Re}_m^{0.6}\ \mathrm{Pr}^{1/3} \tag{8E3.7}$$

where Re_m is Re evaluated at u_{max} and $2d$ is defined as

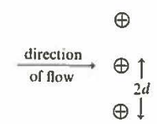

Staggered successive rows of the above type:†

Same as Eq. (8E3.7), but coefficient 0.21 replaced by 0.27 for 3 rows, 0.30 for 5 rows, 0.33 for 10 tube rows or more.

The subject of transport of heat and mass is, we reiterate, an enormously developed area. The present chapter has provided some conceptual guidelines for estimating the quantities of interest. The literature contains a vast number of references for heat- and mass-transfer correlations under a variety of experimental conditions, as indicated in some of the general references of this chapter. Where possible, use of correlations from experimental configurations most apropos to the situation of interest should be practiced, always taking note of the margin of (un)certainty of the correlation.

8.11 STERILIZATION OF GASES AND LIQUIDS BY FILTRATION

Previous sections discussed use of elevated temperature to effect the desired level of sterilization of a liquid. High temperatures can damage medium components, and heat sterilization of gases is not economical. A common alternative approach applicable equally to gases and liquids is the use of appropriate filters to remove undesirable viable cells and, where possible, viruses from the appropriate process stream.

Filters may be made from sintered porcelain, asbestos fiber mats, or synthetic microporous polymer membrane. While the first two categories are important historically, nearly all filtration today associated with sterilization relies on the

† S. E. Charm, *Fundamentals of Food Engineering*, 2d ed., Chap. 4, Avi Publishing, Westport, Conn., 1971.

use of polymeric microporous membranes. These filters may now be routinely used to render sterile a gas flow or dilute liquid suspension entering a bioreactor.

The value of these membrane filters derives from several characteristics:

1. The porous membranes formed, typically from stable gels, have extremely uniform porosity, thereby providing absolute retention of all particles above a certain size (controllable by pore size modification).
2. The extreme porosity (often 70–80%) and thinness (ca. 100 microns) provide low flow resistance, thus allowing a high solvent (water) flux. For example, one liter can be passed through a filter having 0.2 micron pores and 10 cm^2 of filter area in 2–3 min.
3. The membrane filter materials (including cellulose nitrate, cellulose acetate, vinyl polymers, polyamides, and fluorocarbons) are all steam sterilizable and stable against most aqueous suspensions and many organic materials.
4. The quality of the manufactured membrane is easily tested by challenge with a suspension of nearly uniformly sized viable microorganisms. For example, 0.22 micron pore filters are tested with a suspension of *Pseudomonas aeruginosa* bacteria, and *Serratia marcescens* effectively probe a 0.45 micron pore membrane. Viral strains may be used to test filters with very small pore diameters, but uncertainties in virus culture techniques weaken this test for quality control.

The filters of this section are used to remove trace particulates from air or liquid streams, typically to render them sterile (pharmaceuticals) or at least free from pathogens (beverages). Filtration for removal of particles from concentrated suspensions such as fermentation broths is discussed in Chapter 11.

PROBLEMS

8.1 Oxygen diffusivities in protein solutions Stroeve [53] noted that an 1881 derivation of James Clerk Maxwell's (*Treatise on Electricity and Magnetism*, vol. 1, 3d ed.) for diffusion through a fluid containing spherical obstructions simplified to the form below when the obstructions were impermeable:

$$\frac{\mathscr{D}}{\mathscr{D}_0} = \frac{2(1-f)}{2+f}$$

where $\mathscr{D}$ = apparent diffusivity in suspensions
$\mathscr{D}_0$ = apparent diffusivity in pure fluid
f = volume fraction of obstructions

He found that the form gave reasonable fit to experimental data provided that f was defined as $f = f_p + f_h$, where f_p is the volume fraction of protein and f_h the volume fraction of water physically immobilized on the protein surface. Taking the dimensions of the protein to be those of hydrated hemoglobin (spheroid 65 by 55 by 55 Å), calculate and plot $\mathscr{D}/\mathscr{D}_0$ vs. f_p (not f) assuming no, one, or

two monolayers of immobilized water around the protein (range of f_p is 0.1 to 0.5). Compare your results with the following measured values for methemoglobin and comment:

$\mathscr{D}/\mathscr{D}_0$	0.69	0.43	0.17
f_p	0.1	0.2	0.4

8.2 Mass-transfer coefficient Determine k_l for the following conditions:

Liquid volume 10 L
Turbine impeller diameter 10 cm
Vessel diameter 50 cm
Speed (rev/min) 200
Air medium binary diffusion coefficient 0.5×10^{-5} cm^2/s
Airflow rate 2L/min
Medium density 1.2g/cm^3
Medium viscosity 0.01 g/(cm·s)

8.3 Oxygen transfer, nonagitated Consider a 0.5L unstirred aerated chemostat with 10 orifices mounted in the bottom. If each is 1 mm in diameter and has an airflow rate of 5 mL/min, what specific cell growth rate will be maintained if oxygen is limiting? Neglect breakup and coalescence and assume the medium is sufficiently dilute for it to behave like pure water.

μ_{max} 0.5 h^{-1} K_s 0.1 mM σ 72 dyne/cm
g 980 cm/s^2 μ_{gas} 2×10^{-4} g/(cm·s) $\mathscr{D}$ 0.5×10^{-5} cm^2/s
μ_{liq} 10^{-2} g/(cm·s) ρ_{gas} 1.4 g/L H_L 10 cm
$Y_{O/X}$ 1 g O_2/g cell x 1.0 g cells/L

8.4 "Variation" of $k_l a$ with temperature Surface renewal theory provides that the mass transfer coefficient k_l varies as $(\mathscr{D})^{1/2}$. For diffusion in liquids, the Stokes-Einstein relation gives $\mathscr{D}/\mu T$ constant. Thus the variation of k_l with temperature is predicted to follow that of $(T/\mu)^{1/2}$.

(*a*) Using any reference text for the viscosity of water vs. temperature, calculate and plot the expected variation of $k_l(T)/k_l(T = 15\ C)$ in the range 15 to 60 C.

(*b*) The equilibrium dissolved oxygen levels (Table 8.1) vary with temperature. Assuming that the interfacial area volume a is not temperature-dependent, calculate and plot the ratio $\gamma = [k_l a c^*(T)/k_l a c^*(T = 15\ C)]$ as in part (*a*).

Comment on the utility of the nearly constant value of γ predicted in part (*b*). Experimentally, this constancy has been confirmed. [54].

8.5 Batch reactor: growth vs. mass transfer limitation A batch fermentation is conducted at 35 C. Experiments with sodium sulfite oxidation indicate that $k_l a c_l^* = 0.1$ mol/(L·h). The culture has a doubling time, in exponential growth, of 30 min, and an oxygen yield coefficient of 0.6 g cells/g O_2.

(*a*) Calculate the exponential specific growth rate, μ.

(*b*) Use Eq. (8.14) to calculate the dissolved oxygen level, c_l, as the cells increase from $x_0 = 10^{-6}$ g/mL. Plot c_l vs. x. At what biomass level is c_l predicted to become zero?

(*c*) In reality, c_l does not become zero. Rather, μ becomes a function of c_l at low dissolved oxygen levels as in, for example, Eq. (8.15). Use Eq. (8.15) and the same parameter values as above to calculate c_l vs. x. Take $K_{O_2} = 0.05$ m mol/L. (Easiest to assume c_l and calculate x.)

(*d*) For $c_l = 0.9c_l^*$, we have a *growth-limited* condition, while $c_l = 0.1c_l^*$ gives a *mass-transfer* limited condition. Use Eq. (8.15) and your graph in part (*c*) to deduce the ranges of x values corresponding to *growth* and *mass-transfer* limited operation.

(*e*) The right hand side of Eq. (8.15) is simply (dx/dt). Plot (dx/dt) vs. x on the same graph as part (*c*). What expression gives x at $(dx/dt)_{max}$?

8.6 Effect of pressure Oxygen transfer has been increased by augmenting the oxygen partial pressure, p_{O_2}, as may be easily done by use of pure oxygen in place of air feeds. Operation at higher pressures has also been proposed. Unfortunately, cultures may exhibit oxygen inhibition due, for example, to the formation of excess active forms of oxygen within the cell which may damage functions which require a local reducing atmosphere.

(*a*) Assume that growth-dependence on oxygen can be represented as

$$\mu = \frac{\mu_{max} c_l}{K_{O_2} + c_l + c_l^2/K_i}$$

or

$$\frac{\mu}{\mu_{max}} = \frac{\bar{c}}{1 + \bar{c} + \gamma \bar{c}^2}$$

where $\gamma = K_{O_2}/K_i$ and $\bar{c} = c_l/K_{O_2}$. Show that the maximum specific growth rate occurs at $\bar{c} = \gamma^{-1/2}$.

(*b*) Using Eq. (8.15), modified to include the oxygen inhibition term in part (*a*) above, derive an equation that will predict what oxygen pressure, p_{O_2}, should be used at any x value to maintain maximum cell growth. Since μ(max) = constant, give also the required time dependence for $p_{O_2}(t)$.

8.7 Metabolic product export (*a*) At times 1, 2, 3, and 4 h in an L-aspartate producing fermentation, the extracellular product levels are measured as 1, 2, 3, and 4 g/L, respectively. If the surfactant cetylpyridinium chloride is added at $t = 0$, the corresponding measured product levels in the medium are 12, 22, 30, and 35 g/L. Can you say what fundamental process(es) kinetically govern the appearance of product in the original fermentation? in the surfactant-modified medium? (data from Ref. 55).

(*b*) Amino acid export in some *E. coli* appears to be a balance between simultaneous passive transport out of the cell and active transport into the cell. Write a rate equation for amino acid export which is governed by these two phenomena. Using radiolabeled carbon in the amino acid, outline some initial rate measurement experiments by which you could determine all of the parameters in your proposed rate equation.

Mutation programs to eliminate catabolite repression and active transport uptake can lead to transport-limited product export (See Ref. 56).

8.8 Microbead immobilized mycelia The adsorption of spores of a *Penicillium chrysogenum* strain to 300–500 μm porous particles was used to create an immobilized mycelial catalyst, the characteristics of which are compared below with a mycelial suspension culture. Both were propagated in the same bubble column bioreactor.

(*a*) Assuming (roughly) that k_l varies as $(\mu)^{-1/2}$, what was the ratio of viscosities in the cultures: μ (suspension)/μ(immobilized)? What, in your view, allows a broth with a higher biomass level to exhibit a lower viscosity?

(*b*) Discuss the trade-offs in costs of suspension culture vs. immobilized culture which would lead to choice of the most economic process [57].

	Suspension	Immobilized
x_{max}(g/L)	17.0	29.0
p_{max}(g/L)	2.0	5.5
$k_l a \Delta c$ (m moles O_2/L-h-atm)	50–100	100–350
Basis: Power input (kW/m^3)	2.3	2.3
Oxygen transfer economy (kg O_2/kWh)	0.21	0.48
Specific energy consumption (kWh/g pen G)	0.12	0.07

8.9 Scale-up Methods Table 8.5 provides a scale-up basis under various circumstances (e.g., constant P/V).

(*a*) Discuss the (un)desirable effects on other operating variables resulting from scaling-up at constant reference of (P/V), N_i, F_{ij}/V, N_iD_i, or Re_i.

(*b*) It has been suggested that scale-up is best done by keeping k_la and fluid shear (tip velocity) constant, in particular $D_i/T \sim 0.25 - 0.4$ and $N_iD_i = 0.5$ m/s. Use the correlations of this chapter to indicate how (P/V), N_i, F_{ij}/V and Re_i would vary under scale-up with these mass transfer and shear guidelines [58].

8.10 Scaling parameters in aeration (*a*) In agitated aeration, $\mathrm{Sh} = \alpha \mathrm{Re}_i^{m_1}\mathrm{Sc}^{m_2}$ according to many correlations. Assuming constant bubble size, show that achievement of identical values of k_l in two different vessels, e.g., small (I) and large (II) requires that the impeller speed in revolutions per minute N_i scale as follows:

$$\frac{N_i(\mathrm{II})}{N_i(\mathrm{I})} = \left[\frac{D_i(\mathrm{I})}{D_i(\mathrm{II})}\right]^{2-1/m_1}$$

(*b*) Consequently, establish that constant k_l implies

$$\frac{(P/V)_{\mathrm{II}}}{(P/V)_{\mathrm{I}}} = \left[\frac{D_i(\mathrm{I})}{D_i(\mathrm{II})}\right]^{4-3/m_1}$$

For the turbulent correlation in the text, what fortuitous result arises in the previous equation?

(*c*) For conditions where the bubble size itself is determined by impeller conditions, what relations hold for $N_i(\mathrm{II})/N_i(\mathrm{I})$?, $(P/V)_{\mathrm{II}}/(P/V)_{\mathrm{I}}$?

8.11 Bubble-column performance (*a*) Estimate a, H, and k_l for a bubble column under the following conditions:

Gas flow = 20 std ft^3/min

Liquid flow = 25 gal/min (water)

Column ID = 16 in

Average bubble diameter D = 0.25 in

(*b*) An alternate correlation [59] for bubble swarm (liquid or liquid-liquid mass transfer) is

$$\mathrm{Sh} = 2.0 + 0.0187\left[\mathrm{Re}^{0.484}\mathrm{Sc}^{0.339}\left(\frac{Dg^{1/3}}{\mathcal{P}^{2/3}}\right)^{0.072}\right]^{1.61}$$

Compare the explicit dependence of each physical parameter with that of the text formula. Evaluate k_l again and the percentage difference between the two estimates.

8.12 Stream reaeration (rapids and ponds) A moving stream might be approximated by alternating deep and shallow segments of the same width. If the "deep" and "shallow" segments have depths h_D, h_S and lengths l_D, l_S:

(*a*) What is the ratio of aeration mass-transfer coefficients for the shallow to deep segments?

(*b*) Lumping biological activity into a single species, develop an analytic description for substrate utilization by aerobic species of this ponds-rapids configuration, assuming oxygen transfer to be limiting. State your assumptions clearly.

(*c*) Develop expressions (making simplifying assumptions if needed) for the fraction of total microbial growth occurring in the pond and the fraction of total oxygen transfer occurring in the rapids.

8.13 Simplified stream reaeration: (Streeter-Phelps equation) Stream reaeration can be described as a simple plug-flow phenomenon under conditions where organic sedimentation, sediment reactions, and loss of organic volatiles is unimportant. A balance on organic matter S in a stream of velocity u gives

$$\frac{\partial s}{\partial t} = -u\frac{\partial s}{\partial z} - \mu_{\max}s$$

and the oxygen balance is

$$\underset{\text{Gradient}}{\frac{\partial c_0}{\partial t}} = \underset{\text{Gradient}}{-u\frac{\partial c_0}{\partial z}} + \underset{\text{Gain by mass transfer}}{\bar{k}_{O_2}(c^*_{O_2} - c_{O_2})} - \underset{\text{Loss by microbial oxidation}}{\mu_{\max}sY_{O/S}}$$

+ photosynthesis rate − algal respiration rate − sedimentation rate

(*a*) If oxygen is always in excess for the *microbes* oxidizing the nutrients, show that

$$s(z) = s_{z=0}\exp\left(-\mu_{\max}\frac{z}{u}\right)$$

(*b*) At steady state, neglecting photosynthesis, algal respiration, and sedimentation, show that the oxygen-concentration profile satisfies the Streeter-Phelps equation

$$c^*_{O_2} - c_{O_2}(z) = \frac{Y_{O/S}\mu_{\max}s_{z=0}}{\bar{k}_{O_2} - Y_{O/S}\mu_{\max}}\left[\exp\left(-Y_{O/S}\mu_{\max}\frac{z}{u}\right) - \exp\left(-\frac{\bar{k}_{O_2}z}{u}\right)\right] + (c^*_{O_2} - c_{O_2,z=0})\exp\left(-\frac{\bar{k}_{O_2}z}{u}\right)$$

where $\bar{k}_{O_2} = \bar{k}_{O_2}/l$

$\bar{k}_{O_2}$ = eddy-averaged oxygen-transfer coefficient [from (8.88)]

l = stream depth

(*c*) Establish analytically that for the Streeter-Phelps treatment, $c^*_{O_2} - c_{O_2}(z)$, known as the *oxygen deficit*, has a single minimum at

$$c^*_{O_2} - c_{O_2}(z) = \frac{Y_{O/S}\mu_{\max}s_{z=0}}{\bar{k}_{O_2}}\exp\left(-Y_{O/S}\mu_{\max}\frac{z}{u}\right)$$

What is the downstream distance z corresponding to this point of maximum oxygen deficit? Repeat this derivation including constant photosynthesis, algal respiration, and sedimentation rates.

8.14 Heat transfer, bubble size For the stoichiometry given in Prob. 5.13, (*a*) suppose that a batch aerobic fermentor is run in a cylindrical tank of 6-ft diameter with 130 ft of 1-in-diameter cooling coil arranged on 2-in spacing. Assume that all heat transfer is through the coils and that the bubble sparger always maintains a sufficient K_la value so growth is not oxygen-limited. If the average fluid velocity perpendicular to the coiled tubes is 10 percent of the impeller-tip velocity, what is the minimum speed in revolutions per minute needed for heat transfer if the average cooling liquid temperature is 18°C and the fermentor should operate no higher than 28°C? Repeat this calculation for cell densities of 10^6, 10^7, 10^8, and 10^9 cells per milliliter (impeller diameter = 4.5 ft, thickness = $\frac{1}{2}$ in, height = 6 in, single paddle).

(*b*) At 10^9 cells per milliliter, the aeration rate is such that 10 percent of the entering oxygen is consumed by the cells. For a poorly designed sparger, bubble size is too large. What stirrer speed (revolutions per minute) is needed to give adequate bubble size? Can this reasonably be achieved with one large paddle? Would a better design include a second much shorter, high-speed paddle just above the sparger with, for example, $D_2 = 0.2D_1$, $N_2 = 10N_1$?

8.15 Dimensionless groups: Buckingham π theorem In heat transfer by forced flow of fluid over a tube surface, the parameters which are physically important in determining the fluid-side heat-transfer coefficient (a conductance h) are the characteristic diameter of the pipe D, the fluid velocity u, and viscosity μ (in poise), density ρ, specific heat at constant pressure C_p (in calories per mole per degree), and the thermal conductivity of the fluid k_f (in calories per second per centimeter per degree). The Buckingham π theorem states that "the functional relationship between q quantities whose units can

be given in terms of p fundamental units can be written as a function of $q - p$ dimensionless groups. The fundamental units in heat transfer are mass m, length l, time t, and temperature T.

(*a*) Express h, D, u, μ, ρ, C_p, and k in terms of such units, i.e., variable $= m^a l^b t^c T^d$.

(*b*) Four dimensionless groups are commonly formed from these variables: Nu ($\equiv hD/k_f$), Re ($\equiv \rho Du/\mu$), Pr ($\equiv C_p\mu/k_f$) and Stanton number St ($\equiv h/uC_p\rho$). Comment. By inspection, what does the Stanton number represent?

8.16 Power-law fluids: starch hydrolysis Pastes resulting from cooking 1% wt/vol amylopectin in water are pseudoplastic, thus following the power law, $\tau = \eta\dot{\gamma}^n$, with $n < 1.0$. For batch α-amylase hydrolysis of this paste, the following changes with increasing time were observed. [60]:

η, dyn·s^n/cm^2	0.32	0.26	0.20	0.14	0.10	0.03
n	0.73	0.75	0.78	0.83	0.85	0.98

(*a*) Show that these data can be described by

$$\tau_0 = \eta\dot{\gamma}_0^n \qquad \text{where} \quad \tau_0, \dot{\gamma}_0 = \text{const}$$

(*b*) Establish with an appropriate graph that all τ-vs-$\dot{\gamma}$ curves at each degree of hydrolysis pass through a common point.

(*c*) How would the power input at fixed rotation speed vary with time? Could this parameter be used for on-line batch-process control?

8.17 Power input vs. impeller speed in non-Newtonian fluids For non-Newtonian fluids with power-law indices n less than unity, the shear rate $\dot{\gamma}$ may be taken to be proportional to the impeller rotation rate N_i [61]. Show that:

(*a*) For a fluid between concentric cylindrical surfaces, shear stress on the outer cylinder (as the inner-cylinder rotation speed varies) changes according to $(d\tau/dN_i) \propto N_i^{n-1}$.

(*b*) The Reynolds number, $\mathrm{Re} = D_i^2 N_i \rho/\eta_v$, where η_v is the apparent viscosity (shear-rate-dependent), varies as $\mathrm{Re} \propto N_i^{2-n}$.

(*c*) For Reynolds numbers defined above, the data for power number ($\equiv P g_c/D_i^5 N_i^3 \rho$) vs. Reynolds number fall on or just below that correlation for the Newtonian-fluid values. Thus if P_0 varies as Re^a, establish that the power input P varies as $N_i^{3+a(2-n)}$.

(*d*) From the previous information, how would you evaluate the proportionality constant between $\dot{\gamma}$ and N_i for a non-Newtonian fluid?

8.18 Hydrocarbon-fermentation phases (*a*) For the quotation of Mimura et al. (and Fig. 8.14) describing the time course of a particular hydrocarbon fermentation, write a mathematical description of growth and substrate(s) utilization in each phase of the batch fermentation. For each "phase," indicate quantitatively where the controlling resistance(s) to growth may lie, i.e., hydrocarbon solubilization, oxygen transfer, cell metabolism, etc.

(*b*) Postulate various reasons why the cell-hydrocarbon-droplet-air-bubble-solvent system adopts each configuration mentioned by the authors. What obvious experiments are suggested by this direct observation? How would you discriminate between or prove the hypotheses advanced?

8.19 Double-substrate design (both gases) Hamer et al. ["SCP Production from Methane," p. 362 in *Single Cell Protein II*, S. R. Tannenbaum and D. I. C. Wang (eds.), MIT Press, Cambridge, Mass., 1975] report that the utilization of methane in the presence of oxygen in a continuous-flow continuously sparged fermentor can be described by the double Michaelis-Menten form of cell growth:

$$r_x = \mu_{\max} x \frac{c_1}{K_1 + c_1} \frac{c_2}{K_2 + c_2}$$

where 1 is oxygen, and 2 methane.

(*a*) Assuming constant yield coefficients, Y_1 and Y_2 (grams of cell per gram of substrate i, $i = 1, 2$), write down the steady-state balances for a sterile-feed system for cells and substrates 1 and 2.

Take the overall mass-transfer conductance to be $K_{ll}a$ and assume both liquid and gas phases to be completely mixed.

(*b*) As the dilution rate increases, wash-out will again occur. Show by graphical or analytical evaluation that washout occurs at about $D \approx 0.72\ \mathrm{h}^{-1}$ for the following parameter values: $K_1 = K_2 = 5 \times 10^{-4}$ g/L, $Y_l = 1.25$ g cell/g O_2, $Y_2 = 2.0$ g cell/g substrate, $K_{l1}a = K_{l2}a = 100\ \mathrm{h}^{-1}$, $c_1^* = 0.015$ g/L, $c_2^* = 0.007$ g/L, $\mu_{\max} = 0.8\ \mathrm{h}^{-1}$.

REFERENCES

Diffusion:

1. P. Weisz, "Diffusion and Chemical Transformation: An Interdisciplinary Excursion," *Science*, **179**: 433 (1973).

Oxygen demand of cultures and oxygen solubility:

2. R. K. Finn, "Agitation and Aeration," p. 69 in N. Blakebrough (ed.), *Biological Engineering Science*, vol. 1, Academic Press, Inc., New York, 1967.

Interactions between diffusion through liquid films and chemical reactions:

3. P. V. Danckwerts, *Gas-Liquid Reactions*, McGraw Hill Book Company, New York, 1970.
4. G. Astarita, *Mass Transfer with Chemical Reaction*, Elsevier Publishing Company, Amsterdam, 1967.
5. R. B. Bird, W. E. Stewart, and E. N. Lightfoot, *Transport Phenomena*, John Wiley and Son, Inc., New York, 1960.

Fermentation fluids:

6. H. Taguchi, "The Nature of Fermentation Fluids," *Adv. Biochem. Eng.* **1**: (1971).

Problems of scaling microbial reactors:

7. E. L. Gaden, Jr. (ed.), *Biotech. Bioeng.*, **8**: 1966 (Entire volume).

Mass-transfer examples in microbial reactors:

8. A. Moser, in *Proc. Int. Symp. Adv. Microb. Eng.*, **1**: 295–580, 1973.
9. K. Van't Riet, "Mass Transfer in Fermentation," *Trends in Biotechnology*, **1**(4): 113, 1983.

Mass-transfer correlations for oxygen transfer:

10. P. H. Calderbank and M. Moo-Young, "The Continuous Phase Heat and Mass Transfer Properties of Dispersions," *Chem. Eng. Sci.*, **16**: 39, 1961.
11. P. H. Calderbank, "Mass Transfer in Fermentation Equipment," p. 102 in N. Blakebrough (ed.), *Biochemical and Biological Engineering Science*, vol. 1, Academic Press Inc., New York, 1967.
12. K. Akita and F. Yoshida, "Bubble Size, Interfacial Area, and Liquid-Phase Mass Transfer Coefficient in Bubble Columns," *I & EC Process Des. Develop*, **13**: 84, 1974.
13. R. A. Bello, C. W. Robinson, and M. Moo-Young, "Mass Transfer and Liquid Mixing in External Circulating Loop Contactors," *Adv. Biotech.*, **1**: 547, 1981.
14. K. B. Wang and L. T. Fan, "Mass Transfer in Bubble Columns Packed with Motionless Mixers," *Chem Eng. Sci.* **33**: 945, 1978.

Batch oxygen demand:

15. R. T. Darby and D. R. Goddard, "Studies of the Respiration of the Mycelium of the Fungus *Myrothecoum verracaria*," *A. J. Bot.*, **37**: 379, 1950.

$k_l a$ by oxygen-electrode transient response:

16. W. C. Wernan and C. R. Wilke, "New Method for Evaluation of Dissolved Oxygen Response for $K_L a$ Determination," *Biotech. Bioeng.*, **15**: 571, 1973.

Absorption into aqueous films:
17. J. Briffaud and M. Engasser, "Growth and Excretion Kinetics in a Trickle-Flow Fermentor," *Biotech. Bioeng*, **21**, 2093 (1979).
18. K. Livansky, B. Prokes, F. Kihrt, and V. Benes, "Some Problems of CO_2 Absorption by Algae Suspensions," *Biotech. Bioeng. Symp. 4*, p. 513, 1973.

Methane-utilization stoichiometry:
19. D. L. Klass, J. J. Iandolo, and S. J. Knabel, "Key Process Factors in the Microbial Conversion of Methane to Protein," *CEP Symp. Ser.*, [93], **65**: 72, 1969.

Bubble-orifice-diameter correlations:
20. D. W. van Krevelen and P. J. Hoftijzer, "Studies of Gas-Bubble Formation: Calculation of Interfacial Area in Bubble Contactors," *Chem. Eng. Prog.*, **46**: 29, 1950.
21. K. Schügerl and J. Lücke, "Bubble Column Bioreactors," p. 1 in *Advances in Biochemical Engineering, Vol. 7*, T. K. Ghose, A. Fiechter, and N. Blakebrough, ed., Springer-Verlag, Berlin, 1977.

Photographic determination of a, H, D_{Sauter}:
22. P. H. Calderbank and J. Rennie, *Int. Symp. Distill.* (*Inst. Chem. Eng.*), 1960.

Shape-velocity dependence of large bubbles in Eq. (8.36):
23. R. M. Davies and G. I. Taylor, *Proc. Roy. Soc.*, **A200**: 375, 1956.

Free-surface mass transfer to falling film: See Ref 5, p. 540.

Free-surface mass-transfer to turbulent-stream surfaces:
24. G. E. Fortescue and J. R. A. Pearson, "On Gas Absorption into a Turbulent Liquid," *Chem. Eng. Sci.*, **22**, 1163, 1967.
25. D. J. O'Connor and W. Dobbins, "The Mechanism of Reaeration in Natural Streams," *J. Sanit. Eng. Div., Proc. ASCE*, **82**: SA6, 1966.

Turbine power number vs. Re (impeller):
26. J. H. Rushton, E. W. Costich, and H. J. Everett, "Power Characteristics of Mixing Impellers," pt. 2, *Chem. Eng. Prog.*, **46**: 467, 1950.

Aerated vs. nonaerated power requirements:
27. Y. Ohyama and K. Endoh, "Power Characteristics of Gas-Liquid Contacting Mixers, *Chem. Eng. Jpn.*, **19**: 2, 1955.
28. B. J. Michel and S. A. Miller, "Power Requirements of Gas-Liquid Agitated Systems," *AIChE J.*, **8**: 262, 1962.

Mixing by liquid jet injection:
29. H. Blenke, "Loop Reactors," p. 121 in *Advances in Biochemical Engineering, Vol 13*, T. K. Ghose, A. Fiechter, and N. Blakebrough, eds., Springer-Verlag, Berlin, 1979.

Weber number correlations, references: See Ref. 11 above.

Oxygen diffusivities in microbial films:
30. J. V. Matson and W. G. Characklis, "Oxygen Diffusion through Microbial Aggregates," *77th AIChE Meet.*, Pittsburgh, June 1973.

Ionic Strength influence on k_la:
31. C. W. Robinson and C. R. Wilke, "Oxygen Absorption in Stirred tanks: A Correlation for Ionic Strength," *Biotech. Bioeng.*, **15**: 755, 1973.

Surfactants and mass transfer:
32. W. W. Eckenfelder, Jr., and E. L. Barnhart, "The Effect of Organic Substances on the Transfer of Oxygen from Air Bubbles into Water," *AIChE J.*, **7**: 631, 1961.
33. A. Benedek and W. J. Heideger, "Effect of Additives on Mass Transfer in Turbine Aeration," *Biotech. Bioeng.*, **13**: 663, 1971.
34. D. N. Bull and L. L. Kempe, "Influence of Surface Active Agents on Oxygen Absorption to the Free Interface in a Stirred Fermentor," *Biotech. Bioeng.*, **13**: 529, 1971.
35. S. Aida and K. Toda, "The Effect of Surface Active Agents on Oxygen Absorption in Bubble Aeration I," *J. Gen. Appl. Microbiol.*, **7**: 100, 1963.
36. K. H. Mancy and D. A. Okun, "Effect of Surface Active Agents on the Rate of Oxygen Transfer," *Adv. Biol. Waste Treat.*, p. 111 (1963); see also papers by McKeown and Okun, Timson and Dunn, and Carber in this same reference.

Rheology of microbial broths:
37. A. Leduy, A. A. Marson, and B. Corpal, "A Study of the Rheological Properties of a Non-Newtonian Fermentation Broth," *Biotech. Bioeng.*, **16**: 61, 1974 (*A. pullulans* example).
38. J. A. Roels, J. van den Berg, and R. M. Voncken, "The Rheology of Mycelial Broths," *Biotech. Bioeng.*, **16**: 181, 1974 (Penicillin broth example).
39 N. Thompson and D. F. Ollis, "Evolution of Power Law Parameters for Xanthan and Pullulan Batch Fermentations," *Biotech. Bioeng.*, **22**: 875, 1980.
40. H. T. Chang and D. F. Ollis, "Generalized Power Law for Polysaccharide Solutions," *Biotech. Bioeng.*, **24**: 2309, 1982.

Morphology change with tanks in series:
41. D. Vrana: "Some Morphological and Physiological Properties of *Candida utilis* Growing 'Hypertrophically' in Excess of Substrate in a Two-Stage Continuous Cultivation," *Biotech. Bioeng. Symp.* **4**: 161, 1973.

Power-number evolution in non-Newtonian fermentation:
42. H. Taguchi and S. Miyamoto, "Power Requirement in Non-Newtonian Fermentation Broth," *Biotech. Bioeng.*, **8**: 43, 1966.

Cell density and mass transfer:
43. M. R. Brierley and R. Steel, "Agitation-Aeration in Submerged Fermentation, pt. 2: Effect of Solid Dispersed Phase on Oxygen Absorption in a Fermentor," *Appl. Microbiol.*, **7**: 57, 1959 (*A. Niger*).
44. G. F. Andrews, J. P. Fonta, E. Marrota, and P. Stroeve, "The Effects of Cells on Oxygen Transfer Coefficients," *Chem. Eng. J.*, **29**: B39, B47, 1984.

Agitation and cell damage: See Ref. 7 above and
45. M. Midler and R. K. Finn, "A Model System for Evaluating Shear in the Design of Stirred Fermentors," *Biotech. Bioeng.*, **8**: 71, 1966.

Paper-pulp suspensions:
46. N. Blakebrough and K. Sambamurthy, "Mass Transfer and Mixing Rates in Fermentation Vessels," *Biotech. Bioeng.*, **8**: 25, 1966.

Fibrous Filtration:
47. S. K. Friedlander, "Aerosol Filtration by Fibrous Filters," p. 49 in *Biochemical and Biochemical Engineering Science*, Vol. 1. (N. Blakebrough, ed.), Academic Press, New York, 1967.
48. C. N. Davies (ed.), *Air Filtration*, Academic Press, New York, 1973.

Membrane Filtration:
49. J. L. Dwyer, "Filtration in the Food, Beverage, and Pharmaceutical Industries," p. 121 in *Filtration: Principles and Practices, Part II*, Marcel Dekker, New York, 1979.

Heat transfer: Dimensional analysis: pp. 396ff in Ref. 5 and
50. A. I. Brown and S. M. Macro, *Introduction to Heat Transfer*, pp. 85–95, McGraw-Hill Book Company, New York, 1958.

Fermentation heat transfer cost:
51. B. J. Abbott and A. Clamen, "The Relationships of Substrate, Growth Rate, and Maintenance Coefficient to Single Cell Protein Production," *Biotech. Bioeng.*, **15**: 117, 1973.

Fermentation enthalpy balance:
52. C. L. Cooney, D. I. C. Wang, and R. I. Mateles, "Measurement of Heat Evolution and Correlation with Oxygen Consumption during Microbial Growth," *Biotech. Bioeng.*, **11**: 269, 1968.

Problems

53. P. Stroeve, "On the Diffusion of Gases in Protein Solutions," *Ind. Eng. Chem. Fundam.*, **14**: 140, 1975.
54. S. Aiba, J. Koizumi, J. S. Ru and S. N. Mukhopadhyay, "The Effect of Temperature on k_La in Thermophilic Cultivation of *Bacillus stearothermophilus*," *Biotech. Bioeng.*, **26**: 1136, 1984.
55. S. Fukui and Ishida, *Microbial Production of Amino Acids*, Kodansha Ltd., Tokyo and John Wiley, New York, 1972.
56. D. E. Rancourt, J. T. Stephenson, G. A. Vickell, and J. M. Wood, "Proline Excretion by *Escherichia coli* K12," *Biotech. Bioeng.*, **26**: 74, 1984.
57. K. Gbewonyo and D. I. C. Wang, "Enhancing Gas-Liquid Mass Transfer Rates in Non-Newtonian Fermentations by Confining Mycelial Growth to Microbeads in a Bubble Column," *Biotech. Bioeng.*, **25**: 2873, 1983.
58. J. Oldshue, "Fermentation. Mixing Scale-Up Techniques" *Biotech. Bioeng.*, **8**: 3, 1966.
59. G. A. Hughmark, "Holdup and Mass Transfer in Bubble Columns," *Ind. Eng. Chem. Process Des. Dev.*, **6**: 218, 1967.
60. Angel Cruz, "Kinetics and Shear Viscosity of Enzyme Hydrolyzed Starch Pastes," Ph.D. thesis, Princeton University, Princeton, N.J., 1976.
61. A. B. Metzner, R. H. Feehs, H. L. Ramos, R. E. Otto, and J. D. Tuthill, "Agitation of Viscous Newtonian and Non-Newtonian Fluids," *AICHE J.*, **7**: 3, 1961.

CHAPTER
NINE

DESIGN AND ANALYSIS OF BIOLOGICAL REACTORS

Knowledge of biological reaction kinetics and mass transfer, our primary concerns in Chaps. 7 and 8, is essential for understanding how biological reactors work. In order to assemble a complete portrait of biological reactor operation, however, it is necessary to integrate these two fundamental phenomena with the gas and liquid mixing and contacting patterns in the unit. Different design and scale-up procedures are required for reactors with different flow and mixing characteristics. Consequently, our major task in this chapter is to blend these various ingredients to obtain a coherent overall strategy and analysis of biological reactors.

In our considerations of cell kinetics in Chap. 7, the complex multiphase, interactive nature of cellular bioreactors was indicated. In that context, we examined different types of approximations which could be introduced in order to simplify the kinetic description of the cell population to a practical, workable level while at the same time trying to minimize errors introduced by the approximations. Similar problems and needs face us in biological reactor design and analysis. Now, we examine the interaction of the complex cellular kinetic features discussed earlier with an also complicated fluid flow, mixing, and heat transfer situation. We must now consider the effect of scale or size of the reactor on the mixing, flow, and heat and mass transfer patterns inside the reactor and how different flow and transport fields will influence and interact with biocatalyst kinetics. In this chapter we shall focus on different descriptions of contacting in

the reactor and the interaction of contacting patterns with biochemical reactions. In a fashion analogous to that considered earlier for cellular kinetics, we will need to apply approximations judiciously in order to obtain a workable reactor description.

In addressing questions which shall arise in this chapter of approximation strategies for describing bioreactors, it will be extremely useful to consider *relative time scales* and *relative length scales*. The spectrum of time and length scales which we encounter in bioreactor design and analysis is extremely large as suggested by the characteristic times and lengths in Figs. 9.1 and 9.2. A key to analysis of bioreactors is identification of the time and length scales for the phenomena of central interest in a particular reactor design context. Then, it is often possible to analyze phenomena with time or length scales much smaller or much larger than those characteristic of the process of main interest using relatively simple approximations. We have already encountered these ideas in our discussion of the quasi-steady state approximation in Chap. 3 and of structured models in Sec. 7.4.1. Here, comparison of length and time scales shall be used repeatedly in formulating a clear conceptual picture of the bioreactor processes which are most important in the reactor description for a particular design or analysis objective.

Also involved in decisions on appropriate reactor descriptions is the availability of experimental methods for characterizing the transport and reaction processes of interest, and the ability to solve the mathematical models based on

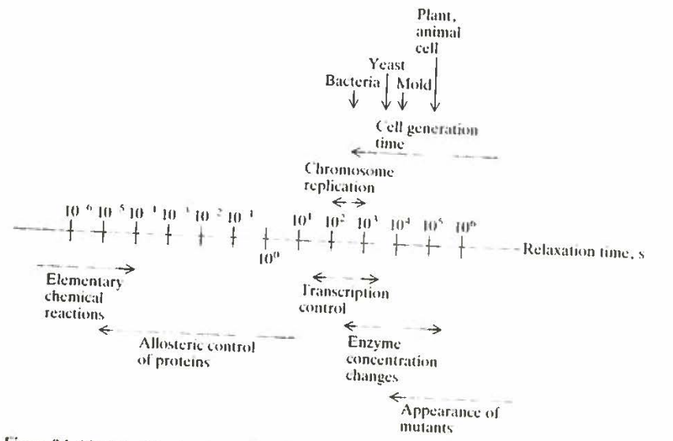

Figure 9.1 Characteristic times for biological responses important in bioreactor engineering (*After Roels [9]*).

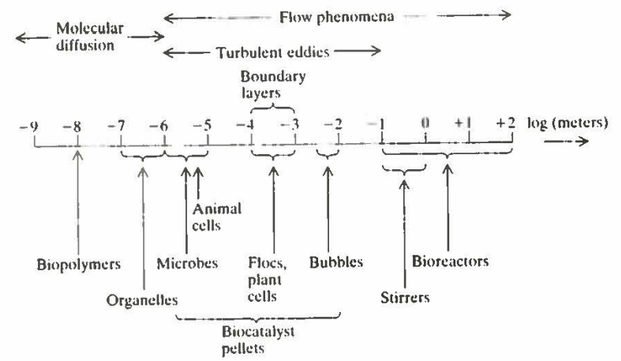

Figure 9.2 Characteristic length scales encountered in bioreactor design and analysis (*After Kossen [8]*).

certain reactor descriptions within reasonable time by currently available numerical methods. We shall see that our ability to arrive at predictive bioreactor models is best for the relatively simple situation of one or a few reactions catalyzed on one or a few enzyme catalysts and that, in the case of cellular reactors with complex multiphase mixing, our lack of knowledge of the structure of the cellular kinetics and of the structure of the physical flow situation hinders predictive analysis at this time. This clearly indicates a major need for additional fundamental research on bioreaction and interacting multiphase flow phenomena. Without more fundamental understanding of these processes, we shall always be faced with a considerable amount of empiricism and need for many scale-up experiments in order to arrive at what may be processes far from optimal.

To begin our consideration of bioreactor design and analysis, we consider elaborations on the ideal batch and continuous-flow stirred-tank (CSTR) reactors introduced in connection with our kinetics discussions in Chap. 7.

9.1 IDEAL BIOREACTORS

In Sec. 7.1, we introduced ideal well-mixed bioreactors. In these systems, mixing is presumed to be sufficiently intense and uniform such that reaction conditions and biocatalyst levels are effectively homogeneous throughout the reactor. This approximation will be valid if any gradients which do exist are sufficiently small so that the reaction rate locally for a given cell or biocatalyst particle is not changed significantly as that catalyst particle moves from one domain of the

reactor to another. Alternatively, if the catalyst particles circulate through different regions of the reactor very rapidly with respect to the characteristic response time of the catalyzed reaction to changing conditions, then calculating reactor performance based on the assumption of average, uniform conditions throughout will usually be satisfactory. Conditions like the ones described may be met in laboratory reactors and even pilot scale reactors, depending upon the process involved. In growth of dense cultures of filamentous organisms or organisms producing extracellular polymer, however, highly non-Newtonian conditions are encountered in which, even in small benchtop reactors, ideal mixing is not approximated.

Examination of the theory of ideal completely mixed bioreactors is important for several reasons. First, such reactors provide well-defined conditions for kinetic studies in the laboratory. Second, such models may frequently be used with reasonable success even when the conditions required for validity of these models are not well satisfied. Finally, such ideal mixing configurations provide a starting point for examination and characterization of nonideal mixing and reactors with significant spatial nonuniformities in reaction conditions. As we shall see, we can sometimes calculate and simulate in the laboratory nonidealities in large-scale reactors using model systems comprised of interconnected ideal reactors. In this section, we first elaborate on the ideal batch and ideal CSTR reactors discussed in Sec. 7.1. Finally we consider an ideal plug-flow reactor in which negligible backmixing occurs.

9.1.1 Fed-Batch Reactors

It is often desirable to add liquid streams to a batch bioreactor as the reaction process occurs. This can be done to add precursors for desired products, to add regulating compounds such as inducers at a desired point in the batch operation, to maintain low nutrient levels to minimize catabolite repression, or to extend the stationary phase by nutrient addition to obtain additional product. When a liquid feed stream enters the reactor, the culture volume is also altered, and this must be taken into account in the equations used to describe the reactor. Letting $F(t)$ denote the volumetric flow rate of the entering feed stream at time t and $c_{if}(t)$ denote the concentration of component i in this entering stream, the material balance on component i takes the following form:

$$\frac{d}{dt}[V_R \cdot c_i] = V_R \cdot r_{f_i} + F(t) \cdot c_{if} \tag{9.1}$$

Assuming that the densities of the entering liquid stream and of the culture fluid are both equal to ρ, a total mass balance on the reactor contents takes the following form:

$$\frac{d}{dt}[\rho \cdot V_R] = \rho \cdot F(t) \tag{9.2}$$

(How would this equation be modified to take into account different feed and reactor content densities resulting from, say, aeration of the reactor contents?) Assuming that the density ρ does not change substantially with time during batch operation, Eq. (9.2) becomes simply

$$\frac{dV_R}{dt} = F(t) \tag{9.3}$$

Carrying out the differentiation indicated on the left-hand side of Eq. (9.1) (remembering that now V_R is a function of time), substituting for dV_R/dt using Eq. (9.3), and rearranging the result gives a useful working form of the component i material balance

$$\frac{dc_i}{dt} = \frac{F(t)}{V_R}[c_{if} - c_i] + r_{f_i} \tag{9.4}$$

Eqs. (9.3) and (9.4) are the mass and component balance equations which describe this system. Assuming that suitable kinetic expressions r_{f_i} are available, these equations can be used to simulate the effect of different batch feeding strategies $F(t)$ on reactor performance.

9.1.2 Enzyme-Catalyzed Reactions in CSTRs

CSTRs used for enzyme-catalyzed reactions assume a variety of configurations (Fig. 9.3), depending on the method employed to provide the necessary enzyme activity. In the simplest design (a), enzymes are continuously added to and removed from the reactor via the feed and effluent lines. Obviously this approach is practical only when the enzymes are so inexpensive that they are expendable.

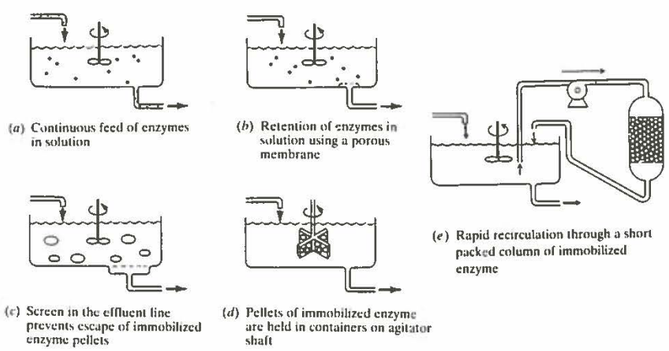

(a) Continuous feed of enzymes in solution

(b) Retention of enzymes in solution using a porous membrane

(e) Rapid recirculation through a short packed column of immobilized enzyme

(c) Screen in the effluent line prevents escape of immobilized enzyme pellets

(d) Pellets of immobilized enzyme are held in containers on agitator shaft

Figure 9.3 Schematic diagrams of CSTR designs for enzyme-catalyzed reactions.

Use of more costly enzymes requires that they be retained in the reactor or recycled. Recalling our discussions of enzyme immobilization in Chap. 4 suggests several possibilities, the first of these (Fig. 9.3*b*) employs an ultrafiltration membrane in the effluent stream with pores sufficiently small to prevent escape of the relatively large enzyme molecules in solution. A screen in the effluent line suffices if the enzyme is immobilized on insoluble particles which are suspended in the reaction mixture as a slurry (Fig. 9.3*c*). Another approach for physical retention of immobilized enzymes within the vessel is shown in Fig. 9.3*d*, where the enzyme is held in screen baskets attached to the agitator shaft. This configuration, which has also been widely used for study of gas-phase reactions on supported-metal catalysts, is intended to minimize mass-transfer resistance between the liquid phase and the immobilized-enzyme pellets. A more conveniently implemented arrangement for achieving the same objective is circulation of reaction mixture from a well-mixed reservoir through a short packed column of immobilized enzyme (Fig. 9.3*e*). So long as the recirculation rate is sufficiently large so that only very small conversion (ca. $< 1\%$) occurs in a single fluid pass through the column, this overall system is equivalent to a CSTR reactor [4]. Thus, this design is especially convenient for laboratory kinetics studies.

Enzyme recycle is feasible only when the enzymes can be readily recovered from the product stream leaving the reactor. Two promising approaches to this problem are containment of enzyme inside liquid-surfactant or phospholipid membranes and immobilization of the enzymes on magnetic supports.

Regardless of which strategy is employed, the common objective is maintenance of the desired enzyme concentration within the CSTR. Assuming that this has been accomplished, we can concentrate our attention on computation of the effluent substrate and product concentrations. The basic principles and general material balances discussed above for microbial growth are applicable, as are additional constraints implied by the relatively simple stoichiometry of these reactions.

For example, for the single reaction

$$\mathrm{S} \longrightarrow \mathrm{P}$$

1 mol of P is formed for each mole of S which reacts, so that the feed (s_0, p_0) and effluent concentrations (s, p) are related by

$$s_0 - s = p - p_0 \tag{9.5}$$

With Eq. (9.5), reaction-rate expressions $v(s, p)$ which are functions of both s and p can be written in terms of s only, simplifying the necessary algebra. The substrate mass balance in this case takes the form

$$F(s_0 - s) - V_R v(s, p_0 + s_0 - s) = 0 \tag{9.6}$$

Table 9.1 gives solutions to this equation for a variety of kinetic forms. These formulas are easiest to use in an indirect fashion: insert the desired substrate conversion into the right-hand side and compute the required residence time

Table 9.1 Relationships among substrate conversions $\delta = (s_0 - s)/s_0$, mean residence time, and catalyst concentration for enzyme-catalyzed reactions in a CSTR†

Reaction-rate expression for v	CSTR design expression for $V v_{max}/F$
Michaelis-Menten: $\dfrac{v_{max} s}{K_m + s}$	$\delta\left(\dfrac{K_m}{1-\delta} + s_0\right)$
Reversible Michaelis-Menten: $\dfrac{v_{max}(s - p/K)}{K_m + s + K_m p/K_p}$	$\dfrac{\delta\left[K_m + s_0 - \delta s_0 + \dfrac{K_m(p_0 + s_0\delta)}{K_p}\right]}{1 - \delta(1 + 1/K)}$
Competitive product inhibition: $\dfrac{v_{max} s}{a + K_m(1 + pK_i)}$	$\dfrac{\delta\left[K_m + s_0 - \delta s_0 + \dfrac{K_m(p_0 + s_0\delta)}{K_i}\right]}{1 - \delta}$
Substrate inhibition: $\dfrac{v_{max}}{1 + K_m/s + s/K_i}$	$\delta s_0\left[1 + \dfrac{K_m}{s_0(1-\delta)} + \dfrac{(1-\delta)s_0}{K_i}\right]$

† R. A. Messing, *Immobilized Enzymes for Industrial Reactors*, p. 158, table 1, Academic Press, New York, 1975.

and/or enzyme concentration. Design equations for more complicated reactions and kinetics are obtained by similar methods.

9.1.3 CSTR Cell Reactors with Recycle and Wall Growth

Addition of a cell separator (see Chap. 11) and a recycle stream containing concentrated cells to a CSTR can be used to increase biomass and product yield per unit reactor volume per unit time. Adopting the notation shown in Fig. 9.4, we take F_0 and F_r as the feed and recycle volumetric flow rates and x_1, x_0, and x as the reactor, recycle-stream, and product-stream biomass concentrations, respectively. These concentrations often differ due to a separator, such as a settling

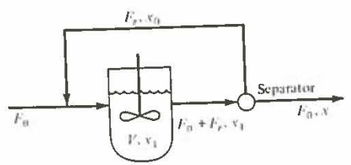

Figure 9.4 Schematic diagram of CSTR with recycle.

basin, at the point where the reactor effluent stream is split. With $a = F_r/F_0$ and $b = x_0/x_1$, the steady-state biomass-conservation equation for the recycle system is

$$F_r x_0 + \mu x_1 V_R - (F_0 + F_r)x_1 = 0 \tag{9.7}$$

so that the overall or external dilution rate D, which is F_0/V_R, is

$$D = \frac{\mu}{1 - a(b - 1)} \tag{9.8}$$

Since the microorganisms in the recycle stream are usually more concentrated than in the reactor effluent, $b > 1$. Then Eq. (9.8) reveals that, with recycle, the dilution rate is larger than the organism's specific growth rate. Thus, with organisms growing at the same rate, use of recycle permits processing of more feed material per unit time and reactor volume than in the nonrecycle situation. This feature of recycle is used to great advantage in biological waste-treatment processes, considered in further detail in Chap. 14. (What is the effect of recycle if $b = 1$? What physical interpretation can you provide for your answer?)

Additional important benefits of recycle are revealed by a few manipulations of the system mass balances. Assuming a constant yield factor, the substrate balance is

$$D(s_0 - s) - \frac{\mu x_1}{Y} = 0 \tag{9.9}$$

Combining this equation with Eq. (9.8) we find that μx_1, the biomass production rate per unit reactor volume, is

$$\mu x_1 = \frac{\mu Y(s_0 - s)}{1 - a(b - 1)} \tag{9.10}$$

This is greater than the nonrecycle production rate by a factor of $[1 - a(b - 1)]^{-1}$. If we assume that μ follows Monod kinetics, we can also show that recycle increases the washout dilution rate by this same factor.

Experiments with CSTRs propagating cell populations sometimes allow higher dilution rates without washout than the theory of the ideal CSTR indicates (recall Sec. 7.1.2). This phenomenon can occur because of wall growth. There may be several solid films of organisms at different points in the vessel. Such colonies can arise, for example, above the liquid level, where splashed droplets have hit the vessel walls, or in crevices and crannies in relatively stagnant zones of the reactor. If we assume that cells on the film at the vessel wall have concentration x_f which is constant with time, reproduction in the film implies addition of cells from the wall into the stirred liquid. In such a situation the steady-state continuous-reactor mass balances take the general form

$$Dx = \mu x + \mu_f x_f \tag{9.11}$$

$$D(s_0 - s) = \frac{1}{Y}\mu x + \frac{1}{Y_f}\mu_f x_f \tag{9.12}$$

where μ_f and Y_f are the specific growth rate and yield factor in the film, respectively. These may differ from the corresponding bulk-liquid parameters μ and Y for a variety of reasons, including diffusion-reaction interactions.

The important thing to notice here is that the $\mu_f x_f$ term in Eq. (9.11) is a source term which is not seriously dependent on D, so that wall growth functions as a second, nonsterile feed which prevents washout. We should note in this connection that laboratory reactors have much larger surface-to-volume ratios than their commercial-sized counterparts, so that in systems involving wall growth, extra care is necessary in scaling up from laboratory data on microbial kinetics.

9.1.4 The Ideal Plug-Flow Tubular Reactor

When fluid moves through a large pipe or channel with sufficiently large Reynolds number (e.g., >2100 in a pipe), it approximates *plug flow*, which means that there is no variation of axial velocity over the cross section. If we assume that plug flow approximately describes fluid movement through the reactor, we can formulate the mass balance on the plug-flow tubular reactor (PFTR) easily using the *differential-section* approach. As Fig. 9.5 suggests, the steady-state conservation equation is applied to a thin slice of the tubular reactor taken perpendicular to the reactor axis. Considering an arbitrary component C, the mass balance on the thin section is

$$Auc\Big|_z - Auc\Big|_{z+\Delta z} + A\,\Delta z\, r_{fc}\Big|_z = 0 \tag{9.13}$$

where r_{fc} is the rate of formation of species C in terms of amount per unit volume per unit time. Rearranging and dividing by $A\,\Delta z$ yields

$$\frac{uc|_{z+\Delta z} - uc|_z}{\Delta z} = r_{fc} \tag{9.14}$$

Taking the limit of this equation and recalling the definition of the derivative gives the final form

$$\frac{d}{dz}(uc) = r_{fc} \tag{9.15}$$

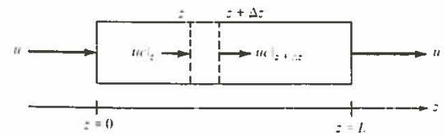

Figure 9.5 Plug-flow reactor.

So long as the reaction does not cause a change in fluid density (would this assumption be valid for a microbial process?), the axial velocity is constant and Eq. (9.15) becomes

$$u\frac{dc}{dz} = r_{fc} \tag{9.16}$$

The quantity z/u is equal to the time required for a small slice of fluid to move from the reactor entrance to axial position z. If we use this transit time t

$$t = \frac{z}{u} \tag{9.17}$$

as a new independent variable, the mass-balance equation (9.16) can be rewritten as

$$\frac{dc}{dt} = r_{fc} \tag{9.18}$$

which is *exactly the same as the batch-reactor mass balance.* This mathematical demonstration can be supplemented by a physical argument: in plug flow with constant velocity, each thin slice of fluid moves through the vessel with absolutely no interaction with neighboring slices. The system is totally segregated, with each thin slice behaving the same as a batch reactor. Consequently, if the initial charge in a batch reactor has the same composition as the feed to the plug-flow reactor, and if the mean residence time L/u in the tube is the same as the batch reaction time, the tube effluent is identical to the batch-reactor product. The boundary condition appropriate for this model is

$$c\Big|_{z=0} = c_0 \tag{9.19}$$

where $z = 0$ denotes the reactor inlet and c_0 is the C concentration in the feed.

As an example, we shall assume that the kinetics used in the Monod chemostat are applicable in the PFTR (or the equivalent batch reactor). The mass balances on cells and substrate in the form of Eq. (9.18) are

$$\frac{dx}{dt} = \frac{\mu_{max} xs}{s + K_s} \tag{9.20}$$

$$\frac{ds}{dt} = -\frac{1}{Y}\frac{\mu_{max} xs}{s + K_s} \tag{9.21}$$

with initial conditions

$$x(0) = x_0 \qquad s(0) = s_0 \tag{9.22}$$

On physical grounds or by manipulations with Eq. (9.20) and (9.21), we can see that the s and x concentrations are bound by the stoichiometric relationship

$$x + Ys = x_0 + Ys_0 \tag{9.23}$$

Using Eq. (9.23) to express x in terms of s and substituting this into Eq. (9.21) gives the single ordinary differential equation

$$\frac{ds}{dt} = -\frac{\mu_{max}}{Y}\frac{[x_0 + Y(s_0 - s)]s}{s + K_s} \tag{9.24}$$

Integration of this equation subject to condition (9.22) can be achieved analytically, with the result

$$x_0 + Y(s_0 + K_s)\ln\frac{x_0 + Y(s - s_0)}{x_0} - K_s Y \ln\frac{s}{s_0} = \mu_{max} t(x_0 + Ys_0) \tag{9.25}$$

The effluent substrate concentration is the s value corresponding to $t = L/u$; then x is found with Eq. (9.23). If viewed as the result of a batch reaction, the kinetics of Eq. (9.20) here shows no lag or death phases but does reach a stationary phase.

In contrast to a CSTR, sterile feed to a PFTR automatically implies zero biomass concentration in the effluent: plug flow prevents a slice of fluid moving through the vessel from ever being inoculated. One way to circumvent this problem is by recycle, so that the incoming stream is inoculated before entering the vessel.

The plug-flow material balances may be readily integrated to relate exit conversion to total reactor residence time L/u for several different common forms of *enzyme* kinetics. Results of such calculations are summarized in Table 9.2.

The relative performance characteristics of ideal CSTRs and PFTRs depend upon the reaction network involved and the corresponding kinetics. For a single reaction with ordinary kinetics (decreasing rate with increasing substrate conversion, such as Michaelis-Menten kinetics), the PFTR provides greater substrate conversion and higher product concentration than the CSTR of equal volume. The opposite is true if the kinetics are autocatalytic (higher rates with decreasing substrate concentration). For microbial processes, the PFTR typically maximizes effluent product concentration. However, the requirement of continuous inoculation and practical difficulties with gas exchange for PFTRs often results in use of their analog, the batch reactor, when high final-product concentration is important. For exponential microbial growth, the CSTR is more efficient than a PFTR or batch reactor. Investigation of the performance of ideal PFTR and CSTR reactors for various simple reaction networks is a major theme of the reaction engineering texts listed in the chapter references. Additional comparisons are explored in the problems.

Table 9.2 Relationships among substrate conversion $\delta = (s_0 - s)/s_0$ and reactor design parameters for enzyme-catalyzed reactions in a PFTR†

Enzymes in solution‡ or in immobilized pellets with negligible mass-transfer limitations

Reaction rate expression for v	PFTR design expression for $\frac{1-\varepsilon}{\varepsilon}\frac{Lv_{max}}{u}$
Michaelis-Menten: $\frac{v_{max}s}{K_m + s}$	$s_0\delta - K_m \ln(1-\delta)$
Reversible Michaelis-Menten: $\frac{v_{max}(s - p/K)}{K_m + s + K_m p/K_p}$	$s_0\left(1 - \frac{K_m}{K_p}\right)\left[\frac{\delta}{b} + \frac{1}{b^2}\ln(1-b\delta)\right] - \left(K_m + s_0 + \frac{K_m}{K_p}p_0\right)\frac{1}{b}\ln(1-b\delta)$ where $b = \frac{K+1}{K}$
Competitive product inhibition: $\frac{v_{max}s}{s + K_m(1 + p/K_i)}$	$s_0\left(1 - \frac{K_m}{K_i}\right)[\delta + \ln(1-\delta)] - \left(K_m + s_0 + \frac{K_m}{K_i}p_0\right)\ln(1-\delta)$
Substrate inhibition: $\frac{v_{max}}{1 + K_m/s + s/K_i}$	$s_0\delta - K_m\ln(1-\delta) + \frac{s_0^2}{K_i}\left(\delta - \frac{\delta^2}{2}\right)$

† Adapted from R. A. Messing, *Immobilized Enzymes for Industrial Reactors*, p. 158, Academic Press, Inc., New York, 1975.
‡ The $(1-\varepsilon)/\varepsilon$ factor in these equations should be set equal to unity for enzymes in solution.

9.2 REACTOR DYNAMICS

In this section we consider dynamic characteristics of bioreactors. Although dynamics of CSTRs are the primary focus here, many of the concepts and principles introduced can be applied to other reactor configurations. We first develop the equations needed to describe unsteady-state reactor performance and then examine use of those equations to characterize transient behavior of the bioreactor. We shall see that successful application of the approaches presented here is often limited by lack of kinetic models which are accurate under transient operating conditions.

9.2.1 Dynamic Models

For dynamic studies of CSTRs the conservation equation (Eq. 7.4) must be modified to give the corresponding unsteady-state mass balance:

$\frac{d}{dt}$ (total amount in the reactor) = rate of addition to reactor

− rate of removal from reactor + rate of formation within reactor

Thus, for a well-stirred vessel we have for component i

$$\frac{d}{dt}(V_R \cdot c_i) = F(c_{iF} - c_i) + V_R r_{f_i} \tag{9.26}$$

Assuming that the feed stream and reactor contents have equal density, equality of inlet and outlet volumetric flow rates means the volume of the reactor contents V_R is constant, allowing rearrangement of Eq. (9.26) into the form

$$\frac{dc_i}{dt} = D(c_{if} - c_i) + r_{f_i} \tag{9.27}$$

This unsteady-state material balance is the starting point for characterization of reactor dynamics. Before introducing some general mathematical tools useful in dynamics analysis, we should comment on the new considerations required to justify the use of a CSTR model to calculate dynamics of a bioreactor. At this point we shall focus entirely on mixing phenomena, saving for later consideration of the required biological kinetics model for transient analysis. As mentioned in Chap. 8, one characteristic parameter of mixing in a vessel is the mixing or circulation time. This is an order of magnitude indication of the time required for an element of fluid to return to a similar region of the reactor after circulating around the reactor according to the existing flow patterns. In order to apply a CSTR model, it is important that this circulation time be short relative to other characteristic times concerning the CSTR.

In particular, a new characteristic time is introduced when we examine dynamic behavior of a CSTR. Now, there is the possibility of time-varying feed rate or feed concentration. In order for the ideal mixing approximation to apply, it is necessary that the circulation time be much less than the characteristic time scale for fluctuations in the feed stream or, for that matter, in any other entering streams such as base additions for pH control. Exactly the same consideration applies to the use of the perfect mixing assumption for the case of fed-batch reactors discussed earlier.

Eq. (9.27) applies to each component considered in the bioreactor model. In all but the simplest case, then, the dynamic reactor model consists of a set of equations of the form of Eq. (9.27) which are usually coupled through the rate of formation terms r_{f_i}. That is, in general the rate of formation of component i may depend on the concentrations of all of the other components in the reactor. It will be very convenient to introduce vector-matrix notation at this point to simplify writing large sets of equations.

We shall adopt the notation convention that lowercase boldface letters like $\mathbf{c}$ denote vectors and that uppercase boldface letters like $\mathbf{A}$ denote matrices. Then, the set of equations indicated by Eq. (9.27) may be written in the form

$$\frac{d\mathbf{c}(t)}{dt} = \mathbf{f}(\mathbf{c}(t), \mathbf{p}) \tag{9.28}$$

where $\mathbf{c}$ is a vector of concentrations with dimension m (with m elements or components; an m-vector) equal to the number of components considered in the model. Here $\mathbf{p}$ denotes a q-vector of model parameters, such as feed concentrations, dilution rate, and kinetic parameters. The ith component of the vector-valued function $\mathbf{f}$ is equal to the right-hand side of Eq. (9.27).

Since the system described by Eq. (9.28) is in general nonlinear, we usually cannot go too far in our analysis without resorting to some approximations. Often we are interested in dynamic properties of the system near a particular steady state $\mathbf{c}_s$. In the notation of Eq. (9.28), the steady state concentration vector $\mathbf{c}_s$ must satisfy

$$\mathbf{f}(\mathbf{c}_s, \mathbf{p}) = \mathbf{0} \tag{9.29}$$

We can attempt to determine behavior near $\mathbf{c}_s$ by expanding the right-hand side of (9.28) in a Taylor's series about $\mathbf{c}_s$ and neglecting all terms of second order and higher in the deviations $c_i(t) - c_{is}$, since they are presumed small. Then we obtain the following linear approximation for our system:

$$\frac{d\mathbf{x}(t)}{dt} = \mathbf{A}\mathbf{x}(t) \tag{9.30}$$

where the vector $\mathbf{x}(t)$ denotes the vector of deviations from the steady state $\mathbf{c}_s$:

$$\mathbf{x}(t) = \mathbf{c}(t) - \mathbf{c}_s \tag{9.31}$$

The element a_{ij} in the ith column of the matrix $\mathbf{A}$ is defined by

$$a_{ij} = \frac{\partial f_i(\mathbf{c}_s, \mathbf{p})}{\partial c_j} \tag{9.32}$$

We should emphasize that $\mathbf{A}$ corresponds to some particular steady state. Some systems have more than one steady state for a given $\mathbf{p}$ and this usually implies that a different $\mathbf{A}$ matrix corresponds to each steady state.

The dynamic properties of the linearized system are relatively easy to determine since all solutions of Eq. (9.30) usually take the form

$$\mathbf{x}(t) = \sum_{i=1}^{m} \alpha_i \boldsymbol{\beta}_i e^{\lambda_i t} \tag{9.33}$$

The quantities $\boldsymbol{\beta}_i$ and λ_i are the corresponding pairs of eigenvectors and eigenvalues of $\mathbf{A}$. Thus $\lambda = \lambda_i$ satisfies the characteristic equation

$$\det(\mathbf{A} - \lambda\mathbf{I}) = 0 \tag{9.34}$$

($\mathbf{I}$ is the identity matrix), and the $\boldsymbol{\beta}_i$ satisfy

$$(\mathbf{A} - \lambda_i\mathbf{I})\boldsymbol{\beta}_i = 0 \qquad i = 1, \ldots, m \tag{9.35}$$

The α_i are constants to be chosen to fulfill the specified initial conditions; consequently they satisfy the linear algebraic equations

$$\sum_{i=1}^{m} \alpha_i \boldsymbol{\beta}_i = \mathbf{x}(0) \tag{9.36}$$

where $\mathbf{x}(0)$ is a specified vector of initial deviations.

This linearized dynamic model of the reactor provides a systematic framework for identification of characteristic response times of the system. Within the framework of local dynamics which are considered here, we can see from Eq. (9.33) that the time scales for decay of disturbances from the reference steady state $\mathbf{c}_s$ are characterized by the eigenvalues λ_i of the matrix $\mathbf{A}$. Thus, in terms of local behavior, the system exhibits a spectrum of characteristic times indicated approximately by

$$t_{c_i} = |\lambda_i|^{-1} \qquad i = 1, \ldots, m \tag{9.37}$$

These values can be used to examine the relative magnitudes of reactor time scales with time scales for input variations, for example.

While the approach leading to the time-scale estimates given in Eq. (9.37) is systematic and locally rigorous, the time scale estimates so obtained are difficult to assign a particular physical significance. The eigenvalues λ_i are in general functions of all entries of the matrix $\mathbf{A}$ and, as such, depend upon the entire vector of steady-state operating conditions $\mathbf{c}_s$ and the entire parameter vector $\mathbf{p}$. This situation does not allow convenient comparison of time scales for mixing, for reaction, and for other interactions in the system. In the case of a CSTR, the eigenvalues may be shown to have the form $-D +$ (a value characteristic of the reaction network).[†] Although providing some guidance, this relationship does not unravel the complex relationships between other parameters and the λ_i. Accordingly, some judgment, experience, and some art is needed in developing a reasonable yet not altogether mathematically rigorous approach for identification of different characteristic lengths and time ratios. Of course one systematic method for achieving this which is well known in chemical engineering is transformation of all system equations to dimensionless form, followed by rearrangements to identify dimensionless groups which characterize the system's behavior. Frequently, such dimensionless groups take the form of ratios of characteristic length or time scales.

9.2.2 Stability

Next we shall examine how the dynamic characteristics of the reactor depend upon the function $\mathbf{f}$ and the selected parameter values $\mathbf{p}$. For our purposes, the *local stability* of a particular steady state $\mathbf{c}_s$ will be of greatest concern. If a steady state is locally asymptotically stable, the system concentrations will return to that steady state after a small disturbance has moved those concentrations slightly away from the reference steady state of interest. For an *unstable* steady state, the concentrations considered will "run away" from the steady-state values following certain small disturbances. To be sure to avoid ambiguity, we shall restate these definitions in more formal mathematical language.

We shall say that the steady state $\mathbf{c}_s$ is *locally asymptotically stable* if $\lim_{t\to\infty} \mathbf{c}(t) \to \mathbf{c}_s$ provided that the initial state $\mathbf{c}_0$ is sufficiently close to $\mathbf{c}_s$. [Our mathematical measure of closeness for vectors is the Euclidean norm, defined by

$$|\mathbf{c}| = \left(\sum_{i=1}^{m} c_i^2 \right)^{1/2}$$

Then "$\mathbf{c}_0$ sufficiently close to $\mathbf{c}_s$" means that $|\mathbf{c}_0 - \mathbf{c}_s|$ is a sufficiently small real number.] The steady state $\mathbf{c}_s$ is *globally asymptotically stable* if $\lim_{t\to\infty} \mathbf{c}(t) = \mathbf{c}_s$ for any choice of $\mathbf{c}_0$ (except ridiculous ones like negative concentrations). If $\mathbf{c}_s$ is an *unstable* steady state, some initial states $\mathbf{c}_0$ arbitrarily close to $\mathbf{c}_s$ lead to trajectories $\mathbf{c}(t)$ which do not approach or stay arbitrarily close to $\mathbf{c}_s$. Thus, in the case of instability, the magnitude of the deviation $\mathbf{x}(t)$ tends to increase from its initial value for some initial deviations.

Local stability is determined in most cases by the eigenvalues λ_i of the matrix $\mathbf{A}$ defined in Eq. (9.32). The steady state $\mathbf{c}_s$ is locally asymptotically stable if all eigenvalues of $\mathbf{A}$ have negative real parts:

$$\text{Re}(\lambda_i) < 0 \qquad i = 1, \ldots, m \tag{9.38}$$

[†] M. Fjeld, O. A. Asbjørnsen, and K. J. Åstrom, "Reaction Invariants and their Importance in the Analysis of Eigenvectors, State Observability, and Controllability of the Continuous Stirred Tank Reactor," *Chem Eng. Sci.*, **29**:1917, 1974.